Ultrafast, Broadband Light Polarization Properties of Vanadium Dioxide Thin Films on Insulating and Metallic Substrates

Vinh Son Tran

A Thesis

In the Department

of

Physics

Presented in Partial Fulfillment of the Requirements

For the Degree of

Doctor of Philosophy (Physics) at

Concordia University

Montreal, Quebec, Canada

October 2018

CONCORDIA UNIVERSITY
SCHOOL OF GRADUATE STUDIES

This is to certify that the thesis prepared

By: Vinh Son Tran

Entitled: Ultrafast, broadband light polarization properties of vanadium dioxide thin films on insulating and metallic substrates

and submitted in partial fulfillment of the requirements for the degree of

Doctor of Philosophy (Physics)

complies with the regulations of the University and meets the accepted standards with respect to originality and quality.

Signed by the final examining committee:

_____ Chair
Dr. Suong Van Hoa

_____ External Examiner
Dr. Ludvik Martinu

_____ External to Program
Dr. Mojtaba Kahrizi

_____ Examiner
Dr. Pablo Bianucci

_____ Examiner
Dr. Laszlo Kalman

_____ Thesis Co-Supervisor
Dr. Truong Vo-Van

_____ Thesis Co-Supervisor
Dr. Alain Haché

Approved by: _____
Dr. Pablo Bianucci, Graduate Program Director

December 11, 2018

_____
Dr. André Roy, Dean
Faculty of Arts and Science

ABSTRACT

Ultrafast, Broadband Light Polarization Properties of Vanadium Dioxide Thin Films on Insulating and Metallic Substrates

Vinh Son Tran, Ph.D.

Concordia University, 2018

The refractive indices of vanadium dioxide (VO_2) abruptly change when its phase transition temperature of 68^{o}C is reached, the point at which it goes from an insulating state to a metallic state. Modifications of complex-valued refractive indices in VO_2 have been shown to produce optical phase shifts that are unequal for the s- and p-components of polarization, thereby causing a relative phase shift Δ between the two. Under certain conditions of Δ, a linearly polarized light can rotate its polarization 90 degrees or transforms between linear and circular. In this thesis, we will demonstrate all possibilities of using a VO_2 thin film to change the polarized light states of reflected or transmitted light on the nanosecond and potentially shorter timescales. Possible applications for high-contrast optical modulation over a wide spectral range are discussed.

ACKNOWLEDGMENTS

This thesis has been completed with the help of many people and organizations. I would like to take this opportunity to thank all who have accompanied me during my doctoral program. Firstly, I would like to express my deep gratitude to Dr. Truong Vo-Van and Dr. Alain Haché, my research supervisors, for their patient guidance, enthusiastic encouragement and financial support. Dr. Alain Haché gave me the opportunity to come to this beautiful country and work in his lab. Thank you for being a good mentor to me and for allowing me to work my own way, with my own schedule. Dr. Truong Vo-Van has supported me in all possible conditions to continue my studies at Concordia University. I have learned a lot from his sharing about all matters of science and life.

My sincere thanks also go to Dr. Jean-François Bisson and Dr. Georges Bader at Université de Moncton, who gave me access to the laboratories and research facilities. Without their precious support it would not have been possible to conduct this research. I would also like to extend my thanks to Richard Vernhes at Polytechnique Montréal for the ellipsometry measurements.

I wish to thank the members of my PhD committee for offering their time to review and comment my work. My sincere thanks to Dr. Pablo Bianucci and Dr. Laszlo Kalman who followed my progress and gave me valuable advices during my studies.

I gratefully acknowledge the funding received towards my PhD from Concordia University through the "Concordia University Full-Tuition International Recruitment Award" and the "Accelerator Award". This support has helped me to concentrate on my research and complete my thesis more quickly.

Thank you to Phuong Anh for fabricating samples, to my fellow labmate Ryan and mom Gibbi for their time checking my thesis and giving me recommendations. I would also like to thank Marie-Anne Cheong-Youne, Assistant to the Chair, Department of Physics, for providing necessary information and documents.

Finally, I would also like to say a heartfelt thank you to my parents and sisters for their unconditional trust and timely encouragement. With endless love, my mother and father worked hard to give me the opportunities to study and explore the world. And I know that they will always follow me on the road ahead. Many thanks to my fiancée, Mai, for her love and for always being at my side.

This thesis is dedicated to my parents.

For their endless love, support and encouragement

TABLE OF CONTENTS

LIST OF FIGURES

LIST OF TABLES

LIST OF SYMBOLS AND ABBREVIATIONS

MIT	Metal-insulator transition
T_{MIT}	Metal-insulator transition temperature
1D	One-dimensional
2D	Two-dimensional
PLD	Pulsed laser deposition
CVD	Chemical vapor deposition
UV	Ultraviolet
IR	Infrared
PIPT	Photoinduced phase transition
LPC	Lattice potential change
CPT	Crystallographic phase transition
$\boldsymbol{F_C^{CPT}}$	Photoexcited fluence threshold for crystallographic phase transition
$\boldsymbol{F_C^{IMT}}$	Photoexcited fluence threshold for metal-insulator transition
VO_2	Vanadium dioxide
ITO	Indium tin oxide
TiO_2	Titanium dioxide
DC	Direct current
RF	Radio frequency
CCD	Charge-Coupled Device
KD*P	Potassium dideuterium phosphate
FWHM	Full width at half maximum

CHAPTER 1

Introduction

Vanadium dioxide (VO_2) is a strongly correlated electron material. It is well known for its ability to change properties from the insulating state to the metallic state at around 68^{o}C due to a rearrangement of its crystal structure. Since the discovery of the metal-insulator transition (MIT) in 1959 [1], this material has attracted significant interest in theoretical as well as applied research. As will be presented in Chapter 2, there have been many theoretical approaches that were proposed to explain the transition mechanism in VO_2, but controversy still exists, and this issue is still a matter of debates when new discoveries about VO_2 are made. VO_2 remains, however, a material of choice among possible MIT materials, exhibiting truly unique properties, whether optical, electrical or magnetic. In terms of optical properties, the topic of this thesis, VO_2, beside being able to change rapidly its crystal structure at a relatively low temperature, can also be activated optically within nanoseconds time scales or faster. This is why we have chosen to further explore the optical properties of this material that offers so much potential for applications.

So far, almost all optical applications of VO_2 have been based on the amplitude variation in optical properties of the material during phase transition as shown in Figure 1.1, some of which can be named as smart coatings [2], optical devices [3], [4], thermal sensors [5], and infrared imaging systems [6], [7]. Although many improvements in fabrication have been made to enhance the applicability of VO_2, all optical applications were found and studied only in the infrared, in particular at wavelengths above 1000 nm where large changes in amplitude happen. In many fields such as sensors, optical switches or smart coatings however, we need to work with visible light. Therefore, there is a strong interest to explorer further the potential of VO_2 in this spectral region.

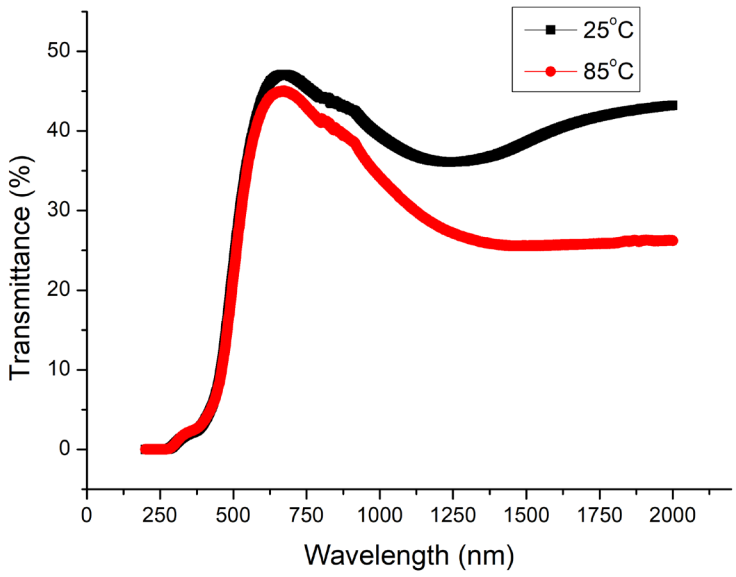

Figure 1.1: Transmittance of a 100 nm VO_2 thin film at temperature of 25°C (black) and 85°C (red).

It is remarked that when light interacts with VO_2 films at different states, not only its amplitude changes, its phase must also change in some way. This interesting aspect has not been studied previously and is our main concern in this thesis. Through our theoretical and experimental findings, we established that the phase of light varies very much too during the phase transition of VO_2. This finding opens for the first time the possibilitiy of applying VO_2 films in a wider spectral range from the visible to the infrared.

Other than using the intensity changes, we focused our attention on the drastic changes of the light polarization state as light interacts with a VO_2 thin film. The variation in refractive index of the film during phase transition alters the phases of the reflected and transmitted s- and p-polarized light. This causes the polarization state of light to change completely. In some cases, a linear polarization can switch to a circular polarization and vice-versa or can rotate to a new orientation. Theoretical calculations and experimental results show that this can be done with wavelengths near the center of the visible spectrum (500 nm) to the infrared and only by using a simple VO_2 film on glass substrate. Using this effect in combination with polarizers could lead to

highly efficient optical modulation and extend applications of VO_2 in many different fields such as electronic devices, perfect absorbers, phase retarders, and energy conservation. To explore the phase and polarization changes of light when it interacts with a thin VO_2 film and to discuss potential applications, we implemented the following studies:

- Calculate and measure phase changes of light as it interacts with a VO_2 thin film at different states of VO_2.
- Find conditions to control polarization of light by thermal activation.
- Measure polarization states of light and optical modulations.
- Induce VO_2 transition by optical pumping to measure switch-on and switch-off time for high speed optical switching applications.
- Enhance ability to control polarization by using metallic substrates.
- Discuss advantages and disadvantages of using phase changes method and propose ideas for new studies.

All details of theories, calculations as well as experimental results of this study will be presented in this thesis through nine following chapters:

Chapter 2 describes metal-insulator transition mechanism through Bloch-Wilson, Mott-Hubbard, Peierls and Anderson models. Each theory has its own advantages to explain the transition. We only show the most fundamental differences and do not go into details as this is not our primary concern. The rest of this chapter is used to show properties of vanadium dioxide materials. Besides mentioning crystal structure, electrical and optical properties, the changes in electronic and crystallographic structures during optical activation of VO_2 also are discussed in detail. Many VO_2 properties in this chapter are used to explain experimental results in Chapters 5-

9. Some promising applications also are covered in this chapter to provide a comprehensive view of VO_2.

Chapter 3 presents theories and equations involved in the interaction between polarized light and a thin film. We described the relationship between polarization states at insulating and metallic states of VO_2 in reflection and transmission through the relative phase shift parameters, functions of temperature, wavelength, film thickness, angle of incidence, and refractive indices. Those parameters play the most important role in all our calculations and is used frequently in this thesis. At the end of this chapter are some equations related to the polarization state and its intensity going through a polarizer.

Chapter 4 provides all steps to fabricate a VO_2 thin film on glass substrates and an ellipsometry method which is used to measure film thickness, refractive indices and other optical parameters related to VO_2 thin films.

Chapter 5 presents our first experimental results in measuring the phase change of light when it interacts with a VO_2 film at different temperatures below and above the transition temperature of the material. It opens the possibility of controlling the phase of light by using VO_2 thin films and leads us to the idea of creating a spatially non-uniform phase shift for reflected light. The VO_2 thin film now acts as a lens to focus or defocus reflected beam in the far field. These findings would be the foundations for later studies on light polarization control.

Chapter 6 analyzes the limitations of using unpolarized light in all published VO_2 applications and polarized light is suggested to overcome these weaknesses. Calculations with polarized light show the possibility to extend the applicable spectral range to visible and increase optical modulation significantly. A vanadium dioxide thin film can be used as a device to control light polarization both in the visible and the near infrared.

Chapter 7 analyzes the influence of thickness, wavelength, and angle of incidence on polarization control to find optimal parameters for fabricating samples and doing experiments. All experimental results with different VO_2 samples and wavelengths from 514 nm to 1550 nm are presented in this chapter. High light contrast ratios are obtained when VO_2 samples are combined with a polarizer. This opens new possibilities for creating high-performance modulators and switches for VO_2 optical devices.

Chapter 8 uses pulsed laser to induce phase transition of VO_2. In this chapter, we repeated similar experiments done by thermal activation in Chapter 7 by optical activation. All experimental results show that VO_2 films can alter the polarization state on nanosecond timescale. This effect is observed with layers of various thicknesses on different substrate materials. VO_2 thin films thus demonstrate a great potential in electronic device applications.

Chapter 9 presents the ability to use metallic substrates to enhance polarization control. This method helps to reduce the angle of incidence for doing experiments to 40^o and increase the reflectivity. However, oxidation layers formed between VO_2 films and metallic substrates cause some differences between experimental and calculated results. This problem will be discussed in this chapter with some potential solutions.

Chapter 10 forms the conclusion with the main features of the present work and new ideas for future studies.

Most of the results in the thesis have been published in the following:

- T. V. Son, P. A. Do, V.-V. Truong, G. Bader, and A. Haché, "Polarization modulation by vanadium dioxide on metallic substrates," *Opt. Commun.*, vol. 427, pp. 511–516, 2018.
- T. V. Son, V. V. Truong, J-F.Bisson, and A. Haché, "Nanosecond polarization modulation in vanadium dioxide thin films", *Appl. Phys. Lett.,* 111, 041103, 2017.

- Patrick Cormier, Tran Vinh Son, Jacques Thibodeau, Alexandre Doucet, Vo-Van Truong, Alain Haché, “Vanadium dioxide as a material to control light polarization in the visible and near infrared”, *Opt. Commun.*, 382, 80-85, 2017.
- T.V.Son, V.V.Truong, P.A.Do, and A.Haché, “Ultra-thin, single-layer polarization rotator”, *AIP Advances,* 6, 095102, 2016.

CHAPTER 2

Properties of vanadium dioxide

2.1 Metal-insulator transition (MIT)

Metal-insulator transition in materials is an interesting subject that has attracted much attention in the past decades. When exposed to stimuli such as temperature, pressure [8], carrier doping or electric fields [9], some materials change their properties completely. Their electrical conductivity can vary by several orders of magnitude, with optical properties changing drastically as well. Although this thesis deals with a phase transition material, namely vanadium dioxide, we are not concerned with the exact nature of metal-insulator phase transition, a topic that has already been the subject of countless studies in solid state physics [10]–[14]. Instead, our goal is to understand the properties of light when it interacts with a material undergoing a phase transition. From this optics point of view, the refractive indices of the material are sufficient to fully characterize the problem. Nevertheless, for the sake of completeness and to understand the underlying causes, we outline here the key findings in solid state physics relating to metal-insulator phase transitions.

The first successful theory of MIT transition was introduced in the early 1930s [15]–[18]. In this model, the periodic lattice structure of atoms in crystals form a band structure with all the allowed bands and forbidden bands. For insulators, the highest filled band is completely filled, while for metal it is partially filled. An insulator in this band theory is called a band insulator or Bloch-Wilson insulator. However, de Boer and Berwey [19] found that this theory could not explain why many metal oxides with a partially filled d-electron bands are poor conductors. Following this finding, Mott [20] pointed out that the interaction between electrons must be considered. The strong Coulombic repulsion between the electrons could be the origin of the

insulating behaviour. According to Mott, a conduction electron in a screened Coulomb interaction from each proton and the other electrons has a potential energy.

$$U(r) = -\frac{e^2}{r}\exp(-qr) \tag{2.1}$$

The activation energy in the insulating state needs to be higher than this potential energy to make a phase transition. In Eq. 2.1, the constant q relates to electron-electron interactions effect and is calculated by the Thomas-Fermi appoximation $q^2 = 4me^2(3N_0/\pi)^{1/3}/\hbar^2$, which depends on the free electron density N_o. At high densities, the potential $U(r)$ has no bound states and we have a metal. The critical free electron density N_c, at which the transition occurs is given by

$$N_c{}^{1/3} a_H \approx 0.2 \tag{2.2}$$

where a_H is the effective Bohr radius of the material. This theory agrees well with observation from doped materials such as germanium or silicon [21], [22]. When increasing the doped concentration of the donor or acceptor atoms in the semiconductor, the transition to the metal phase will occur at approximately the predicted concentration. This MIT model is named the Mott MIT or Mott-Hubbard MIT with some modifications of the Hubbard model [23] in the potential energy calculation.

However, metal-insulator transitions are not only explained by interactions among electrons, it can be the result of interactions between electrons and lattices, known as the Peierls MIT theory.

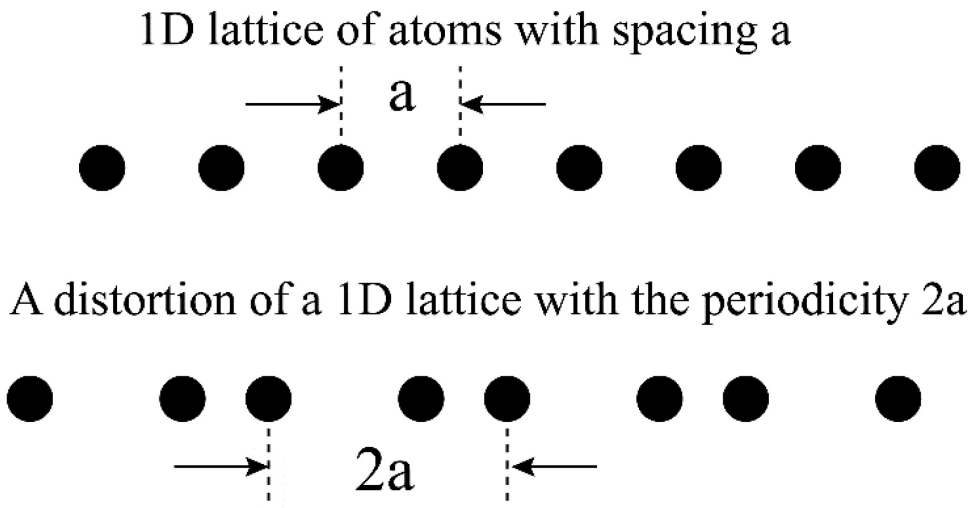

Figure 2.1: A distortion of the Peierls one-dimensional lattice model.

In general, the Peierls MIT theory is based on a distortion in the structure of lattice [24]. In the simple one-dimensional model of Peierls, every lattice node (ion) carries one electron. At the metallic state, all atoms are arranged in a periodic system with equal lattice spacing, denoted by *a*. This structure is unstable and easy to change when the metal is cooled down or under a stimulus. To a first order, a periodic distortion in the structure can alter the periodicity such that the lattice constant doubles to *2a*, as shown in Figure 2.1. As a consequence of this transition, the periodic ionic potential in the material is distorted with a new energy gap created in the energy spectrum of electrons. The electrons now need more energy to swap positions so they are stuck in their locations. Effectively this means that the system is no longer conducting, but rather insulating. Among the many MIT materials we know, $NbSe_3$ and $K_{0.3}MoO_3$ [25] are two typical examples of Peierls insulator, which undergo a phase transition at 145 K and 180 K with significant changes in conductivity as results of their structural changes. Since the development of that theory, properties of electrons in the deformation structures receive a lot of research attention. Anderson [26] suggested that when increasing in the degree of lattice disorder to a critical point, all electrons in the lattice will be trapped in local areas and the electrical conductivity of the material vanishes

altogether, a phenomenon known as Anderson localization. To explain this effect, he used a tight-binding model of an electron in a disordered lattice. This electron feels a random potential and can tunnel to nearest neighbor sites. However, instead of assuming that conduction electrons are the extended plane waves with short lifetime and small mean free paths, Anderson sees them as standing waves which are confined in space and thus have long lifetimes [27]. This makes all conduction electrons localized by a random well in the random potential energy picture, see Figure 2.2. This Anderson MIT is commonly used to explain properties of strongly disordered materials [28], [29] and materials with strong impurity scattering, such as heavily doped semiconductors [30], [31].

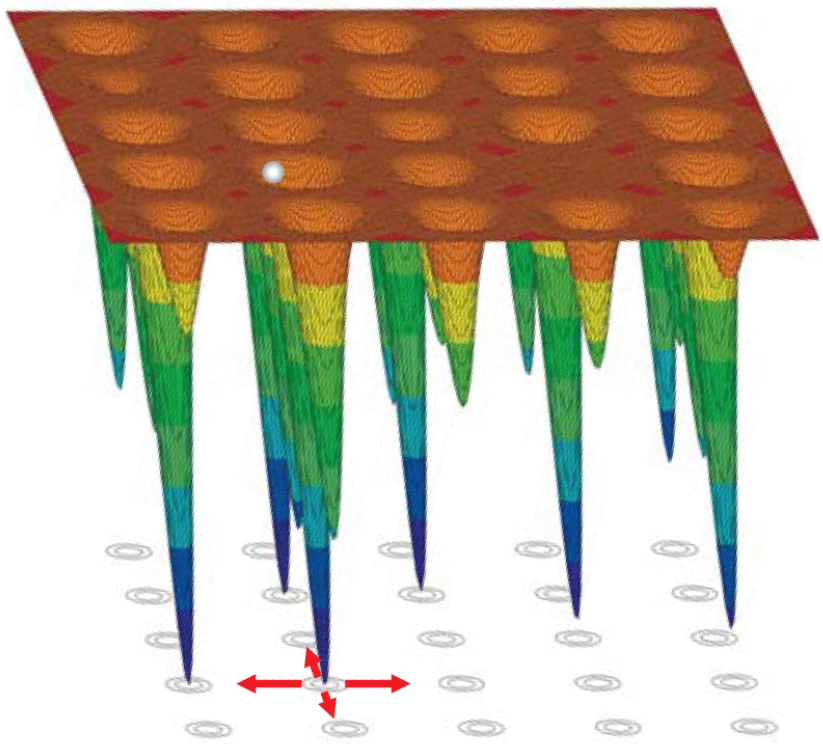

Figure 2.2: An electron in 2-D random potential energy of the Anderson model. Reproduced from ref. [27].

Table 2.1 summarizes the four most widely accepted theories of metal-insulator transition with different mechanisms. Each has its own advantages and disadvantages and can be used to

explain properties quite well for a group of materials or a specific material. Although, much progress in experiment and theory has been accomplished to explain how MIT transitional mechanism works over the past 70 years [16], [32]–[36], there is no comprehensive theory that can explain this problem thoroughly. The true nature of the metal-insulator transition in some materials remains a mystery.

Table 2.1: Metal-Insulator transition (MIT) classification.

Type	Origin of MIT
Bloch-Wilson insulator	Conventional band theory
Mott-Hubbard insulator	Electron-electron interaction
Peierls insulator	Electron-phonon (lattice) interaction
Anderson insulator	Disorder-induced localization

2.2 Vanadium dioxide and its crystal structures

2.2.1 Vanadium dioxide

One of the first observations of metal-insulator transition effect in oxides was published in 1959 by Morin [1]. He reported the sudden change in electrical conductivity of titaninum and vanadium oxides as they undergo a certain temperature. Since then many correlated oxides with the same properties were found such as FeO, CoO, and NiO [37], [38]. Each material has its own specific metal-insulator transition temperature (T_{MIT}), ranging typically from 70 K to 1000 K, as shown in Figure 2.3. Among those materials, the metal-insulator transition temperature of vanadium dioxide (VO_2) is about 340 K (68^{o}C) in bulk crystals. This is close to ambient temperature, and this property, coupled with a large change in resistance across the transition, makes VO_2 an interesting material in research and manufacturing of electronic and optical devices. Therefore, VO_2 is the chosen material to discuss throughout this thesis. All its interesting

properties will be analyzed in detail in the following sections for the purpose of providing an overview of the metal-insulator transition in oxide materials. It is worth noting that vanadium also makes other oxides (V_4O_2, $V_2O_{3,\ldots}$), each with its own phase transition temperature.

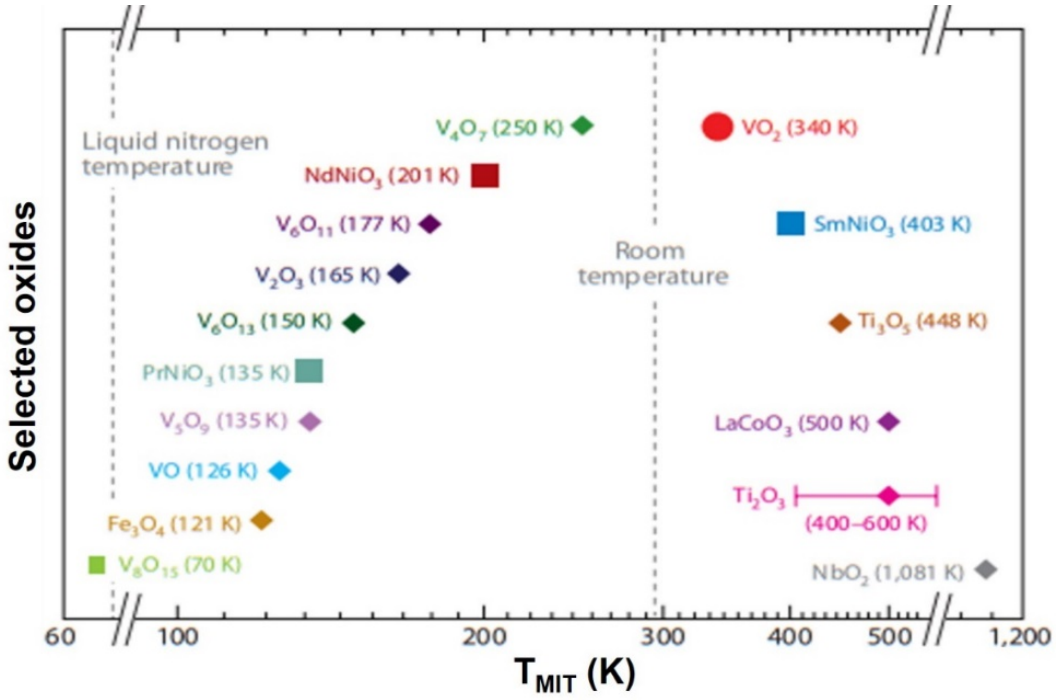

Figure 2.3: Metal-insulator transition temperature (T_{MIT}) of some selected bulk oxides. Reproduced from ref. [39].

2.2.2 Vanadium dioxide crystal structures

Vanadium dioxide (VO_2) is an insulator at room temperature, with a monoclinic crystalline structure (M_1). At temperatures above 68°C, vanadium and oxygen atoms are rearranged to a rutile (R) structure. Those structures belong to the P21/c (M_1) and P42/mnm (R) space group [39] with different lattice symmetries, as shown in Figure 2.4. A unit cell of the rutile structure contains two vanadium cations V^{4+} and four oxygen anions O^{2-}. The vanadium atom sits at the center of the oxygen octahedron and forms six bonds by hybridizing its orbital with orbitals of 6 oxygen atoms on the top of the octahedron [40]. Each oxygen atom has 3 sp^2 hybrid orbitals and creates three

sigma bonds with vanadium atoms in near-neighbor unit cells. At the low-temperature phase, the chain V-V is tilted along the c axis with unequal gaps between cations, namely 2.65 Å and 2.87 Å, unlike the constant 2.87 Å in the rutile phase at high temperature. This structural change constitutes a lowering of symmetry and a doubled size of the unit cell (the monoclinic unit cell now has 4 vanadium and 8 oxygen atoms). It also causes deformation of the oxygen cages around vanadium atoms. In order to compare the differences in structure between VO_2 (M_1) and VO_2 (R), we compare lattice parameter in Table 2.2 [41].

Table 2.2: Lattice parameters for VO_2 at Monoclinic (M_1) and Rutile (R) phases.

	VO_2 (M_1)	**VO_2 (R)**	**Difference**
a or a' (Å)	5.375	5.383	0.008
b or b' (Å)	4.526	4.554	0.028
c or c' (Å)	5.753	5.712	-0.041
β (degrees)	122.6	122.1	-0.5
V ($Å^3$)	118.07	118.44	0.37

It can be seen that the unit cells expand slightly along the axes a and b, while the distance along V-V in the c axis shrinks. The entire monoclinic structure is compressed and twisted by a small angle from 118.07° to 118.44° in the rutile structure. This makes the volume changes by approximately 0.31%. Although the change of VO_2 structure during the transition is small, it causes significant changes in the energy band structure leading to changes in electrical and optical properties. One of the most widely accepted explanations of VO_2 band energy structure for both the metallic and the insulating phases was presented by Goodenough [42]. He assumed that each vanadium atom $[Ar]3d^34s^2$ contributes four electrons to fill the valence band and leaves one d-electron in the conduction band. At high temperature, the d-level of the V^{4+} is first split into doubly

degenerate e_g levels and triply degenerate lower lying t_{2g} levels in the octahedral crystal field. The e_g orbitals lie higher in energy and are strongly hybridized with the 2p orbital of O^{2-}. They have large bandwidth and are empty. The t_{2g} levels are further split into $d_{\|}$ and π^* levels by the orthorhombic component of the tetragonal crystal field. Those levels are located at the lowest energies around the Fermi level. Since the π^* orbitals are easily hybridized with the 2p orbitals of O compared with $d_{\|}$ orbitals, the π^* band have higher energies and a wider bandwidth. On the other hand, the $d_{\|}$ orbitals in V are relatively nonbonding. In the rutile phase, the $d_{\|}$ and π^* bands overlap at the Fermi level as depicted in the schematic diagram in Figure 2.4. In the monoclinic phase, the dimerization and tilting of the V-V pair results in two important effects. First, V-V pairing within the vanadium chain parallel to the rutile c axis cause the $d_{\|}$ band splits into two subbands, each contains half the number of levels of the initial $d_{\|}$ band. The lower-energy bonding subband is almost completely filled with electrons, and the upper-energy antibonding one is empty. Second, distortion of V-O bonds lifts the antibonding π^* to a higher in energy above the Fermi level, as in Figure 2.4. With these changes when VO_2 undergo phase transition, a bandgap $E_g \sim$ 0.6-0.7 eV is formed in the insulating phase.

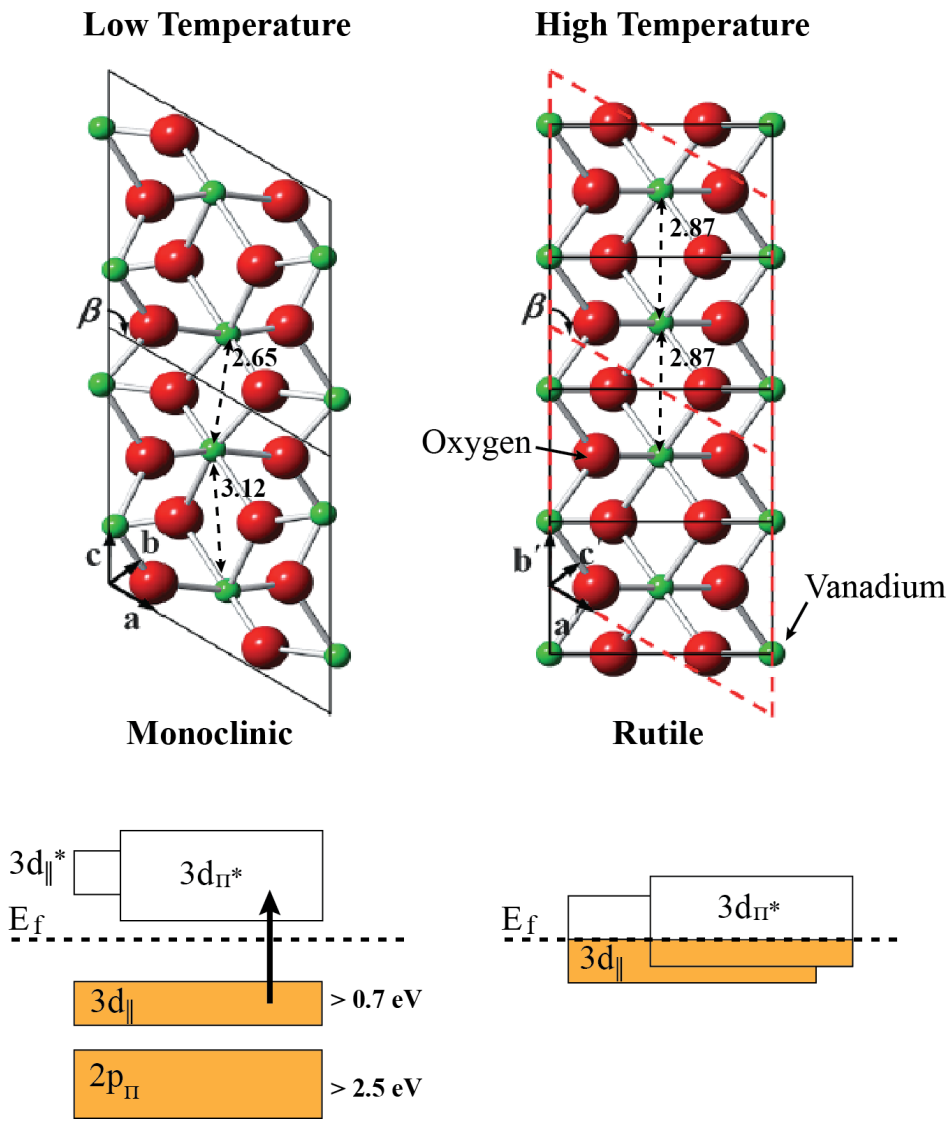

Figure 2.4: VO_2 monoclinic and rutile crystal structures and their energy band structures. Modified from ref. [43].

Many studies on structural changes and electronic behaviour of VO_2 during MIT have been done to determine whether the above structural change induces MIT (a Peierls mechanism) or structural changes as a result of carrier concentration increases causing transition (Mott-Hubbard mechanism) [10]. Recently, this issue was taken into consideration again after more than four decades of debate with the hope that new advances in science could find the answer. Cavalleri [12] is one of the pioneers who has used ultrafast spectroscopy to investigate a time-domain between

the structural and electronic effects in VO_2. He and his colleagues created the metallic phase of VO_2 by photo-doping holes into the valence band of the low-T insulator and observed that MIT is delayed with respect to hole injection. This makes him suggest that the atomic arrangement is necessary for the formation of the metallic phase of VO_2, so that the insulator phase has bandlike character [12]. Huffman et al. [44] and Kim et al. [14] on the other hand affirms that insulating VO_2 has a Mott-Hubbard nature. This issue will certainly continue to be debated when more concrete evidences are revealed. It is also possible that the metal-insulator transition in VO_2 has a combined nature, having the features of both the Mott-Hubbard and Peierls transitions [45], [46].

2.3 Properties of vanadium dioxide

VO_2 thin-films have been prepared by numerous methods including pulsed laser deposition (PLD) [47], [48], chemical vapour deposition (CVD) [49], sputtering [50]–[53], sol-gel coating [50], [54], electron beam evaporation [55], and ion beam deposition [56]. These studies have shown that the electrical and optical properties of the film have strong dependence in the level of residual stress caused by the deposition technique. In addition, the crystalline nature of substrates also plays an important role to the structure of films [47], [53], [57], [58]. Because there are so many factors affecting the quality of film, creating a single crystal and an uniform VO_2 film is not easy. The main problem in the preparation of VO_2 film is that many other oxides such as V_2O_2, V_2O_5, etc may grow simultaneously during deposition and form mixed structures [59].

In general, when a VO_2 thin film with good quality is obtained and induced into a phase transition, the film shows a metallic nature with an abrupt decrease in electrical resistivity. This is accompanied by a dramatic decrease in optical infrared light transmittance, with smaller changes in the visible spectrum [60]. The following sections will present the basic electrical and optical properties of VO_2 thin films as well as analyze the factors that directly affect those properties.

2.3.1 Electrical properties of vanadium dioxide

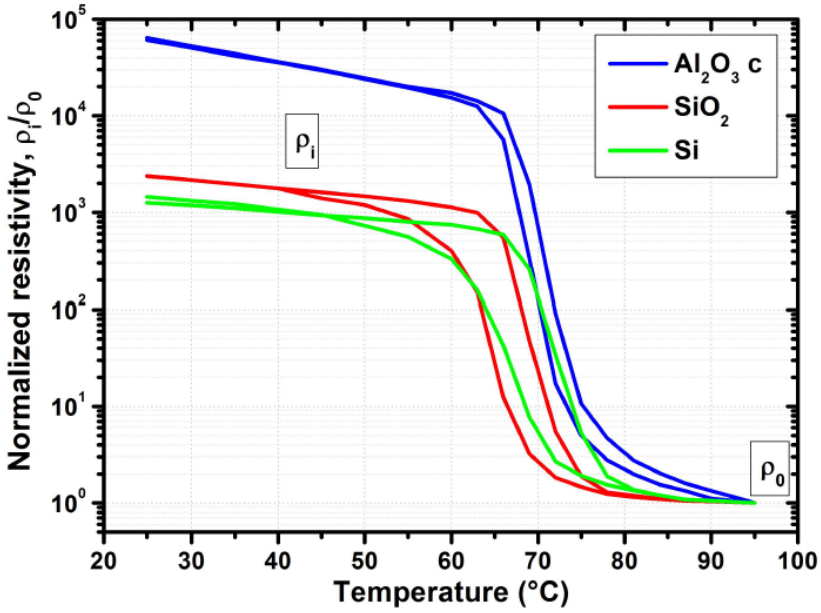

Figure 2.5: Resistivity as a function of temperature for VO_2 thin films on varying substrates (Blue: VO_2 on Al_2O_3; Red: VO_2 on SiO_2; Green: VO_2 on Si). Reproduced from ref. [57].

As discussed above, at room temperature VO_2 has monoclinic structure and possesses insulator or semiconductor properties. Hall effect measurement [61] shows that it is a n-type material with carrier density around $n_s \sim 10^{18} - 10^{19}\ cm^{-3}$ [62]. At temperatures higher than 68°C, the resistivity of VO_2 changes suddenly and decreases by up to 5 orders of magnitude, as Figure 2.5 shows. This conductivity jump is due to the change in the free carrier density ($n_m = 10^{22} - 10^{23} cm^{-1}$) while the mobility of charge carrier seems to keep constant at $0.5 - 1\ cm^2/V.s$ [63]. Experimental observations show that the properties of VO_2 will return to original states when cooled, but this process offers resistance, thereby causing a hysteresis effect. The transition temperature during the cooling cycle is always lower (by about 10°C) than the one for the heating cycle and this difference depends strongly on the grains size [53], [64], film thickness, and the film quality.

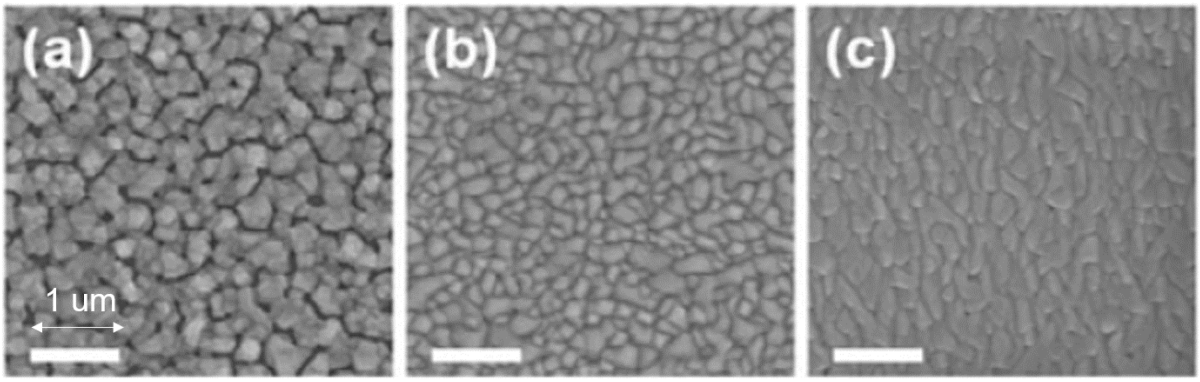

Figure 2.6: Surface morphology of 120 nm VO_2 films grown on (a) c-plane, (b) m-plane, (c) r-plane sapphire substrates. Reproduced from ref. [53].

In all VO_2 fabricating methods, the substrate role is important. The crystalline nature of substrate will determine how crystals in the thin film grow, so it greatly affects the morphology and properties of the film. For example, for VO_2 made on silicon (Si), fused silica (SiO_2) and sapphire (Al_2O_3), the films on sapphire showed the highest changes, up to five orders of magnitude, as compared with the three orders of magnitude change on the other substrates [57], Figure 2.5. The type of the substrate also has an influence on T_{MIT} and the resistivity hyteresis widths (ΔT), varying all figures by a few ^oC. Furthermore, thin films formed on the same type of sapphire material but on different crystallographic orientations also have difference in properties. Figure 2.6 shows the crystalline morphology of VO_2 film grown on c-, r-, and m-plane sapphire substrates under identical fabrication conditions; in all films the nano-grain size vary with the substrate orientation [53]. The VO_2 film on the c-plane substrate has many voids in the structure which makes film semi-continuous. In constrast, the size of grains in m-plane and r- plane samples are smaller and are connected together by a uniform plane which exhibits a continuous film. Resistivity vs temperature characteristics also indicate the T_{MIT} of samples on m- and r-planes are reduced by several degrees compared to that of samples on c-plane. Reference [65] also reported a reduction in T_{MIT} down to 45^oC (318 K) for reactively sputtered VO_2 films deposited on sapphire

(0001) substrates. These results suggested that the lattice mismatch between the film and substrate affects on the stress along the c-axis of film and causes the change in $T_{MIT.}$

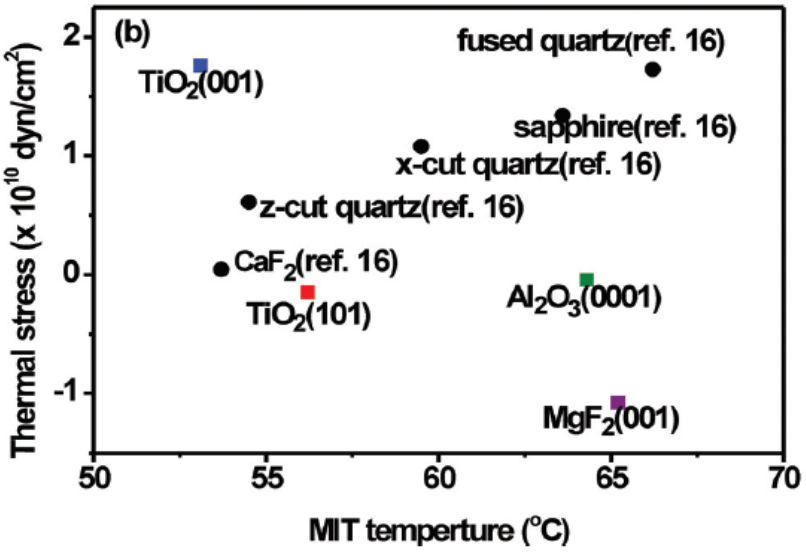

Figure 2.7: Calculated thermal stress vs metal-insulator transition temperature for VO_2 films on different substrates. Reproduced from ref. [58].

Among many substrates such as fused quartz, sapphire, MgF_2, CaF_2, TiO_2 which have been tested to optimize the properties of VO_2 film, TiO_2 (001) is rated highest because of strong enhanced oxidation durability [58], [66]. In addition, the VO_2 films grown on TiO_2 (001) surface have their c-axis perpendicular to the plan of the substrate with the minimum distance V^{4+}-V^{4+} [47]. This reduction in length between vanadium atoms affects directly the overlap of the d orbitals as analyzed in the energy structure of the material. It expands the width of the d band and helps transform the material into metallic phase easier. Thus, VO_2 films formed on the TiO_2 (001) have a lower T_{MIT} than that of the bulk material [47], [58], as shown in Figure 2.7.

Another factor that greatly influences the electrical properties of VO_2 films is carrier concentration. As known from Mott's theory discussed in section 2.1 , when the free electron concentration in VO_2 increases to the certain level, the insulator-metal transition will occur. Thus, by injecting more carriers into VO_2 film we can shift the T_{MIT} of material either towards a higher

temperature or towards a lower temperature. For example, at 2% W donor doping in VO_2, the material increases room temperature carrier concentration and its transition temperature has reduced from 68°C to 25°C [67].

2.3.2 Optical properties of vanadium dioxide

Similar to the electrical properties, the optical properties of VO_2 also vary depending on the metal or semiconductor properties of the material. Figure 2.8 is the typical transmittance of the VO_2 thin films in the UV-vis-IR region at different temperatures from 20°C to 85°C. The transmission intensity in the visible range of 200-650 nm is almost independent of the phase of VO_2, while the gap between the transmittances at 20°C and 87°C increases with longer wavelengths. Most of the light at 1500 nm can not pass through the VO_2 thin film at temperatures higher than the T_{MIT} and the change in transmission at this wavelength reaches 45%.

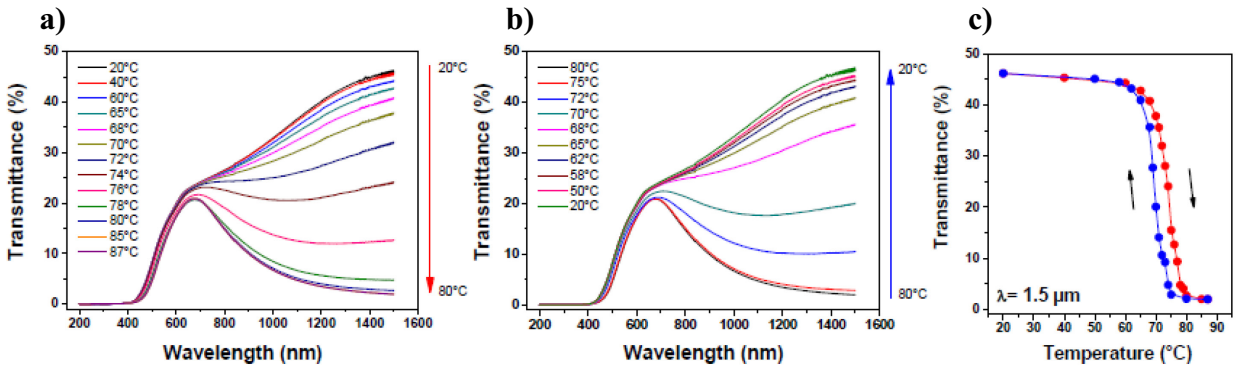

Figure 2.8: Transmission as a function of temperature for light from 200 nm to 1600 nm through a 100-nm thick VO_2 film during (a) heating cycle, (b) cooling cycle, and (c) the hysteresis cycle at λ=1500 nm. Reproduced from ref. [57].

2.4 Optical activation of VO_2

Electron-phonon interactions and structural changes during phase transition in VO_2 occur at a short time scale. Thus, to better understand the MIT dynamics, we need to excite and probe MIT states as fast as possible. The best way to do this is using a femtosecond laser to activate

phase transition and characterize either the electronic or crystallographic structure of VO_2 at different states. Roach and Balberg [68] were the first to observe the photoinduced phase transition (PIPT) in VO_2 by using optical excitation. They showed that VO_2 changes its dielectric and exhibits a metal-like state after 20 ns of interacting with a pulsed laser. These results promised that with improving time resolution in time-resolved spectral measurement, the mystery in the driving mechanism of the MIT phase transition would be unraveled. Indeed, measurements in photoemission, Raman spectroscopy and diffraction techniques were used extensively during the last decade to study either the electronic or the crystallographic structure and achieved considerable progress. In recent years, the techniques of characterizing the combination of both structural and electronic properties of VO_2 have gained a lot of attention. Many important discoveries have been made that help us understand better the mechanisms of electrons, ions and lattices during the phase transition. Basically, the structural transformation from monoclinic (insulator) to rutile (metal) during the photoexcited phase transition in VO_2 must go through the series of processes described in Figure 2.9. This mechanism is drawn from many studies and is widely accepted, but some details remain controversial.

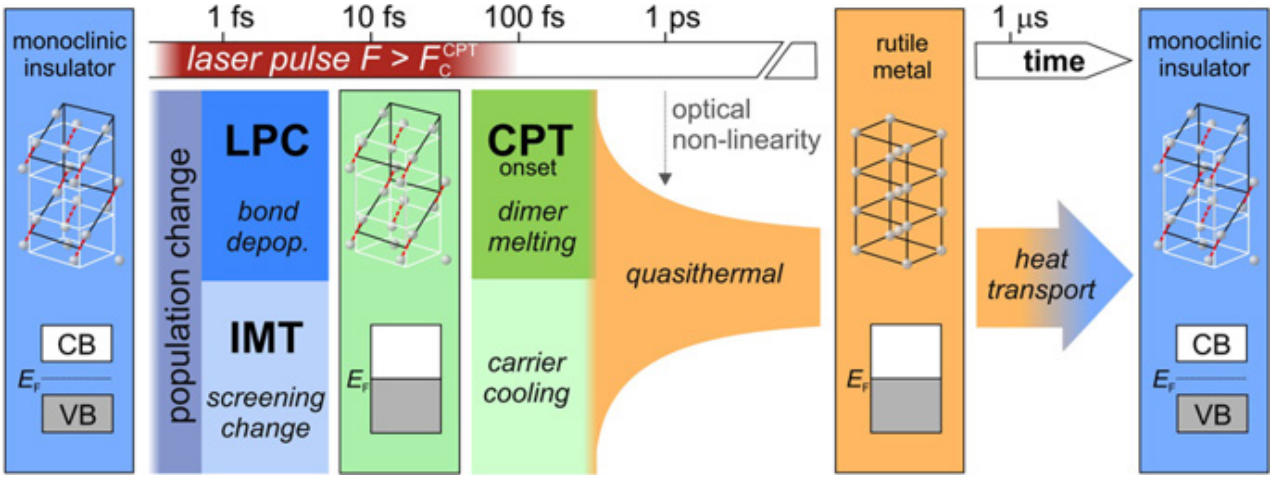

Figure 2.9: Timescales of optically-induced MIT in VO_2. Reproduced from ref. [69].

At low-temperature equilibrium phase, VO_2 owns monoclinic structure and is insulating with the energy gap around 0.7eV between the valence and conduction bands. When excited by above a certain critical fluence, the population of electronic states in VO_2 changes instantly that creates a highly non-equilibrium plasma and changes the screening of the Coulomb interaction. The insulating band gap is collapsed and the VO_2 has metal-like optical responses. This non-thermal MIT process and lattice potential change (LPC) occur instantaneously (i.e. femtosecond time scale) with the photoexcitation. However, the crystal structure of VO_2 remains the same, monoclinic. But this structure in new lattice potential is extremely unstable. The new charge distribution changes the forces that push all the ions toward the new stable positions and leading to rutile arrangement, as shown in Figure 2.10. This crystallographic phase transition (CPT) process takes place within a few hundred fs and involves many complex pathways and multitude of ionic motions. At the excited state, the excess energy of electrons and holes is transferred to the lattice and brings the subsystems into thermal equilibrium. Then the whole system is cooled down due to heat transport through the substrate and recovers its monoclinic state at low-temperature phase. This relaxation process is slower and often takes place in several nanoseconds to few hundred microseconds depending on the characteristics of the VO_2 thin film and the substrate. This issue will be discussed in more details in Chapter 8.

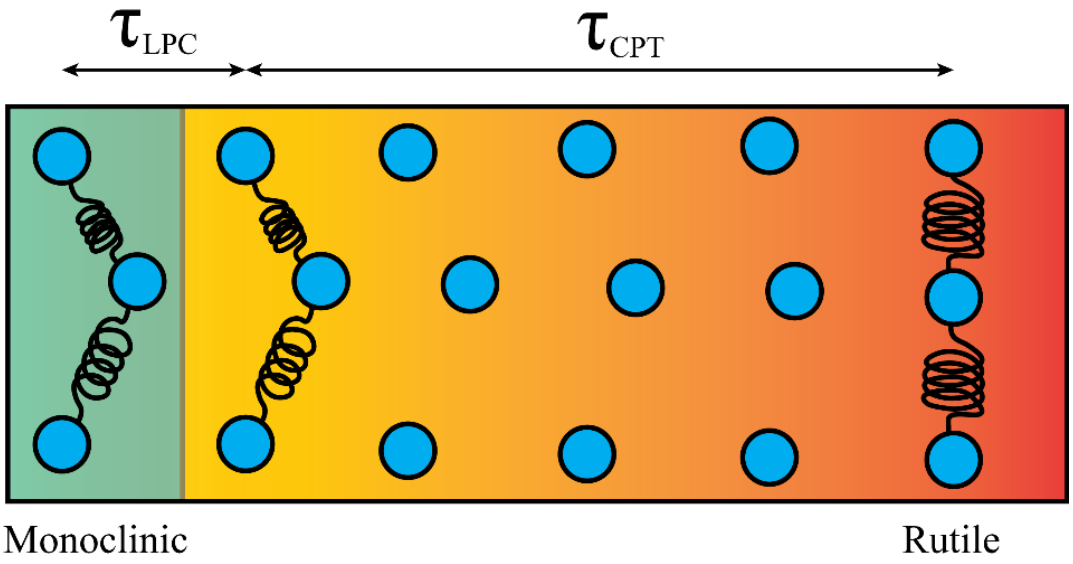

Figure 2.10: Structural change from monoclinic to rutile during the photoexcited phase transition in VO_2.

The above-discussed dynamics of the PIPT occur only for sufficiently high values of the photoexcited fluence $F > F_C^{CPT}$. In the limit of weak pump pulses, below a threshold value F_C^{IMT}, the change in measured reflectivity did not last long and quickly returned to its original value. This is due to the fact that the number of electron-hole excitations created by photoexcitation is not high enough to induce a lattice deformation. Excited electrons from the conduction decay quickly to the valence band of the monoclinic structure and restore the original state.

The MIT mechanism is more complex for intermediate values of the fluence $F_C^{MIT} < F < F_C^{CPT}$. In this case, the pump pulse creates enough electron-hole excitations to trigger the coherent structural deformation. However this intensity is not strong enough to transform the whole sample lattice from monoclinic to rutile. Initially, optical pumping induces small domains in the sample to change their structure to rutile. This procees happens very fast, on the subpicosecond time scale. Next, these metallic seeds stimulate the surrouding monoclinic areas and drive them to the rutile phase, as well. It takes a longer time, from few picoseconds to few hundred picoseconds for all the

domains to complete this process. Finally, the separated rutile regions are formed in the sea of insulating monoclinic phase [70], [71]. This phase transition formation explains why the observed reflectivity keeps increasing on the time scales of the order of tens of picoseconds [70]. The experimental results in Figure 2.11 regarding the probe reflection over time under different photoexcited fluence represent the above analysis. At 14.9 mJ/cm^2 pump intensity, the reflection increases sharply in less than 1ps after photoexcitation, and then the reflection rises gradually up to 50 ps, achieving the maximum reflection change.

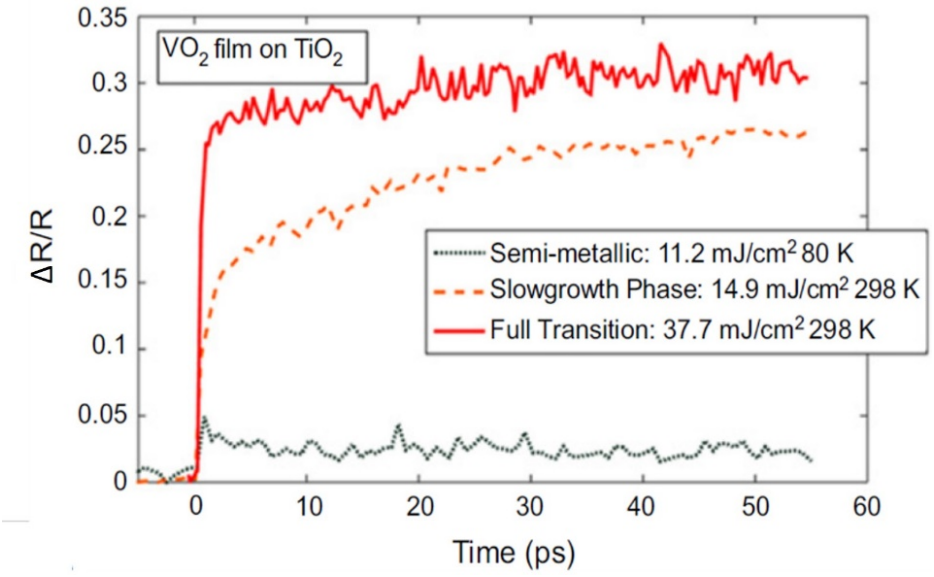

Figure 2.11: Changes in the probe reflection over time under different photoexcited fluences 11.2 mJ/cm^2, 14.9 mJ/cm^2, and 37.7 mJ/cm^2 measured for VO_2 on TiO_2 at a temperature well below the phase transition temperature. Reproduced from ref. [70].

The above analysis has shown the importance of photoexcited fluence on the MIT mechanism in VO_2. At different intensity, the pump beam will create different effects on the whole phase transition process. To investigate this problem, Cavalleri et al. [72] excited the VO_2 sample using 1.55 eV pulses from the amplifier laser and monitored the conductivity change as a function of the optical pump fluence at 300K. At the maximum tested fluence 19.1 mJ/cm^2, the VO_2 thin film transforms its phase completely from insulator to metal at long times, Figure 2.12(a). This

was verified carefully by comparing the conductivity changes in both the optical and thermal activation cases. The maximum obtained induced conductivity decreases with decreasing fluence and reaches zero (extrapolation) at the fluence of ~ 7mJ/cm^2, as in Figure 2.12(b). This value is considered as the photoexcited fluence threshold for VO_2 sample at 300K. Besides the study of Cavalleri et al., there are many other studies of fluence threshold for VO_2 thin film. Generally, this value varies depending on the properties of VO_2 thin films [73], temperature of substrate [70], [72], excited wavelength [74], or pressure on the surface of the sample [74].

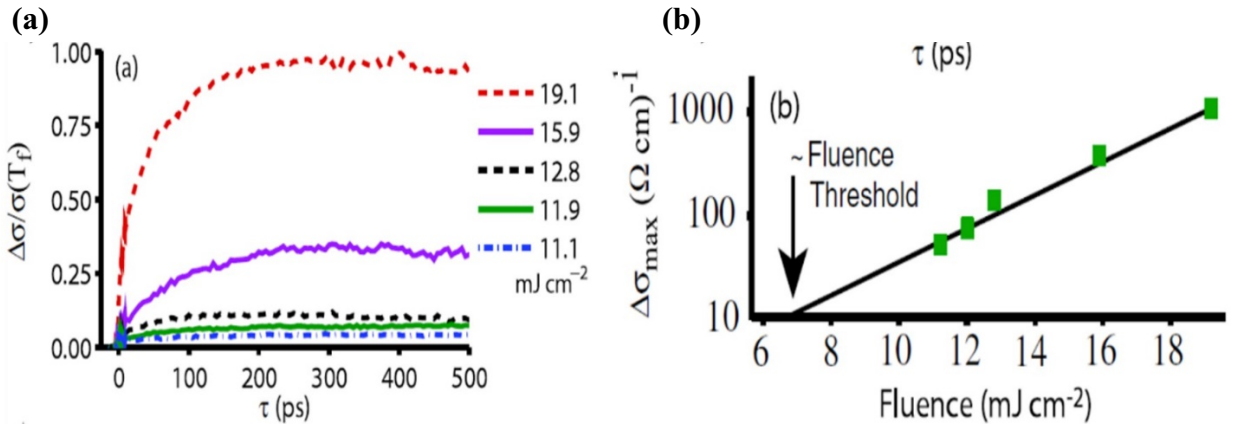

Figure 2.12: (a) The conductivity changes over time under different photoexcited fluences, (b) The maximum conductivity changes versus photoexcited fluence. Reproduced from ref. [72].

2.5 Vanadium dioxide applications

With the ability to change the properties rapidly under various stimuli such as temperature, electric field, pressure or pulsed laser, and the transition temperature can be customized to almost any desired temperature, vanadium dioxide has been considered for a wide variety of applications. In the following sections, I will describe some of the promising applications in using VO_2 to create electrical and optical switches. In addition, VO_2 thin films coated on glasses for smart windows are highly appreciated in saving the energy comsumption of building. This also will be discussed in details with the evaluations of the potential and the obstacles that need to be overcome.

2.5.1 Electro-optical switch

Soltani et al. [3] fabricated $VO_2/TiO_2/ITO/glass$ structure by reactive pulsed laser deposition for optical switch test, Figure 2.13. In this device, TiO_2 film is very thin and was used as a buffer layer to enhance the properties of the 200 nm VO_2 layer on the top while indium tin oxide (ITO) was used as transparent positive electrode at the bottom. The external DC voltage was applied between ITO and VO_2 electrodes with different values from 0 to 20V. The whole device was probed by 1.55 μm wavelength laser which was verified to be easily transmitted via TiO_2 layer. The reflectance and transmittance were measured as a function of voltage applied to the whole structure. The transmittance decreases while the reflectance increases as the applied voltage increases and both change abruptly at around 11.5 V. At this value, the insulator-metal transition in VO_2 occurs, resulting in significant change in reflectance (5 dB) and transmittance (12 dB). The simple structure acts as an optical switch between two states ON (insulator) and OFF (metal) without needing any moving parts and can work at fast speed at a few nanoseconds [75].

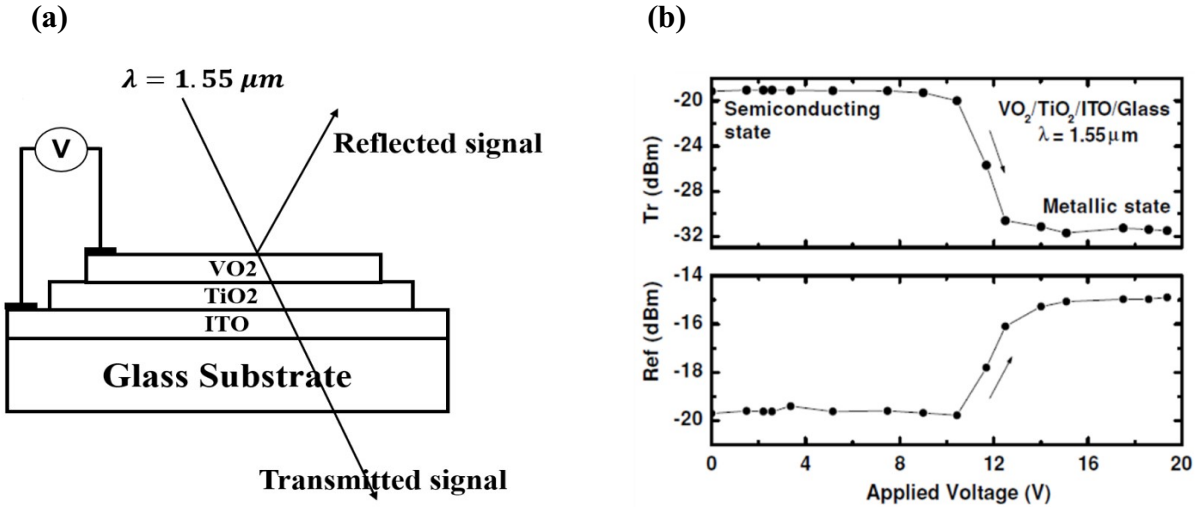

Figure 2.13: (a) The VO_2 electro-optical switch structure, (b) The transmittance and reflectance of λ=1.55 μm at different voltages applied to the whole electro-optical structure. Reproduced from ref. [3].

2.5.2 Smart coating for windows

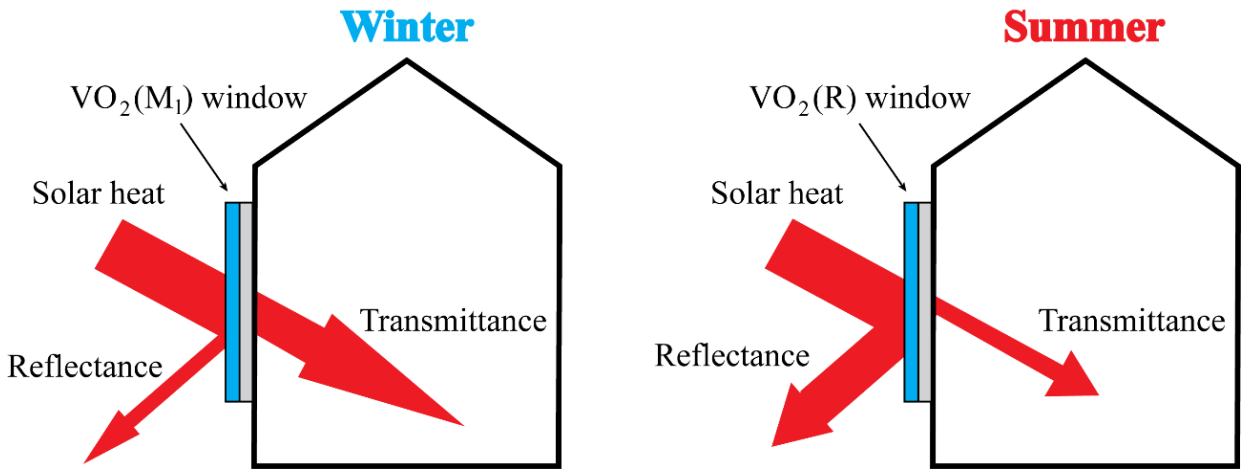

Figure 2.14: The VO_2 windows allow more light to enter in the room in winter and less light to enter in the room in summer to balance temperature.

The use of lighting, air-conditioning, and heating in buildings cost a lot energy and emit hamful gases to environment. Therefore, finding an effective way to cut down the energy consumption of buildings is an urgent demand. One possible approach is to control the amount of light entering buildings. For example, when the room temperature is low, windows can allow more light to enter the room to warm it up and balance the light when the temperature reaches the comfortable temperature, Figure 2.14. This can be done by coating VO_2 film on windows. Based on the ability to transform phase from semiconductor (more light goes through) to metal (less light goes throught) and the transition temperature can be changed to the desired temperature, VO_2 is believed to contribute positively to reducing energy consumption for buildings. However, to commercialize VO_2 thin films as smart coatings for energy efficient windows, the following issue need to be addressed thoroughly.

- The phase transition temperature for pure VO_2 (68^{o}C) is high. It needs to be reduced to 30^{o}C – 40^{o}C without effecting abilities to block or allow light go through.

- The transmission variation in VO_2 is predominantly in the near-infrared region which only accounts for about 43% of the solar spectrum at the Earth's surface. We need to improve VO_2 film properties or use multilayer structures to cover all the solar spectrum.
- VO_2 will transform into the V_2O_5 phase in the real enviroment, which is the most stable phase of vanadium oxide but does not possess the thermochromic property [76]. Therefore, it is necessary to improve the durability of VO_2 in the environment if we want to use it as smart coating for windows.

CHAPTER 3

Polarization state of light interacting with thin films

3.1 Polarization states of light

Light is a electromagnetic consisting of an electric $\vec{E}$ and a magnetic $\vec{B}$ components. The electric field and magnetic field amplitudes are represented by wavefunctions with harmonic time dependence:

$$E = E_o e^{i(kz-\omega t+\varphi)} \tag{3.1}$$

$$B = B_o e^{i(kz-\omega t+\varphi)} \tag{3.2}$$

where E_o, B_o, ω, φ, k are amplitudes of electric and magnetic fields, angular frequency, initial phase of wave and wave number, respectively. If a wave has oscillations taking place in a specific direction, we call it polarized light. All normal light sources such as the sun or a filament lamp emit light as a result of random processes taking place in atoms of those objects. As a result, electromagnetic waves coming from these objects have oscillations in random directions and they are considered as unpolarized light. Polarized light can be produced by passing unpolarized light through a polarizer.

Let's consider a monochromatic plane wave travelling in the z direction, its electric field lies in the x-y plane and is generally described by two orthogonal wave functions in x-axis and y-axis.

$$\vec{E}_x(z,t) = \hat{\boldsymbol{x}} E_{ox}\cos(kz - \omega t + \varphi_x) \tag{3.3}$$

$$\vec{E}_y(z,t) = \hat{\boldsymbol{y}} E_{oy}\cos(kz - \omega t + \varphi_y) \tag{3.4}$$

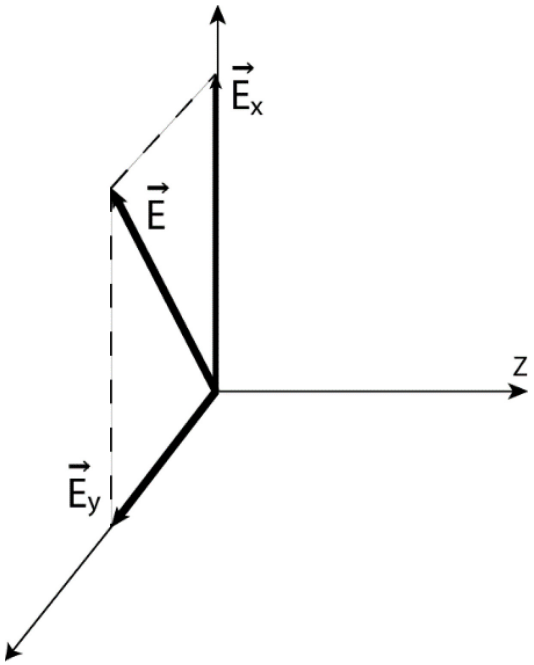

Figure 3.1: A plan wave $\vec{E}$ travels in the z direction of Cartesian coodinates and its projection on the ox and oy axes.

where $\hat{\boldsymbol{x}}$, $\hat{\boldsymbol{y}}$ are unit vectors in x and y directions and φ_x, φ_y are the initial phases of $\vec{E}_x(z,t)$ and $\vec{E}_y(z,t)$. The phase difference between the two waves is defined by:

$$\delta = \varphi_y - \varphi_x \tag{3.5}$$

The general expression for an electric field of a plane wave propagating along z axis is:

$$\vec{E}(z,t) = \overrightarrow{E_x}(z,t) + \overrightarrow{E_y}(z,t) \tag{3.6}$$

With some rearrangement, Eq. 3.5 and Eq. 3.6 can be put together in the form of:

$$\left(\frac{E_x}{E_{ox}}\right)^2 + \left(\frac{E_y}{E_{oy}}\right)^2 - 2\frac{E_x}{E_{ox}}.\frac{E_y}{E_{oy}}cos\delta = sin^2\delta \tag{3.7}$$

Eq. 3.7 represents an ellipse with axes E_x and E_y as shown in Figure 3.1. The major (minor) axis of the ellipse making an angle of α with E_x (E_y) is given by:

$$tan2\alpha = \frac{2E_{ox}E_{oy}cos\delta}{E_{ox}^2 - E_{oy}^2} \tag{3.8}$$

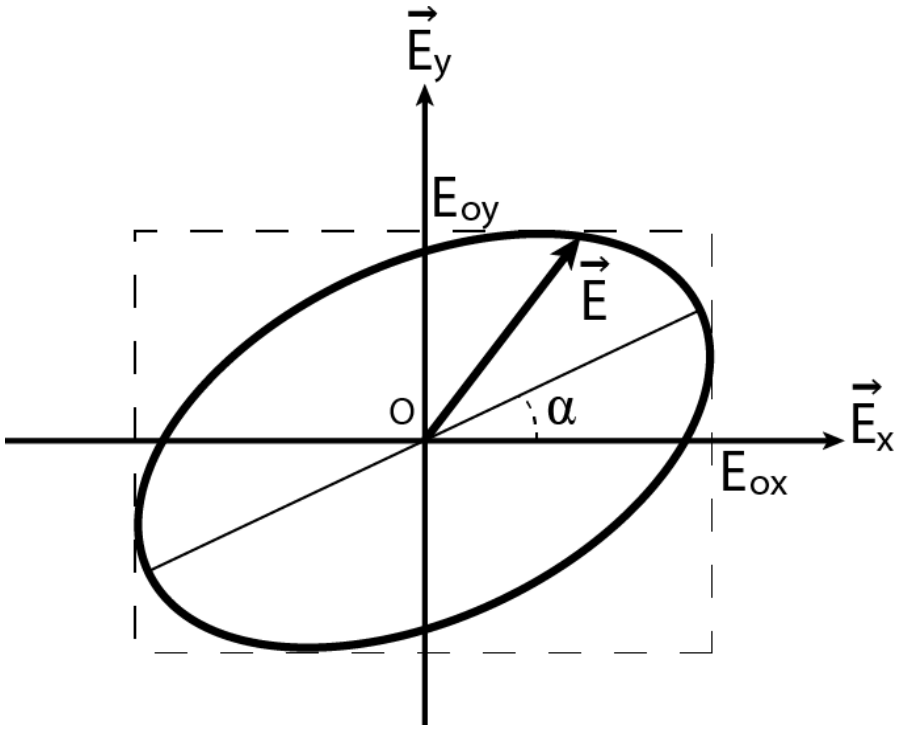

Figure 3.2: The tip of vector $\vec{E}$ moves in an ellipse in the xy-plane as the vector travels along the oz axis.

The state of polarization is specified by the ratio of the electric field amplitude components $\frac{E_{oy}}{E_{ox}}$ and the phase difference δ.

- **Linearly polarized light**

If the phase difference is $\delta = n\pi$ with $n = 0, \pm 1, \pm 2$ ..., Eq. 3.7 becomes:

$$E_y = \pm\left(\frac{E_{oy}}{E_{ox}}\right) E_x \tag{3.9}$$

This is an equation of a straight line with a slope of $\pm\frac{E_{oy}}{E_{ox}}$. In this case, the electric field of light is confined to a single plane along the direction of propagation. This state of polarization depicts a linealy polarized light.

- **Circularly polarized light**

If $\delta = \pm\frac{\pi}{2} + n\pi$ and $E_x = E_y = \frac{1}{\sqrt{2}}E_o$, Eq. 3.7 becomes

$$E_x^2 + E_y^2 = E_o^2 \tag{3.10}$$

The results is an equation for a cirle. In this case, the electric field rotates in a cirle around the direction of propagation. Also, with $\delta = \frac{\pi}{2}$ and a fixed position z, the electric field rotates in a clockwise direction when viewed towards the direction of propagation. This light is right-handed circularly polarized. The case $\delta = -\frac{\pi}{2}$ corresponds to counterclockwise rotation and is said to be left-handed circularly polarized light.

In the general case, the intensity of electromagnetic $\vec{E}$ is determined by:

$$I = |E|^2 \tag{3.11}$$

3.2 Interaction between polarized light at interfaces and thin films

When light at a single frequency strikes a thin film sample, this light can be absorbed, reflected, scattered or transmitted through the sample depending on the interaction between the light and the material, as seen in Figure 3.3. Normally, the total loss due to absorption and scattering is defined as κ, the extinction coefficient of medium, that sometimes is referred to as the opacity.

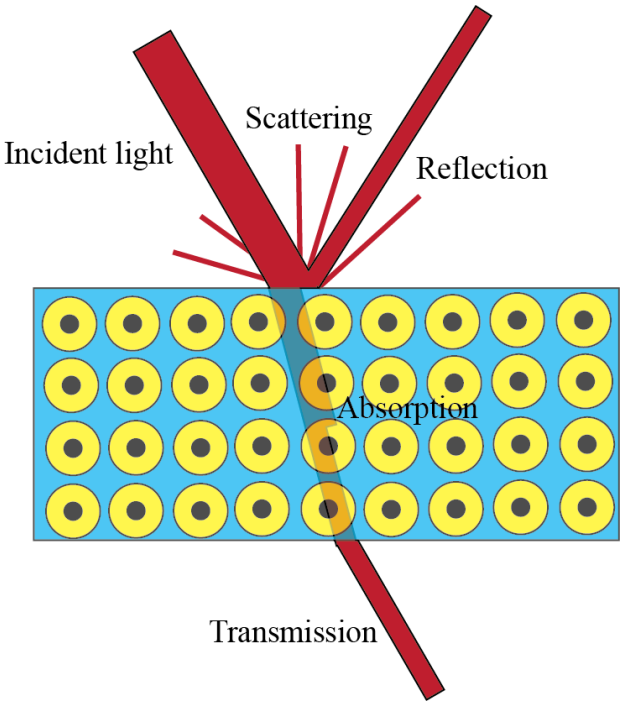

Figure 3.3: Absorption, reflection, transmission and scattering mechanisms.

In calculation, the optical properties of material are often expressed through the complex refractive index:

$$N = n + i\kappa \tag{3.12}$$

where n is the real part of complex refractive index. By replacing $k = \frac{2\pi N}{\lambda} = \frac{2\pi(n+i\kappa)}{\lambda}$ in Eq. 3.1, where λ is the wavelength of light in vacuum, we obtain:

$$\begin{aligned} E &= E_o e^{i\left(\frac{2\pi N}{\lambda}z-\omega t+\varphi\right)} = E_o e^{i\left(\frac{2\pi}{\lambda}(n+i\kappa)z-\omega t+\varphi\right)} \\ &= E_o e^{-\frac{2\pi\kappa}{\lambda}z} e^{i\left(\frac{2\pi n}{\lambda}z-\omega t+\varphi\right)} \end{aligned} \tag{3.13}$$

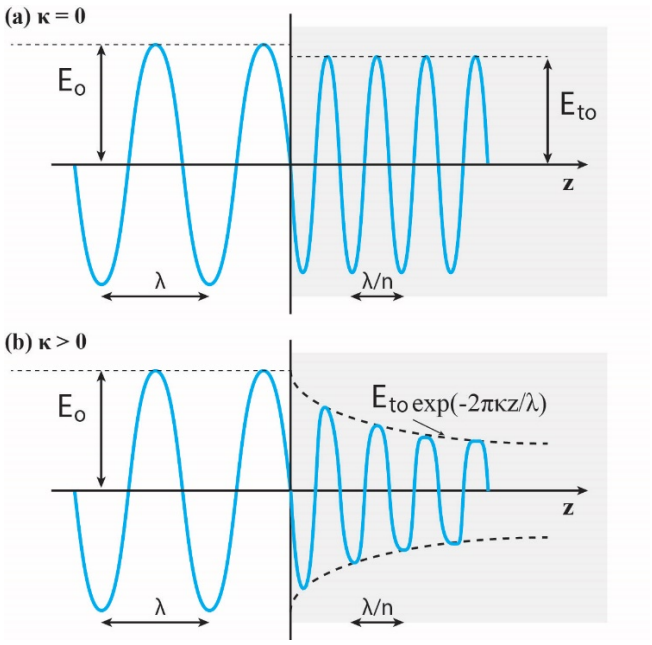

Figure 3.4: Propagating waves in (a) non-absorbing, (b) absorbing media.

Figure 3.4 describes a wave propagating through a non-absorbing medium (a) and an absorbing medium (b). We can see that the wavelength of light in the absorbing and non-absorbing medium is reduced n times. Thus, the absorption of light does not affect the wavelength transmitted in the medium. However, when absorption occurs, the amplitude of the electromagnetic wave decreases exponentially with increasing distance in the direction of propagation.

3.2.1 Reflection and refraction at interface

When a beam of light hits a planar interface between two homogeneous dielectric media with permittivity ϵ_1 and ϵ_2 and permeability μ_1 and μ_2, as illustrated in Figure 3.5, all boundary conditions for field components perpendicular ($\perp$) and parallel ($\parallel$) to the interface plane have to satisfy Maxwell equations. These conditions are expressed by:

$$\epsilon_1 E_1^{\perp} = \epsilon_2 E_2^{\perp} \tag{3.14}$$

$$B_1^{\perp} = B_2^{\perp} \tag{3.15}$$

$$E_1^{\parallel} = E_2^{\parallel} \tag{3.16}$$

$$B_1^{\parallel}/\mu_1 = B_2^{\parallel}/\mu_2 \tag{3.17}$$

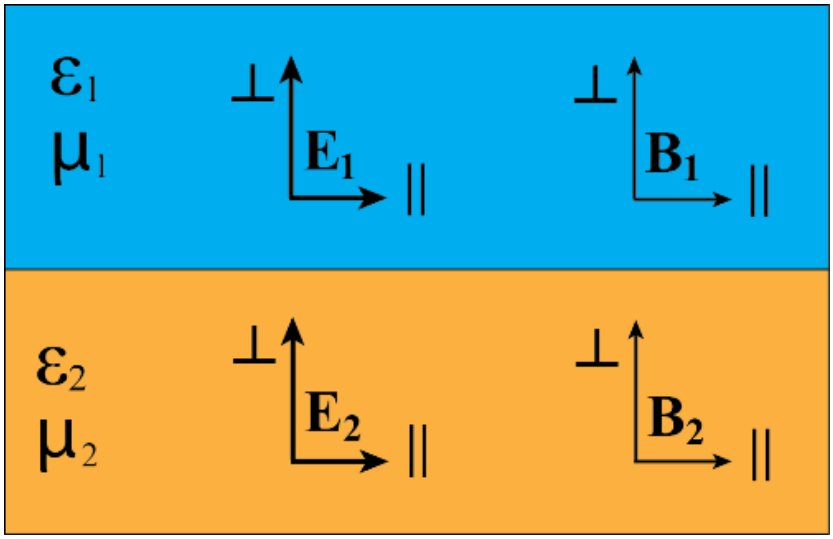

Figure 3.5: Field components at an interface between two homogeneous dielectric media.

Let's suppose that we have non-magnetic materials $\mu_1 = \mu_2 = 1$ so that Eq. 3.17 can be simplified to

$$B_1^{\parallel} = B_2^{\parallel} \tag{3.18}$$

As mentioned before, reflection and refraction depend on the state of polarization. For better understanding and calculations, we divide the electric field of the electromagnetic wave into two orthogonal electric fields. The p-polarized light has the electric field oriented parallel to the plane of incidence and the s-polarized light has the electric field oriented perpendicular to this plane (Figures 3.6 and 3.7).

Now we apply Eq. 3.16 and Eq. 3.18 to transform all boundary conditions for electromagnetic waves at the interface in terms of s- and p- components.

s-polarized light

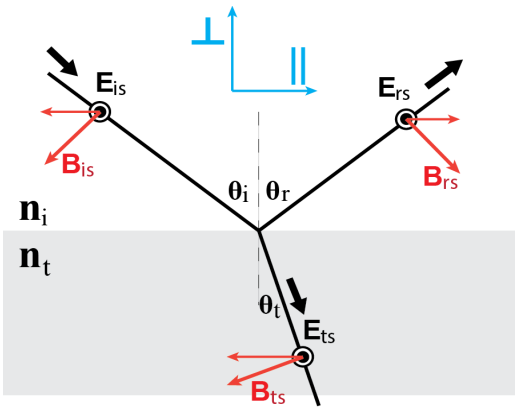

Figure 3.6: Reflection and refraction of a s-polarized light at an interface between two media.

From Eq. 3.16

$$-E_{is} + E_{rs} = E_{ts} \quad (3.19)$$

From Eq. 3.18

$$-B_{is}cos\theta_i + B_{rs}cos\theta_r = -B_{ts}cos\theta_t \quad (3.20)$$

p-polarized light

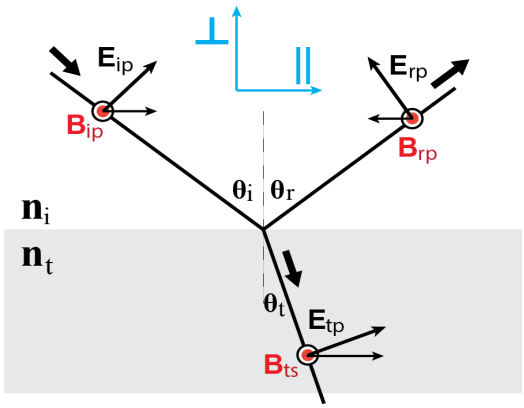

Figure 3.7: Reflection and refraction of a p-polarized light at an interface between two media.

From Eq. 3.16

$$E_{ip}cos\theta_i - E_{rp}cos\theta_r = E_{tp}cos\theta_t \quad (3.21)$$

From Eq. 3.18

$$B_{ip} + B_{rp} = B_{tp} \quad (3.22)$$

where subscripts is, rs, ts, ip, rp, tp denote the incident, reflected and refracted components for s- and p- polarized light, respectively. As shown in Figures 3.6 and 3.7, the angles of reflection θ_r and incidence θ_i must be equal, $\theta_i = \theta_r$. The angles of incidence and refraction must satisfy Snell's law:

$$n_i sin\theta_i = n_t sin\theta_t \quad (3.23)$$

With n_i and n_t are the complex refractive indices of two dielectric media, now n means N in Eq. 3.12. By solving the Eq. 3.23 above with the boundary conditions and the relationship between amplitudes of electric and magnetic field $E = \frac{c}{n}B$, we get

$$r_{it,s} = \frac{E_{rs}}{E_{is}} = \frac{n_i cos\theta_i - n_t cos\theta_t}{n_i cos\theta_i + n_t cos\theta_t} \tag{3.24}$$

$$t_{it,s} = \frac{E_{ts}}{E_{is}} = \frac{2n_i cos\theta_i}{n_i cos\theta_i + n_t cos\theta_t} = 1 + r_s \tag{3.25}$$

$$r_{it,p} = \frac{E_{rp}}{E_{ip}} = \frac{n_t cos\theta_i - n_i cos\theta_t}{n_t cos\theta_i + n_i cos\theta_t} \tag{3.26}$$

$$t_{it,p} = \frac{E_{tp}}{E_{ip}} = \frac{2n_i cos\theta_i}{n_t cos\theta_i + n_i cos\theta_t} = \frac{n_i}{n_t}(1 + r_p) \tag{3.27}$$

From Eq. 3.23 =>

$$\cos\theta_t = [1 - sin^2\theta_t]^{1/2} = \left[1 - \left(\frac{n_i}{n_t}\right) sin^2\theta_i \right]^{1/2} \tag{3.28}$$

Since the value in parentheses can be negative, in general, all reflection and refraction coefficients are complex, as well as angles.

3.3 Phase shifts and polarization changes by thin films

Let's consider a thin film with a complex refractive index n_2 and a thickness d on a thick substrate characterized by a complex refractive index n_3, both located in medium n_1, as shown in Figure 3.8. The incident wave strikes the thin film creating many reflected and transmitted beams. These have different phases and amplitudes. All reflected beams will interfere to create the total reflection. Similarly, the combination of all transmitted rays will form the total transmission.

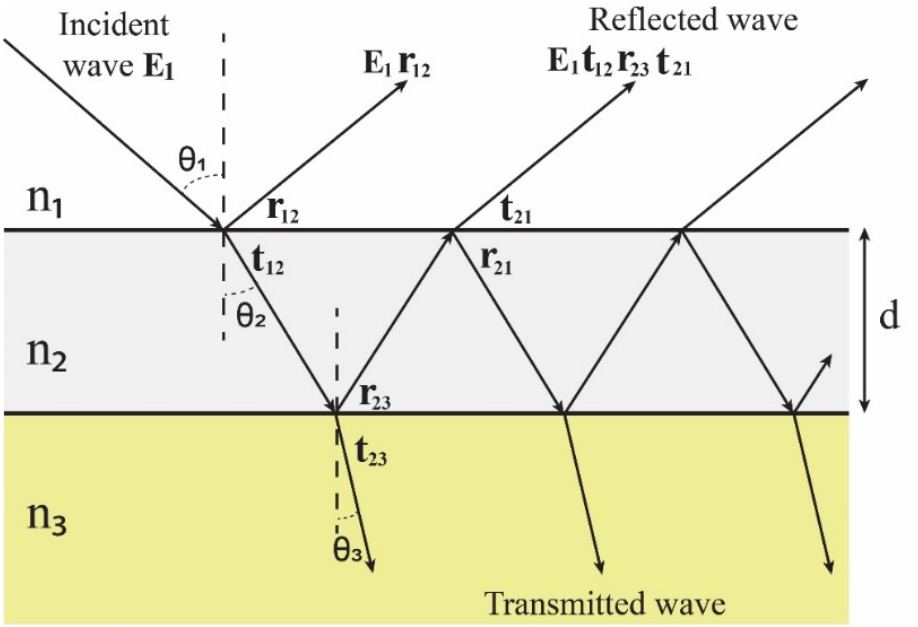

Figure 3.8: Reflection and refraction of a light on a thin film sample.

In Figure 3.8, the ratio between the two nearest reflected wave amplitudes is $r_{21}r_{23}$ and their phases shift an amount β based on the optical path difference. In general, the l[th] reflected wave can be expressed by

$$E_1 t_{12} r_{23} (r_{21} r_{23})^{l-2} t_{21} e^{-i(l-1)\beta} = E_1 t_{12} r_{23} t_{21} e^{-i\beta} \left(r_{21} r_{23} e^{-i\beta}\right)^{l-2} \tag{3.29}$$

So the total reflected wave is calculated with:

$$\begin{aligned} E_{123}^r &= E_1 r_{12} + E_1 t_{12} r_{23} t_{21} e^{-i\beta} + E_1 t_{12} r_{23} (r_{21} r_{23}) t_{21} e^{-i2\beta} + \cdots \\ &= E_1 \left(r_{12} + t_{12} r_{23} t_{21} e^{-i\beta} \sum_{l=2}^{\infty} \left(r_{21} r_{23} e^{-i\beta}\right)^{l-2} \right) \end{aligned} \tag{3.30}$$

Because we always have $\sum_{n=1}^{\infty} x^n = \frac{1}{1-x}$, the total reflected wave can be simplified to

$$E_{123}^r = E_1 \left(r_{12} + \frac{t_{12} r_{23} t_{21} e^{-i\beta}}{1 - r_{21} r_{23} e^{-i\beta}} \right) \tag{3.31}$$

In a similar way, any two of the nearest transmitted waves also differ by an amount of β in phase. The total transmitted wave through the thin film is calculated as

$$E_{123}^{t} = E_1 t_{12} t_{23} + E_1 t_{12} r_{23} r_{21} t_{23} e^{-i\frac{\beta}{2}} + E_1 t_{12} (r_{21} r_{23})^2 t_{23} e^{-i\left(\frac{\beta}{2}+\beta\right)} + \cdots$$

$$= E_1 \left(\frac{t_{12} t_{23} e^{-i\frac{\beta}{2}}}{1 - r_{21} r_{23} e^{-i\beta}} \right) \tag{3.32}$$

From Fresnel's equations at interface (See Eqs. 3.24, 3.25, 3.26, 3.27) we have the relationships $t_{12}t_{21} = 1 - r_{12}^2$ and $r_{21} = -r_{12}$. So the reflection and transmission coefficients in Eq. 3.31 and Eq. 3.32 can be simplified to:

$$r_{123} = \frac{E_{123}^{r}}{E_1} = \frac{r_{12} + r_{23} e^{-i\beta}}{1 + r_{12} r_{23} e^{-i\beta}} \tag{3.33}$$

$$t_{123} = \frac{t_{12} t_{23} e^{-i\frac{\beta}{2}}}{1 + r_{12} r_{23} e^{-i\beta}} \tag{3.34}$$

The phase difference β can be calculated based on Figure 3.9.

$$\beta = \frac{2\pi n_2}{\lambda} (\overline{AB} + \overline{BC}) - \frac{2\pi n_1}{\lambda} \overline{AD} \tag{3.35}$$

Replacing $\overline{AD} = \overline{AC} sin\theta_1 = 2dtan\theta_2 sin\theta_1 = 2d \frac{sin^2\theta_2}{cos\theta_2} \frac{n_2}{n_1}$, and

$\overline{AB} = \overline{BC} = {}^{d}/_{cos\theta_2}$, we get

$$\beta = \frac{4\pi d n_2}{\lambda} cos\theta_2 = \frac{4\pi d}{\lambda} \sqrt{n_2^2 - n_1^2 sin^2\theta_1} \tag{3.36}$$

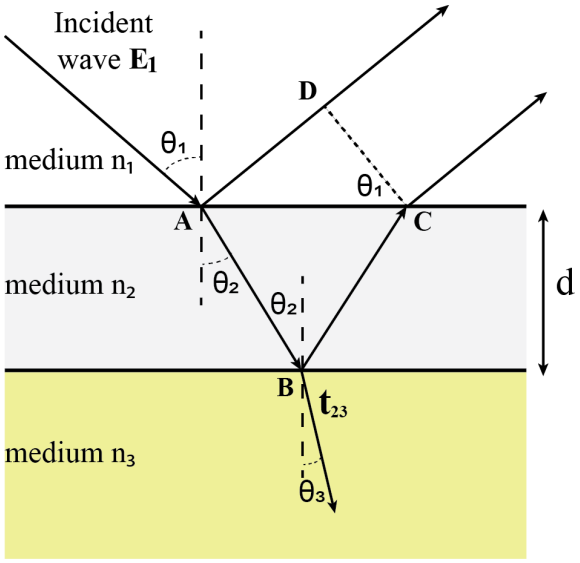

Figure 3.9: Optical path difference between two nearest reflected light.

In general, the reflection and transmission coefficients for a thin film are function of the light wavelength λ in vacuum, the thickness of film d, the complex refractive indices of all media n_1, n_2, n_3, and the incidence angle θ_1. Table 3.1 summaries all the reflection and transmission coefficients for s- and p- polarized light. They are used often in all our calculations later.

Table 3.1: Reflection and transmission coefficients for s- and p-polarized light interacting with a thin film.

S-polarized light	**P-polarized light**
$r_s = r_{123,s} = \dfrac{r_{12,s} + r_{23,s}e^{-i\beta}}{1 + r_{12,s}r_{23,s}e^{-i\beta}}$ (3.37)	$r_p = r_{123,p} = \dfrac{r_{12,p} + r_{23,p}e^{-i\beta}}{1 + r_{12,p}r_{23,p}e^{-i\beta}}$ (3.39)
$t_s = t_{123,s} = \dfrac{t_{12,s}t_{23,s}e^{-i\frac{\beta}{2}}}{1 + r_{12,s}r_{23,s}e^{-i\beta}}$ (3.38)	$t_p = t_{123,p} = \dfrac{t_{12,p}t_{23,p}e^{-i\frac{\beta}{2}}}{1 + r_{12,p}r_{23,p}e^{-i\beta}}$ (3.40)

with $\beta = \frac{4\pi d}{\lambda}\sqrt{n_2^2 - n_1^2 sin^2\theta_1}$

In this thesis, VO_2 thin films and their ability to change the polarization of light are discussed throughout the whole text. The most important property of VO_2 resides in the fact that

its complex refractive index changes significantly during the phase transition process around 68°C. That leads to drastically different reflected light states on VO_2 at above and below the transition temperature. This problem will be discussed in the following part.

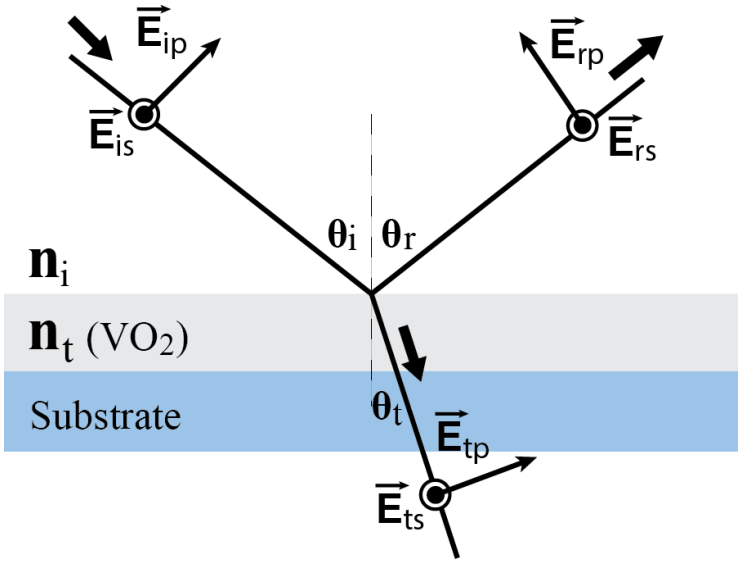

Figure 3.10: Incoming, reflected and refracted electric fields components.

Let's call $\vec{E_\iota}$ the incoming electric field, that can be described by the Jones matrix.

$$\vec{E_\iota} = \begin{pmatrix} E_{i,p} \\ E_{i,s} \end{pmatrix} \tag{3.41}$$

When VO_2 is at temperature T_L below transition temperature, the reflected electric field relates to the incoming electric field by:

$$\vec{E}_{rL} = r_L \vec{E_\iota} \tag{3.42}$$

With r_L is the reflection coefficient matrix at low temperature T_L of the form:

$$r_L = \begin{pmatrix} r_{L,p} & 0 \\ 0 & r_{L,s} \end{pmatrix} \tag{3.43}$$

where $r_{L,p}$ and $r_{L,s}$ are the complex, overall coefficients of reflection of the VO_2 layer for the p- and s- polarization, see Eqs. 3.37 and 3.39. At high temperature above phase transition

temperature, matrix r_H has the same structure as r_L, but with coefficients for temperature T_H and the electric field as:

$$\vec{E}_{rH} = r_H \overrightarrow{E_\iota} \tag{3.44}$$

From Eq. 3.42 and Eq. 3.44, we have a relationship between reflected fields at low and high temperatures

$$\vec{E}_{rH} = r_H r_L^{-1} \vec{E}_{rL} \tag{3.45}$$

We can call $r_{LH} = r_H r_L^{-1} = \begin{pmatrix} \frac{r_{H,p}}{r_{L,p}} & 0 \\ 0 & \frac{r_{H,s}}{r_{L,s}} \end{pmatrix}$ as the transformation matrix of a VO_2 thin film following the transition temperature. This matrix can be written in the form

$$r_{LH} = a_r \begin{pmatrix} 1 & 0 \\ 0 & z_r \end{pmatrix} \tag{3.46}$$

With $a_r = \frac{r_{H,p}}{r_{L,p}}$ and $z_r = \frac{r_{H,s}}{r_{L,s}} \frac{r_{L,p}}{r_{H,p}}$. Since a_r affects both the s- and p-components of $\vec{E}_{rL}$ equally. It does not change the relative phase or amplitude between the two and the polarization state remains the same. On the other hand, the phase of z_r will have an effect on the polarization state. It changes the phase difference between s- and p- components by an amount $\arg(z_r)$.

In the most general case, r_{LH} will transform an elliptically polarized field $\vec{E}_{rL}$ into a differently polarized field $\vec{E}_{rH}$. Since the phase between s- and p- of the reflected wave in general is not the same due to the effect of r_s and r_p, even if the incoming wave E_i is linearly polarized, the reflected light in general will be elliptically polarized. In some applications, we would like to attain high contrasts of modulation using a polarizer, so it is best to operate with linear polarization for at least one of $\vec{E}_{rH}$ or $\vec{E}_{rL}$. This can be done by adjusting phase of the incoming field $\overrightarrow{E_\iota}$ with a phase compensator.

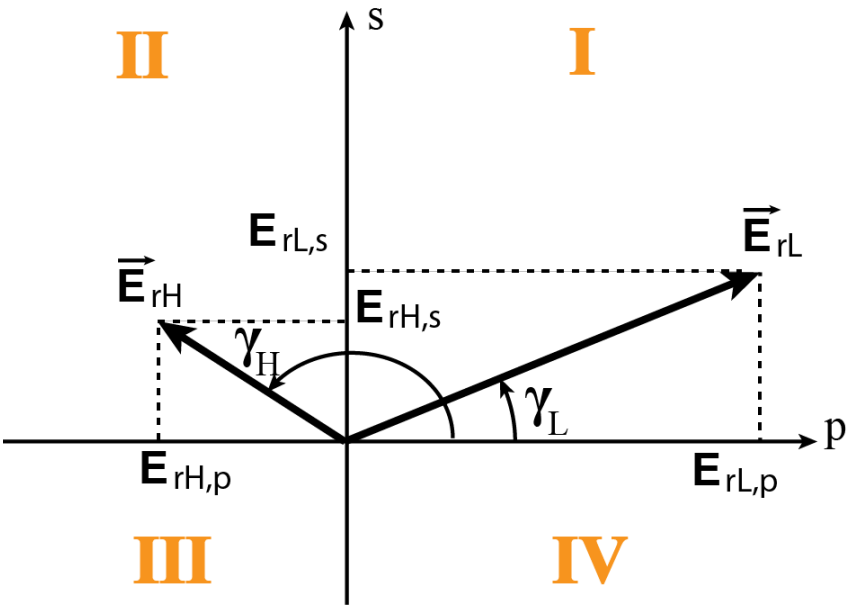

Figure 3.11: Reflected electric fields at a low temperature ($T < T_{MIT}$) and a high temperature ($T > T_{MIT}$) VO_2 sample.

If $\vec{E}_{rL}$ is linearly polarized, and the tranformation coefficient z_r has $\arg(z_r) = \Delta$, there are the following cases in Table 3.2.

Table 3.2: A linearly polarized field transforms into a new polarized field corresponding to different value of Δ.

$\Delta = m\pi$ with $m = 0, \pm1, \pm2$ ...	A linearly polarized field at low temperature will transform into a new linearly polarized field at different polarization direction at high temperature.
$\Delta = \left(\frac{1}{2} + m\right)\pi$ with $m = 0, \pm1, \pm2$ ...	The linearly polarized field at low temperature will transform into a new circularly polarized field at high temperature if the amplitudes of $E_{rH,s}$ and $E_{rH,p}$ are equal. Otherwise, it will be elliptically polarized.
All the remaining cases of Δ	The linearly polarized field at low temperature will transform to a new elliptically polarized field at high temperature.

From this, we consider two special cases:

a. Transformation from linear to linear polarization with a rotation of 90º

In this case, Δ must be equal to $\pi + m2\pi$. If $\arg(z_r) = m2\pi$ both the electric fields at low and high temperatures are in the first quarter as seen in Figure 3.11, so we can-not achieve a rotation of 90º. Also it is important to remember that we can easily attain high contrasts of modulation using a polarizer if two electric fields are perpendicular to each other.

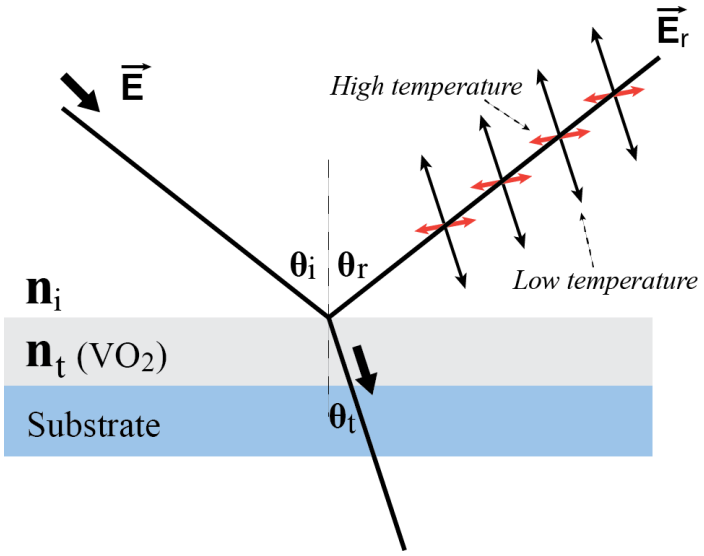

Figure 3.12: A reflected linear polarization transforms to a linear polarization with a rotation of 90º.

And because $\Delta = \pi + m2\pi,\ z_r = |z_r|(cos\pi + isin\pi) = -|z_r|$. Thus, we obtain

$$\begin{pmatrix} E_{rH,p} \\ E_{rL,p} \end{pmatrix} = a_r \begin{pmatrix} E_{rL,p} \\ -|z_r|E_{rL,s} \end{pmatrix} \tag{3.47}$$

so that

$$cot\gamma_H = \frac{E_{rH,p}}{E_{rL,p}} = \frac{E_{rL,p}}{-|z_r|E_{rL,s}} = -\frac{1}{|z_r|}cot\gamma_L \tag{3.48}$$

from which the rotation angle $\Delta\gamma = \gamma_H - \gamma_L$ is obtained. The condition under which the rotation angle becomes $\pm 90^o$ is

$$cot\gamma_L cot\gamma_H = -1 \tag{3.49}$$

And with Eq. 3.48 we find the condition that:

$$cot\gamma_L = \sqrt{|z_r|} \tag{3.50}$$

With known initial parameters such as incidence angle, film thickness, wavelength, and refractive indices of all media, the value of $|z_r|$ is calculated. From that, we can choose the polarization state of the incoming wave at which the reflected wave is linear and satisfies the condition $cot\gamma_L = \sqrt{|z_r|}$. But the most important condition is that $\arg(z_r) = \pi$. Not all VO_2 samples can satisfy this condition. As a result, it needs an appropriate combination of all the above parameters to meet this condition.

b. Transformation from linear to circular polarization

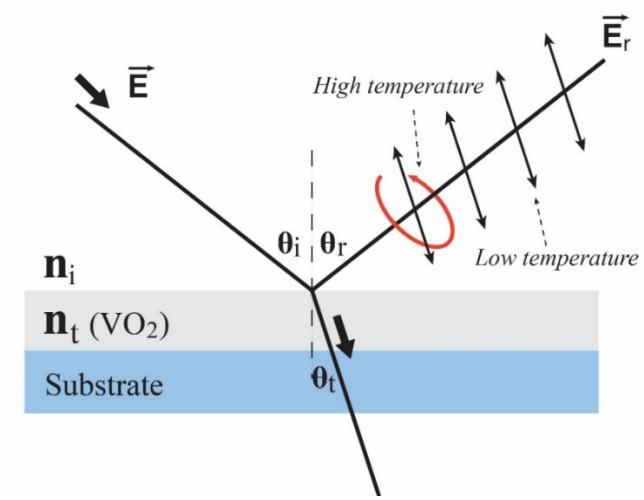

Figure 3.13: A reflected linear polarization transforms to a circular polarization.

The conditions for a circularly polarized field $\vec{E}_{rH}$ are that the s- and p- components have the same amplitudes and the phase difference between them is $\pm\frac{\pi}{2}$. Because s- and p- components of $\overrightarrow{E_{rL}}$ have the same phase (linearly polarized), $arg(z_r) = \pm\frac{\pi}{2}$.

We have:

$$\frac{E_{rH,p}}{E_{rL,s}} = e^{\pm i\frac{\pi}{2}} = \pm i \tag{3.51}$$

But

$$\frac{E_{rH,p}}{E_{rH,s}} = \frac{E_{rL,p}}{z_r E_{rL,s}} = \frac{1}{z_r} cot\gamma_L \tag{3.52}$$

From Eq. 3.51 and Eq. 3.52, that leads to the condition:

$$cot\gamma_L = |z_r| \tag{3.53}$$

❖ **Theory in transmission**

All the above results can be extended to the electric field transmitted through the VO_2 film. In transmission, the transformation matrix has the same form as in Eq. 3.46 and is expressed by

$$t_{LH} = a_t \begin{pmatrix} 1 & 0 \\ 0 & z_t \end{pmatrix} \tag{3.54}$$

where $a_t = \frac{t_{H,p}}{t_{L,p}}$ and $z_t = \frac{t_{H,s}}{t_{L,s}} \frac{t_{L,p}}{t_{H,p}}$

For a rotation of 90° from linear to linear polarization, matrix z_t must satisfy that $arg(z_t) = (1 + 2m)\pi$, with $m = 0, \pm 1, \pm 2$ ..., and that the condition $cot\gamma_L = \sqrt{|z_t|}$ is met.

For transformation from linear to circular polarizations, it requires that $arg(z_t) = \left(\frac{1}{2} + m\right)\pi$ with $m = 0, \pm 1, \pm 2$ ..., and the condition for a transmitted electric field at low temperature has $cot\gamma_L = |z_t|$.

3.4 Transmission of polarized light through a polarizer

The state of a polarization often is analyzed by measuring the power transmitted through a polarizer. Let's start by looking at general elliptically polarized field, the end point of the vector $\vec{E}$

creates an ellipse with semi-major axis a and semi-minor axis b and its polarization direction makes an angle α with the X axis, Figure 3.14(a).

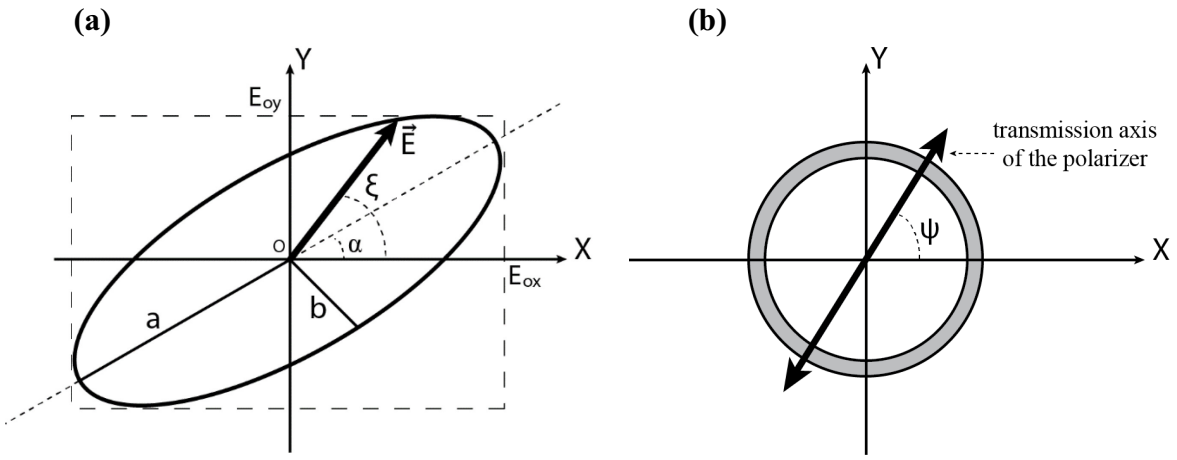

Figure 3.14: (a) An elliptically polarized light in Cartesian coordinate, (b) A polarizer with its transmission axis creating an ψ angle with the ox axis.

The equation of vector $\vec{E}$ in polar coordinate system can be expressed as

$$E(\xi) = \sqrt{\frac{a^2 b^2}{a^2 sin^2(\xi - \alpha) + b^2 cos^2(\xi - \alpha)}} \tag{3.55}$$

where the angle ξ depends on time t and can be written as $\xi = \xi(t)$. When this field meets the polarizer with its transmission axis at an angle ψ to the horizontal, Figure 3.14(b), there is only an orthogonal projection of the vector $\boldsymbol{E}$ in the direction of transmission axis of the polarizer that can pass through. This electric field is written as:

$$\boldsymbol{E}_\psi(t) = E[\xi(t)].cos[\xi(t) - \psi].\hat{\boldsymbol{e}}_\psi \tag{3.56}$$

where $\hat{\boldsymbol{e}}_\psi$ is the unit vector in the ψ direction. Since the transmitted intensity is proportional to the square of electric field $I = |\boldsymbol{E}|^2$ so we have

$$I_\psi(t) = \left|\boldsymbol{E}_\psi(t)\right|^2 = \frac{a^2 b^2}{a^2 sin^2[\xi(t) - \alpha] + b^2 cos^2(\xi(t) - \alpha)}.cos^2[\xi(t) - \psi] \tag{3.57}$$

In optical laboratories, photodiode devices are used to measure the intensity of light through its electric field. And because the electric field has a high frequency (10^{14} Hz), the signal detected by photodiodes is actually the time-averaged intensity . That is the average intensity of different electric fields at detector for one period (vector $\vec{E}$ rotates a full ellipse).

$$I_{RMS}(\psi) = \sqrt{\frac{1}{T}\int_0^T I_\psi^2(t)dt} \tag{3.58}$$

$$\Rightarrow \qquad I(\psi) = I_{RMS}(\psi) = a^2cos^2(\psi - \alpha) + b^2sin^2(\psi - \alpha) \tag{3.59}$$

The Eq. 3.59 shows the intensity of a polarized light through polarizer as a function of angle between the direction of polarization and the polarizer transmission axis. This one also contains all information about the polarization state which can be calculated by fitting the curve $I(\psi)$ according to the parameters a_1, a_2, a_3.

$$I(\psi) = a_1^2cos^2(\psi - a_3) + a_2^2sin^2(\psi - a_3) \tag{3.60}$$

Comparing with Eq. 3.59, it is clear that

$$a_1 = a,\ a_2 = b, a_3 = \alpha \tag{3.61}$$

Let's set the new expressions p, q, r as:

$$p = \frac{a_1^2 + a_2^2}{2} \tag{3.62}$$

$$q = \frac{a_1^2 - a_2^2}{2}cos(2a_3) \tag{3.63}$$

$$r = \frac{a_1^2 - a_2^2}{2}sin(2a_3) \tag{3.64}$$

From Eq. 3.60 and Figure 3.14(a), we see that the maximum or amplitudes of $\overrightarrow{E_x}$ and $\overrightarrow{E_y}$ can be calculated by putting $\psi = 0$ for E_{ox} and $\psi = {}^{\pi}/_{2}$ for E_{oy}.

$$E_{ox} = \sqrt{a^2cos^2\alpha + b^2sin^2\alpha} \tag{3.65}$$

$$E_{oy} = \sqrt{a^2 sin^2\alpha + b^2 cos^2\alpha} \tag{3.66}$$

And the phase difference between $\overrightarrow{E_x}$ and $\overrightarrow{E_y}$ can be rewritten from Eq. 3.8.

$$cos\Delta = \frac{E_{ox}^2 - E_{oy}^2}{2E_{ox}E_{oy}} tan2\alpha \tag{3.67}$$

Substituting Eq. 3.65 and Eq. 3.66 into Eq. 3.67 with some rearrangements, we can find the expression for phase information. Finally, all the parameters of the incoming polarization state can be found to be correlated to p, q and r in the following forms.

Ellipticity $$\varepsilon = \sqrt{\frac{p - \sqrt{q^2 + r^2}}{p + \sqrt{q^2 + r^2}}} \tag{3.68}$$

Amplitude $$E_o = \sqrt{2p} \tag{3.69}$$

Azimuth $$tan2\alpha = \frac{r}{q} \tag{3.70}$$

Phase $$cos\Delta = \frac{r}{\sqrt{p^2 - q^2}} \tag{3.71}$$

CHAPTER 4

Fabrication of VO_2 and ellipsometry measurement

4.1 Vanadium dioxide fabrication

The samples used in this study were made by sputtering metallic vanadium followed by post-treatment in oxygen method. The steps for fabricating VO_2 samples are described in the Figure 4.1.

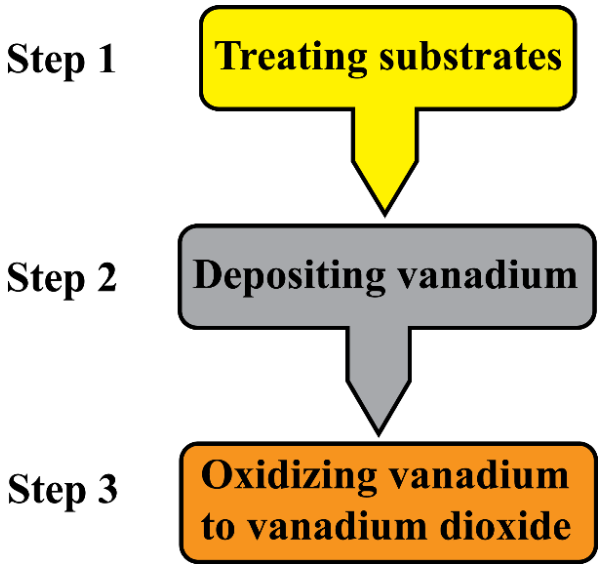

Figure 4.1: Steps for fabricating VO_2 samples.

❖ ***Step 1: Treating substrates***

Only in certain studies, such as determining the impact of substrate on recovery time of VO_2 film, the Zerodur, sapphire or quartz substrates were used. This study will be presented in Chapter 8. In most of the experiments, we use VO_2 samples fabricated on glass. Typically, there are many impurities in Corning glass substrates. They influence the VO_2 film quality and optical measurement results. Thus, we always treat the substrates by annealing them at 500^{o}C in the oven for an hour and clean their surfaces by H_2SO_4 acid after that. Next, the substrates are washed with

distilled water, acetone in ultrasound and dried. The whole process is done carefully to ensure that the substrates are of good quality before coating the vanadium on their surface in the next step.

❖ ***Step 2: depositing vanadium layer***

The metallic vanadium thin films are made by RF sputtering in the vacuum chamber. The substrate is mounted on the sample holder and heated to 450^{o}C to remove any water vapor from the substrate. Then it is cooled down to room temperature. This process is carried out simultaneously while decreasing the pressure. After 1 hour, the vacuum in the chamber is about 10^{-6} torr and is ready for depositing thin film. The thickness of film depends on the sputtering time. Normally, it takes about 4 minutes depositing metallic vanadium for VO_2 samples with a thickness of 100 nm after oxidation. In the end of the step 2, a metallic vanadium thin film on the glass substrate is created and taken out of the chamber for the oxidation process in step 3.

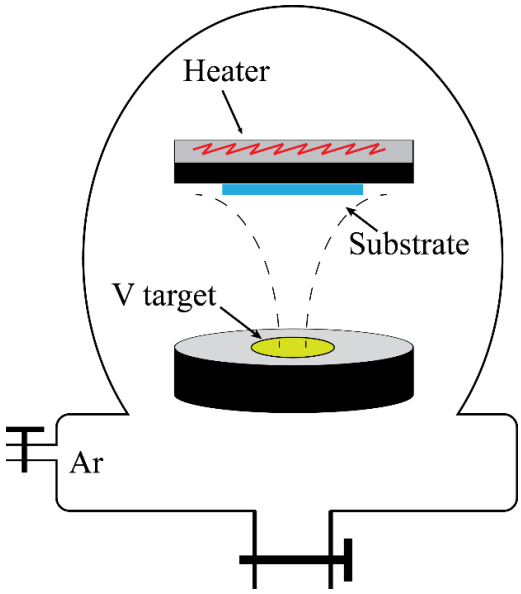

Figure 4.2: Vanadium sputtering method.

❖ ***Step 3: Oxidizing vanadium to vanadium dioxide***

This step is done in the oven system which was designed to anneal samples in oxygen environment at high temperature. To convert vanadium to vanadium dioxide, the metallic

vanadium sample is heated at 500°C for 1 hour in 150 mtorr oxygen. Those are standardized parameters for VO_2 samples of 100 nm. This process requires more time for a thicker sample. The whole system is then kept running overnight to cool down to room temperature. In the end of the step 3, the sample is taken out of the oven system and is ready for doing analysis and experiments.

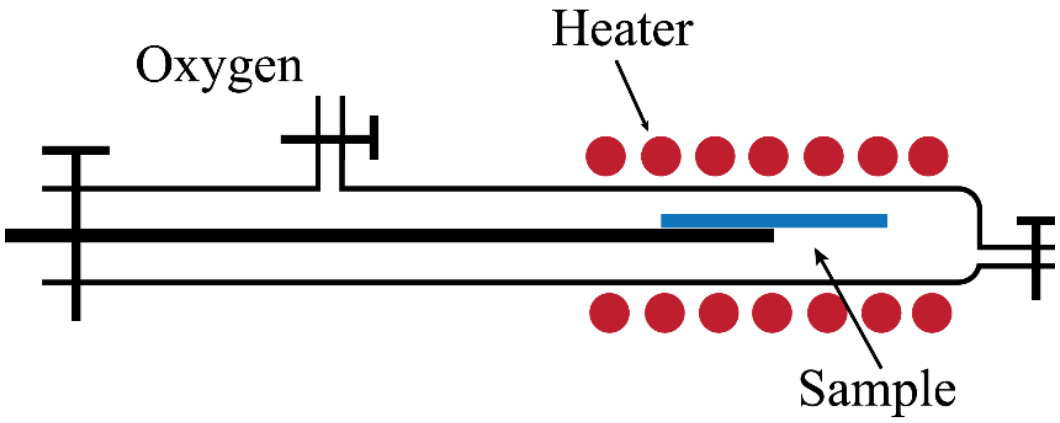

Figure 4.3: Oxidizing vanadium to vanadium dioxide in the oven system.

4.2 Ellipsometry measurements

The VO_2 samples after fabrication will be checked for their properties through the transmittance spectra at room temperature and at 85°C. This measurement only provides a general view of the samples' optical properties. To know the specific parameters such as thickness, complex refractive indices of VO_2 layer, the samples are usually checked by ellipsometry in our lab. The home made ellipsometry system can operate well with wavelengths from 400 nm to 2200 nm. And both polarizations of light reflected on or transmitted through the VO_2 samples are measured simultaneously by the detectors. The sample holder can be tilted for different incidence angles from 10° to 70° and is used to heat samples to 100°C. These ellipsometry measurements are time-consuming but they give accurate results.

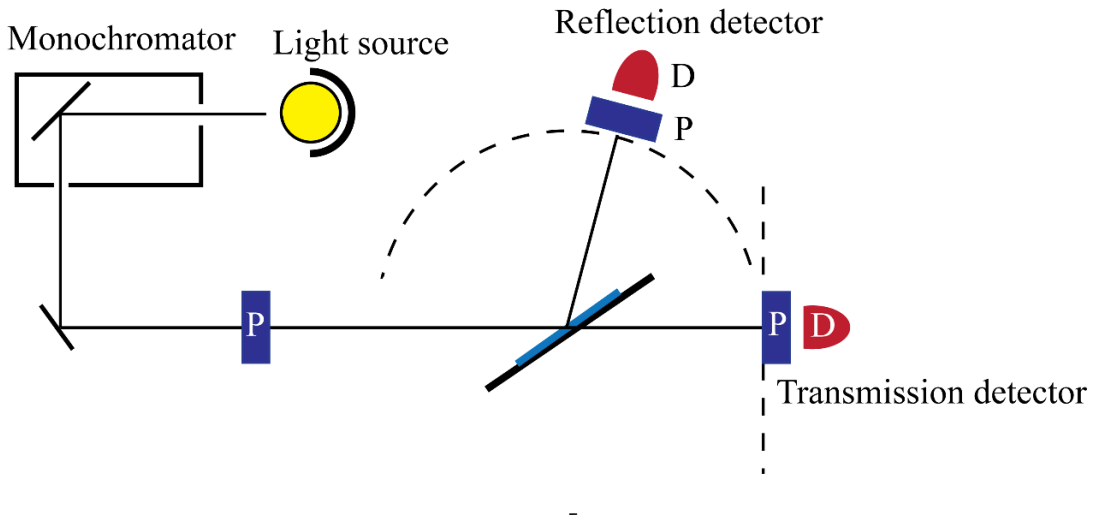

Figure 4.4: The ellipsometry system for measuring optical parameters of VO_2 samples.

CHAPTER 5

Phase control experiments

In this section, we present two pioneering works that opened the way to new optical phase control applications for vanadium dioxide.

The first experiment demonstrates the possibility of controlling the phase of light by means of changing the phase of the material. This was done without modifying the amplitude or any other properties of light, hence the term ‘’pure phase control’’. Typically, such phase control is achieved by mechanically varying the path length of light, like moving a mirror mounted on a piezoelectric transducer in an interferometer, or by using some kind of electro-optic effect, like in Pockels cells or liquid crystals. In addition to using a different physical mechanism, the approach using vanadium dioxide presents fundamental differences in that it works in transmission or reflection, and over much shorter distances (nanometer versus micrometers to centimeters).

The second experiment uses the effect on a light beam of a spatially non-uniform phase shift. The simplest optical elements which work on this principle are lenses and curved mirrors, where non-uniform distortion of the phase front leads to focusing or defocusing of the light beam. In this experiment, a non-uniform optical phase shift is created by heating a VO_2 film non-uniformly by a strongly absorbed laser beam. A second beam is then focused in reflection from the resulting distorted wavefront. This effect demonstrated an ultrathin flat lens with adjustable focus, the first of its kind.

5.1 Pure optical phase control with vanadium dioxide thin films

In our first study [51] on the phase of light interacting with VO_2 layer during phase transition process, we studied monochromatic light passing simultaneously through a bare glass substrate and a film VO_2. This was done by depositing vanadium on only half of the glass substrate, as shown in Figure 5.1. Two half-beams interacting respectively with the glass and the VO_2 on the glass sample were created, and because both come from the same laser source, they interfere with each other and create interference fringes in the far field. When the whole sample is heated slowly from room temperature to 80°C, any relative phase difference between the two paths will manifest itself in the interference fringes pattern.

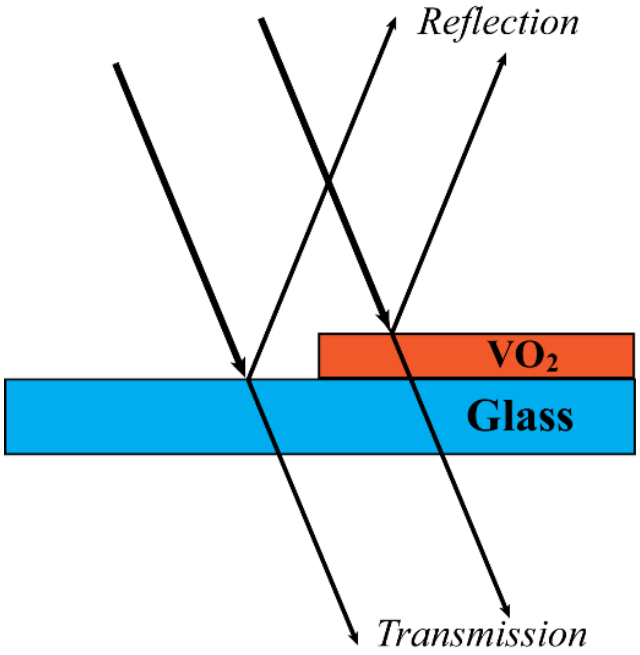

Figure 5.1: The sample with VO_2 deposited on a half of the glass substrate for interference measurements.

Figure 5.2 shows the experimental setup for measuring the phase change of light. In a sample holder, a small hole was made to allow the transmitted light to go through. The edge between the bare glass and VO_2 sides of the sample remains on the center of the hole. The shapes

of the transmitted interference fringes were monitored with a CCD camera (Thorlab-DCU224C) which has 4.65 µm x 4.65 µm in size for each pixel. In reflection measurement, a linear array 512 InGaAs detector (Jobin Yvon Spectrum One) was used. The sample temperature was measured and controlled entirely by computer with a precision of 0.2°C. The computer also was used to collect all images from the CCD cameras and analyzed the movement of the fringes. For accurate results, 800 nm and 1310 nm lasers were used as probe beams for transmission and reflection, respectively. Those wavelengths were chosen because the transmittance at 800 nm and the reflectance at 1310 nm do not change during the VO_2 phase transition in that sample, as shown in Figure 5.3.

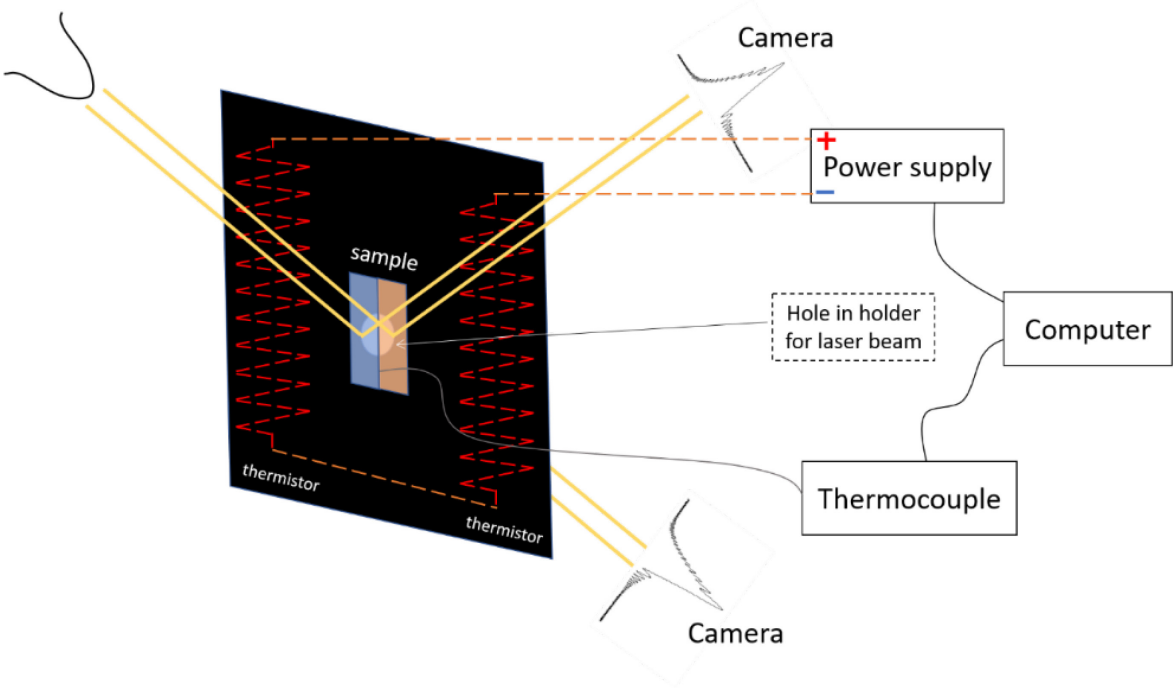

Figure 5.2: Experimental setup for measuring optical phase changes in light beams interacting with VO_2 during the phase transition.

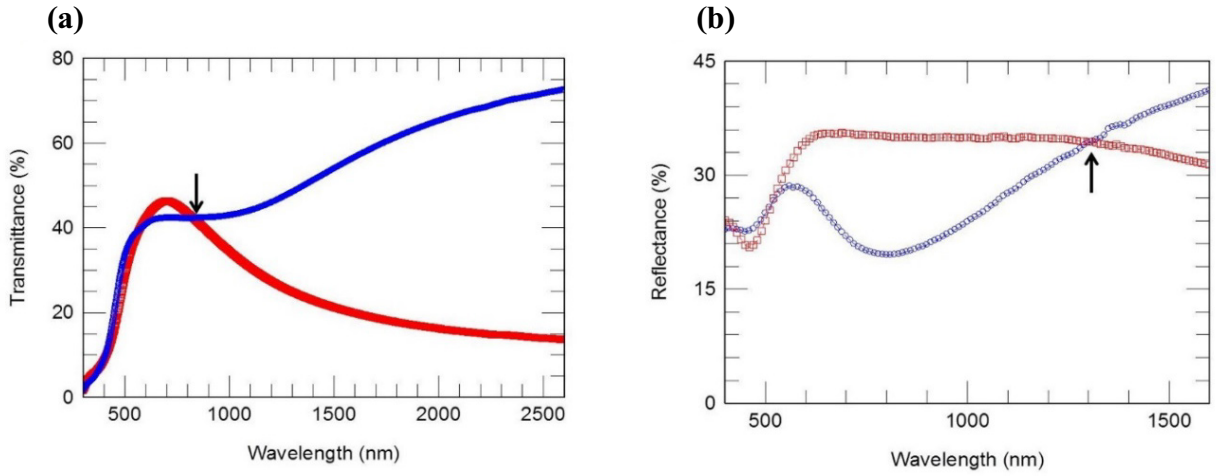

Figure 5.3: (a) Transmittance and (b) Reflectance of a VO_2 thin film at temperature of 23°C (blue) and 80°C (red) for an 86 nm VO_2 thin film on glass. Reproduced from ref. [51].

The sizes of the laser beams in our experiment are small, with less than 2 mm in diameter. They all have the Gaussian energy distribution and this distribution does not change when the beams are positioned entirely on the glass side or on the VO_2 side, Figure 5.4(a). However, when they are centered at the edge between the glass and the VO_2 film, the combined profile of two half beams appears with interference fringes, as seen in Figure 5.4(a). Any change in the optical thickness of the film causes the fringes to move. For this reason, the relative phase changes of the light are inferred by the position of the fringes. For experiments done near the normal incidence angle, the optical phase difference for the 1310 nm reflected light between the insulating and metallic VO_2 states is 0.8 radians, as Figure 5.4(b) shows. This corresponding value for the 800 nm transmitted light is 0.4 radians (Figure 5.4(c)). Both results are close to the calculated values based on the real and imaginary refractive indices of the VO_2 film. A hysteresis during the heating and cooling cycle also is observed, as for other properties of VO_2.

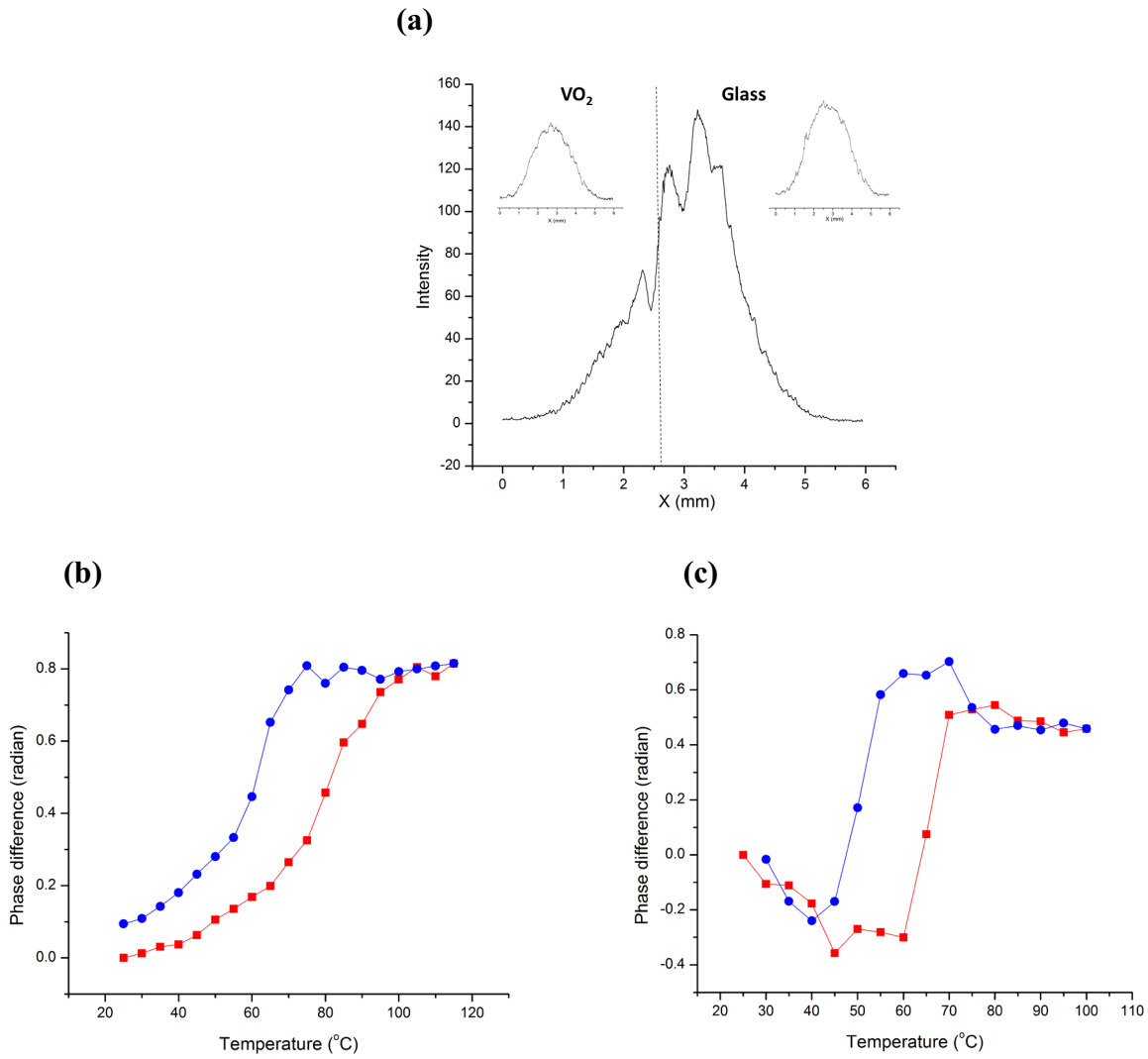

Figure 5.4: (a) Self-interference of a Gaussian laser beam probing the edge of a VO_2 thin film. Insets show beam profiles when positioned entirely on the VO_2 film and the glass substrate, (b) Phase difference for 1310 nm reflected light and (c) Phase difference for 800 nm transmitted light in heating cycle (red) and cooling cycle (blue).

This study showed that despite the constant reflectance and transmittance during the phase transition of VO_2, there are significant optical phase shifts, which promise some new applications in controlling the polarization of light. The possibility of using phase effects instead of amplitude effects, which are typically limited to wavelengths above 1000 nm, opens the door to applications of VO_2 in the visible spectrum for the first time.

5.2 Ultrathin flat lens with adjustable focus

The possibility of controlling the phase of light by changing the temperature of a VO_2 film lead us to the idea of creating a spatially non-uniform phase shift for reflected light. This makes the light beam focus or defocus in the far field [51]. The spatial phase profile would be controlled by a second, stronger (pump) laser beam that heats the sample according to some Gaussian intensity profile [77].

In our experiment [78], we used a 100 nm uniform VO_2 thin film to focus a 1.3 μm laser beam, with the focus point adjusted by controlling the pump laser intensity. As we known from Figures 5.4(b) and 5.4(c), optical phase shift in VO_2 vary almost linearly with temperatures near the phase transition temperature 50°C and 70°C. Since the surface temperature is linear with the local pump intensity, the phase shift should resemble the intensity profile of the pump and take the same curvature.

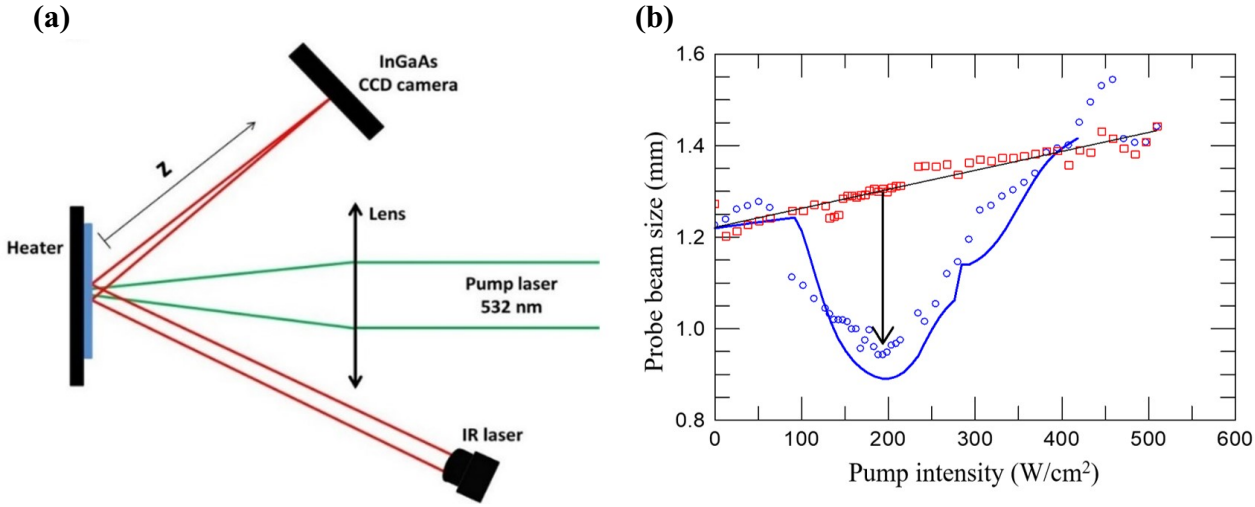

Figure 5.5: (a) The setup for adjustable lens experiments, (b) Probe beam size at 50 cm away from the sample as a function of pumping intensity when the sample is externally heated at 85°C (squares), kept at room temperature 22°C (circles). The curve is a theoretical calculation based on Fresnel-Huygens theory. Reproduced from ref. [78].

The experimental setup is shown in Figure 5.5(a). A 1310 nm light produced by a diode laser (LPS-PM1310-FC) with 2.5 mW continuous average power was used as probe beam. At this low intensity, the probe beam can-not induce a phase change in the VO_2 film. The pump beam was generated by a frequency-doubled Nd:YVO_4 laser operating in continuous mode at 532 nm, a wavelength which absorbs well into the VO_2 film. The sizes of the probe (w = 0.96 mm) and pump (w_p = 0.5 mm) beams on VO_2 were choosen to optimize the focusing effect.

Figure 5.5(b) show the probe beam size (FWHM) measured at a distance z = 50 cm away from the sample at various conditions. This result shows clearly evidence of beam focusing. When the sample is kept at 85^{o}C (via external heating), the VO_2 sample is in the fully metal state so the pump laser can-not make any change in phase of the sample as well as the optical phase of the probe beam. But the heat from the pump beam creates a diverging lens due to local thermal expansion of the substrate [79]. By this reason, the probe beam at the detector (InGaAs detectors) widens steadily as the intensity of the pump increases.

The result changes completely when the sample is at a room temperature 22^{o}C. Local heat from the pump beam creates a temperature gradient and a phase curvature. At threshold intensity (~ 50 W/cm^2), the shape of the probe beam begins to change with a higher peak and a narrow width. The beam gets minimum width (at focus point) at 200 W/cm^2 at which we assume that temperature at the center beam reaches 70^{o}C. The size of the probe beam at the detector reduces from 1.3w to 0.9w as seen by the arrow in Figure 5.5(b). These results have demonstrated well the ability to use a VO_2 thin film as flat lens. In addition, focal length can be adjusted easily by changing the pumping intensity or size of the pump beam. Details of this issue was presented clearly in ref. [78]. The above experimental results are the foundation for the research on using VO_2 in controlling polarization of light that will be presented in the following chapters.

CHAPTER 6

Polarization and amplitude modulation of light by VO_2

6.1 The limits of amplitude modulation

In most applications of VO_2, light is modulated by changes in reflectance and transmittance. This kind of modulation has two disadvantages:

1. Reflectance and transmittance change substantially only for wavelengths in the infrared region (>1000 nm) and almost no change is observed in the visible spectrum.
2. The maximum ratio between reflected intensities at two states for both R_1/R_0 and R_0/R_1 (1 and 0 indices for activated and not activated states, respectively) is limited, as Figure 6.1(a) shows. While, for transmission, the ratio can go up to 1000 or higher, it occurs for thick samples where transmittance is very low. Also, for opaque substrates, the use of transmitted beams is not possible.

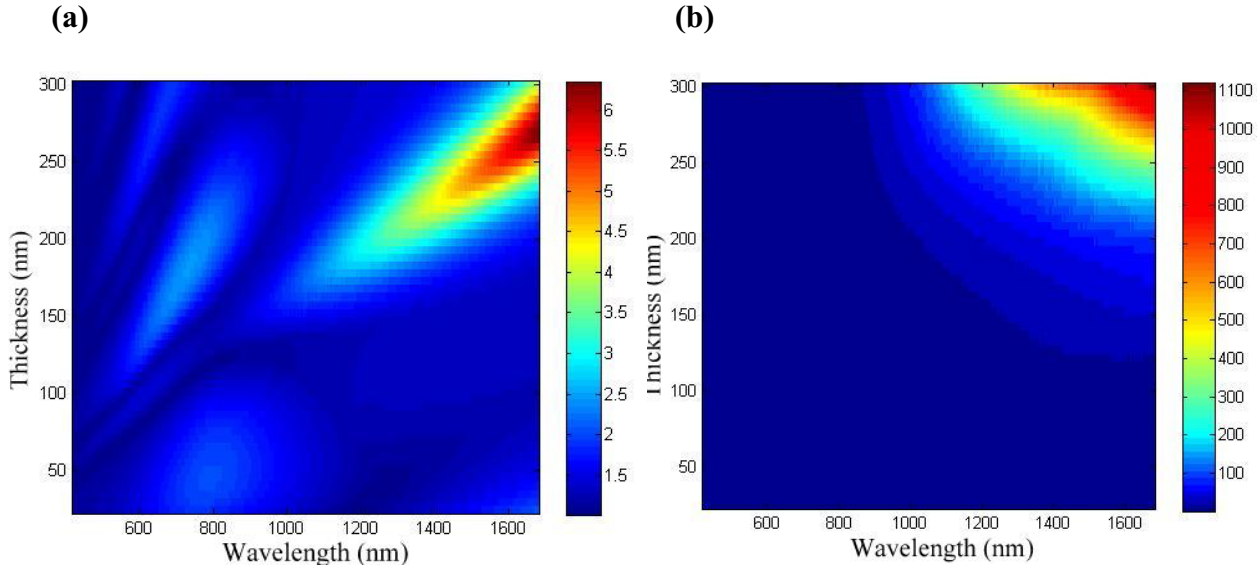

Figure 6.1: The maximum intensity ratio between two VO_2 states for (a) reflection and (b) transmission are calculated for normal light at different incidence angles.

In this section, we will describe the principles to achieve high intensity modulation in the infrared and visible using VO_2 thin films (less than 100 nm). The new concept is based on the change in the phase of s- and p-components of the polarization as they interact with VO_2 thin film in different states [80]. This opens new possibilities for controlling the polarization of light and creating high modulation optical switches that can operate with different wavelengths. The calculated results based on this idea will be presented in the following parts.

As discussed in Section 3.3, when a beam reflects on or transmits through a VO_2 sample, the amplitude as well as the phase of the beam will change, and they depend strongly on the properties of VO_2. At different states of VO_2, the polarization of the reflected and transmitted beams can vary completely. In some cases, a linear polarization after interacting with VO_2 sample at low temperature can be transformed into a linear polarization in a new direction or into a circular polarization when the sample is heated to above the phase transition temperature. This change is determined by the phase difference $\arg(z_r)$ or $\arg(z_t)$ as described in Table 3.2.

To calculate these quantities for a VO_2 film on glass, the model in Figure 3.8 is used. In that, $n_i = 1$ for air, and n and k of VO_2 and glass are taken from the ellipsometry measurements. Figure 6.2 shows the values of n and k obtained from our VO_2 sample which are similar to many published articles [81], [82]. The most important factor is to choose the appropriate conditions such as the thickness of VO_2 film, the angle of incidence, and the wavelength to achieve the greatest possible phase difference.

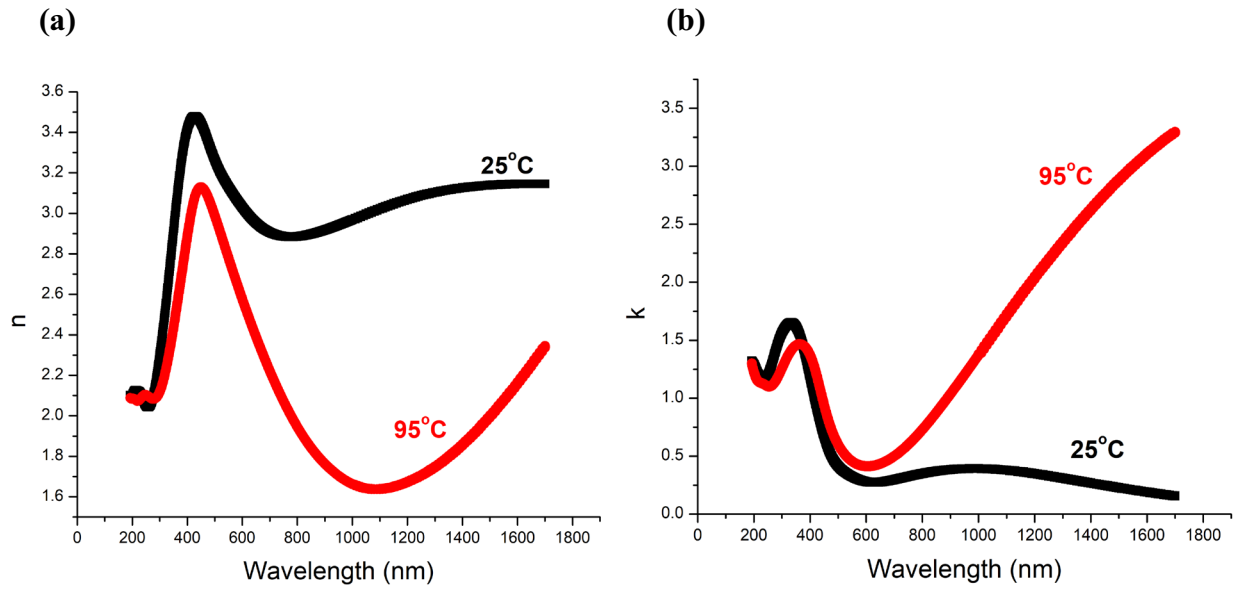

Figure 6.2: (a) Real and (b) imaginary refractive indices of the VO_2 film on Zerodur sample in its insulating state (25°C) and its metallic state (95°C).

Figure 6.3(a) maps the maximum absolute value of $\arg(z_r)$ at different incidence angles and wavelengths, each combination taking the best film thickness, ranging from 25 nm to 300 nm, at which $\arg(z_r)$ achieves maximum value. This graph indicates that π radians relative phase shift can be attained for wavelengths in the visible and infrared, if the incidence angle is in the range between 60° and 75°. These angles stay near the pseudo-Brewster angle for the VO_2 on glass sample. This is further confirmed by the reflectance of p-polarization corresponding to the maximum $\arg(z_r)$ as demonstrated in Figures 6.3(b) and 6.3(c). In both insulating and metallic VO_2 states, the p-reflectance is very small. Meanwhile, the s-reflectance increases as the angle of incidence increases and achieves more than 0.5 with the angles higher than 60°. Figures 6.3(d) and 6.3(e).

(a) Relative phase shift_arg(z_r)

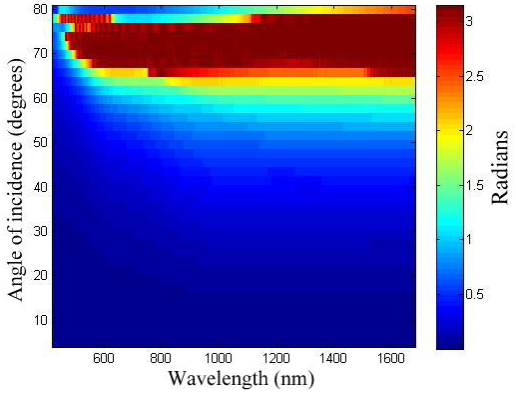

(b) Reflectance of p-polarized light at low temperature

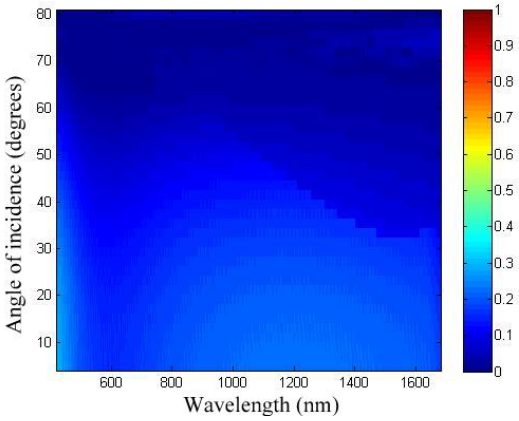

(c) Reflectance of p-polarized light at high temperature

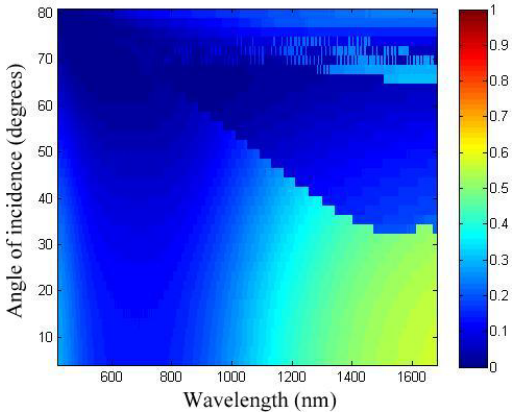

(d) Reflectance of s-polarized light at low temperature

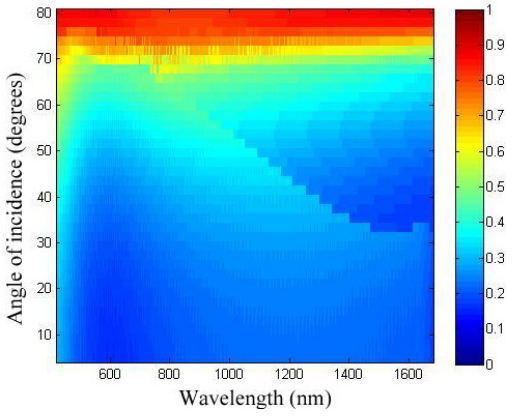

(e) Reflectance of s-polarized light at high temperature

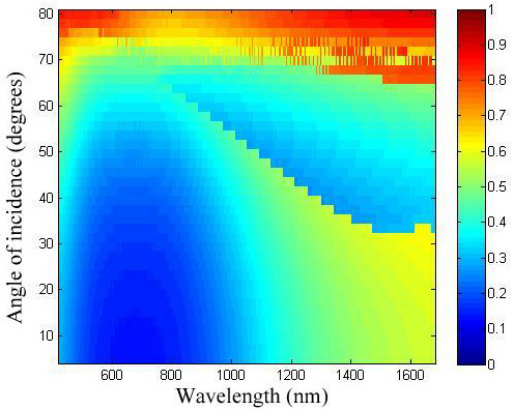

Figure 6.3: (a) Maximum relative phase difference arg(z_r), (b)-(e) p-reflectance at low temperature, p-reflectance at high temperature, s-reflectance at low temperature, s-reflectance at high temperature corresponding to maximum relative phase difference (in radians) calculated for VO_2 on glass sample with thickness in range 25-300 nm.

For light transmitted through VO_2 on glass, the phase difference $\arg(z_t)$ does not change much, as Figure 6.4(a) shows. At 1.7 μm wavelength and the very large angle of incidence 80^o, only a 1 radian phase difference is achieved. However, the transmission for both s- and p-polarizations is almost zero at this condition, as shown by Figures 6.4(b)-(e). This would have little practical applications. At the insulating state of VO_2, light can go through the sample while at metallic state, the sample blocks completely all light. The ratio between the transmission at two states for IR can be very high as the result shows in Figure 6.1(b). Because of the limitations of $\arg(z_t)$ and amplitudes analyzed above, we do not use transmitted light in our experiments.

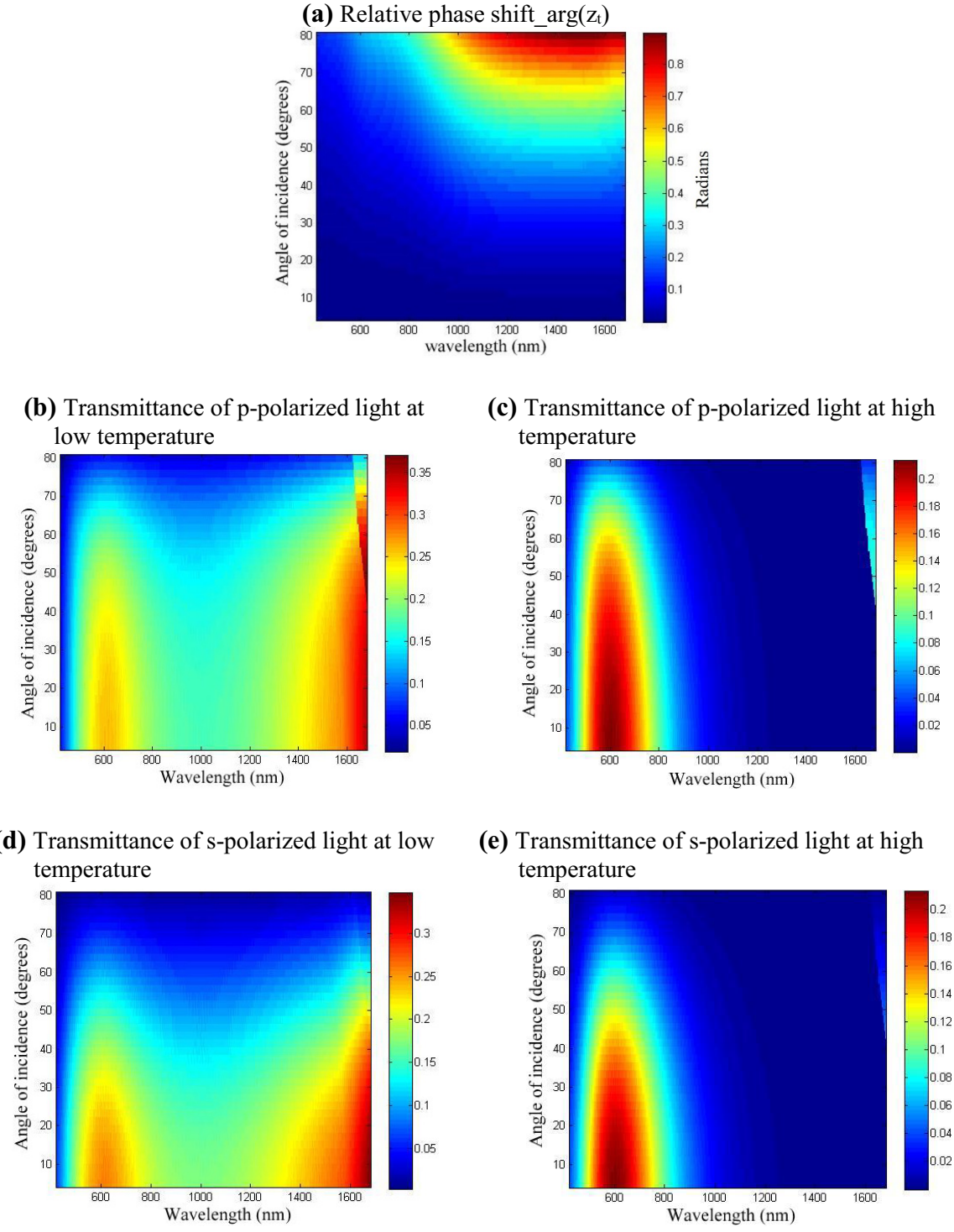

Figure 6.4: (a) Maximum relative phase difference arg(z_t), (b)-(e) p-transmittance at low temperature, p-transmittance at high temperature, s-transmittance at low temperature, s-transmittance at high temperature corresponding to maximum relative phase difference (in radians) calculated for VO_2 on glass sample with thickness in range 25-300 nm.

In this thesis, we propose to use polarized light in reflection from VO_2 samples and exploit relative phase changes between s- and p-polarizations to alter the polarization state of light. This ability when combined with a polarizer could lead to high switching amplitudes over a wide range of wavelengths. The following analysis will analyze this effect in detail.

6.2 Intensity modulation with polarizers

Figure 6.5 shows a schematic to exploit polarization changes to modulate light interacting with a VO_2 layer.

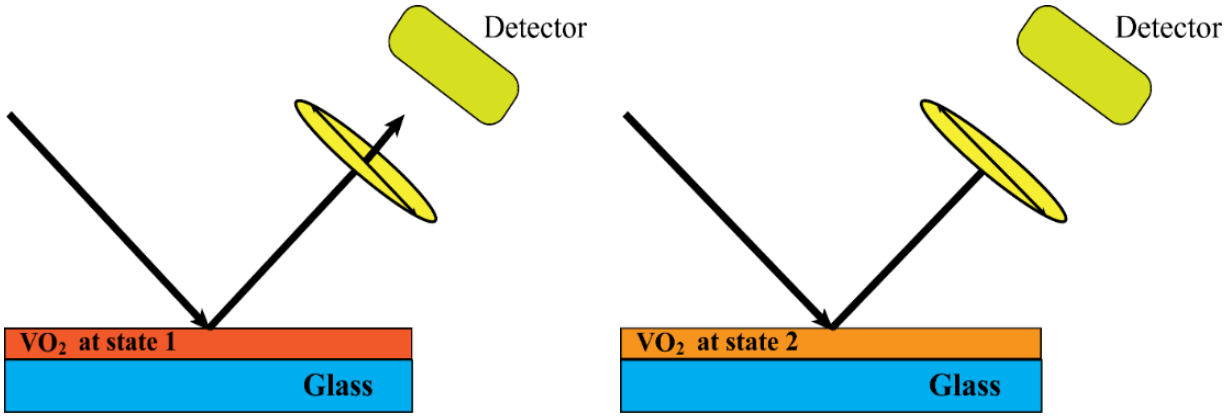

Figure 6.5: The reflected light goes through the polarizer at state 1 of VO_2 and is blocked by the polarizer at state 2 of VO_2.

Let's suppose that at insulating state of VO_2, the reflected light has elliptical polarization with semi-major axis a_L and semi-minor axis b_L, and its polarization direction makes an angle α_L with the X axis as shown in Figure 3.14(a). When heating VO_2 to its metallic state, the reflected light gains new polarization. This state is characterized by semi-major axis a_H, semi-minor axis b_H, and angle of polarization direction α_H. The intensity of the reflected light in both cases after passing through the polarizer with transmission axis at angle ψ are demonstrated by Eq. 3.59. The relative light intensity between them is written as

$$R(\psi) = \frac{a_H^2 cos^2(\psi - \alpha_H) + b_H^2 sin^2(\psi - \alpha_H)}{a_L^2 cos^2(\psi - \alpha_L) + b_L^2 sin^2(\psi - \alpha_L)} \quad (6.1)$$

The result of Eq. 6.1 can achieve high value if the denominator is near zero. It requires $b_L = 0$ and $\psi - \alpha_L = 0$, corresponding to linear polarization for reflected light at low temperature and the transmission axis of the polarizer perpendiculars to the electric field vector of light. A less optimal but still acceptable situation is when the reflected light is linearly polarized in either one of the two states of VO_2, so long as the polarizer is cross-aligned with it. Because of this reason, in most of our following experiments, the light reflected on VO_2 sample at low temperature will be prepared in the form of linear polarization. This can be done by using a birefringent crystal as phase compensator to set the phase difference between s- and p- components in such a way that after reflection from VO_2, it becomes linearly polarized light. Generally speaking, the film will impart a phase shift δ_o and thus the compensator must yield a phase $-\delta_o$ to compensate. Note that δ_o is not constant but depends on the angle of incidence. Alternatively, we also operate in the regime where the light reflected is linearly polarized when VO_2 is activated instead of when it is in its insulating state.

In all these cases, the ratio of light passing through the polarizer with VO_2 activated by thermal heat or photoinduction to the light passing when VO_2 is not activated can be high. It could reach values in the thousands and depends much on the quality of the polarizer (its extinction ratio). This high modulation can happen if the amplitudes and phases of the s-and p-components satisfy some conditions as discussed in Section 3.3. The most important condition is that the relative phase difference $arg(z_r)$ must reach a value of π.

CHAPTER 7

Polarization modulation by thermal activation

In Chapters 5 and 6, we confirmed through experimental results that the phase of light reflected on or transmitted through VO_2 are different at the metallic and insulating states. And this phase shift can reach π radians if the appropriate conditions for the sample and experiment are used [80]. This leads to new potential for optical applications when the polarized light is passed through a polarizer. In this chapter, the influence of film thickness, incident angle and wavelength on the phase difference and polarization will be discussed in more details with calculations. Additionally, we will also present experimental results where polarization is controlled effectively with high contrast ratios of light achieved by using a single VO_2 layer.

In order to choose the best thickness for VO_2 films, angle of incidence and wavelength of light in a polarization control experiment, we did calculations with the model (Figure 3.8) for a VO_2 layer on glass (fused silica) sample as mentioned in Section 6.1. In Figure 7.1, the incidence angle is scanned from 10° to 80° for each pair of thickness and wavelength, and the maximum phase shift $arg(z_r)$ is plotted. As mentioned in Section 6.1, in order to achieve π radians relative phase shift, the angle of incidence typically needs to be near the pseudo-Brewster angle for VO_2 on glass, namely around 65° to 75°. Note that we cannot find a VO_2 film thickness from which π radians can be achieved for all wavelengths from 500 nm to 1700 nm, but some thickness can be good for multiple wavelengths. For doing experiments at a specific wavelength, we can choose the most suitable thickness for the thin film. However, the results in Figure 7.1 will change slightly if different sets of VO_2 refractive indices are used. From these calculations, we found that a thickness of 75-100 nm is consistent with the experiments in the visible and infrared regions. Therefore, most of the VO_2 samples for this study were made with a thickness of around 100 nm.

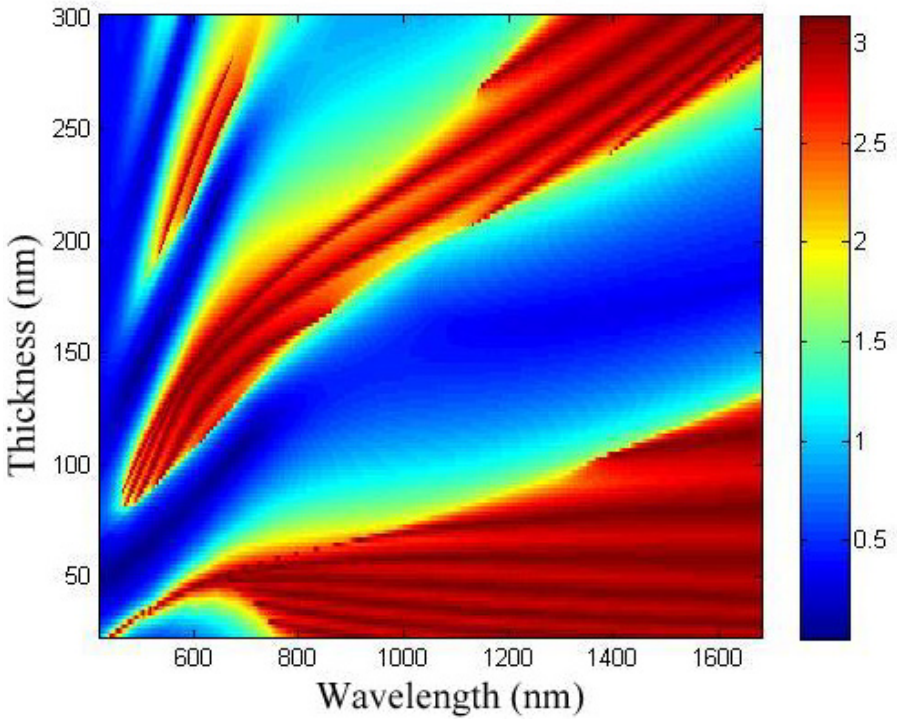

Figure 7.1: Maximum $\arg(z_r)$ obtained (in radians) for different combinations of wavelength and film thickness.

In summary, for VO_2 on glass, a 100 nm thick layer was selected for experiments in the wavelength range of 400 nm to 1700 nm. And all experiments must be performed at the incidence angle from 65°C to 75°C to achieve a high relative phase shift. The following part will present the experimental results under the above conditions.

As stated in Chapter 6, the purpose of this study is to use a VO_2 thin film to control polarization of light based on the large change in refractive indices at different VO_2 states. The combination of polarization change with transmission through a polarizer can create very high intensity ratios. This can be achieved if the light reflected on VO_2 sample in one of the VO_2 states is linearly polarized light. Because of this, we attempted create linear polarization for the reflected light at low temperature and researched conditions to have a polarization at high temperature which is as different as possible.

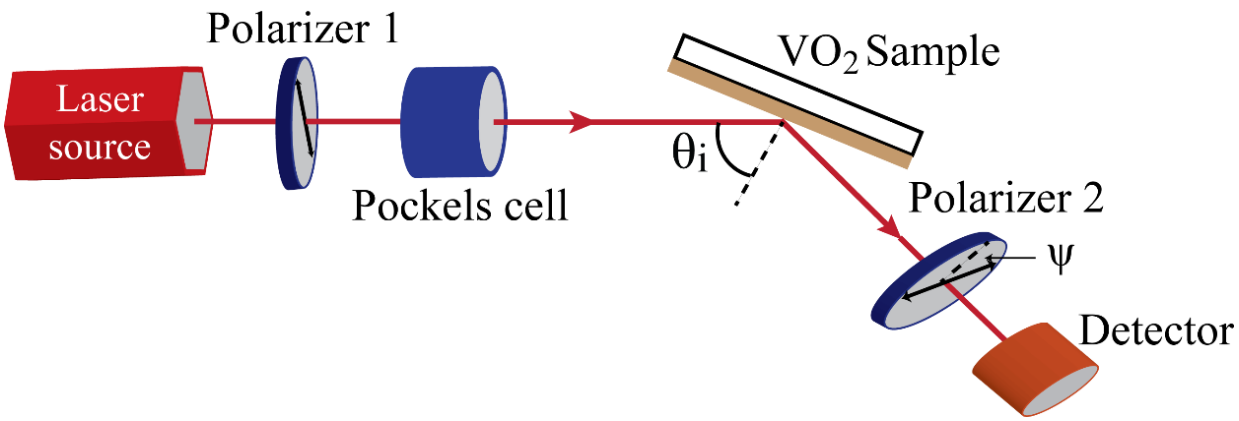

Figure 7.2: Experimental setup for controlling light polarization.

The setup in Figure 7.2 was used to examine the polarization of light reflected on VO_2 sample at the insulating and metallic states. We used different wavelengths, from 500 nm to 1700 nm, for our experiments. All came from the laser sources listed in Table 7.1. The first optical device on the path of laser beam is polarizer 1. By rotating this polarizer, we adjust the ratio between amplitudes of s- and p- components of the electric field. And because the phases of s- and p- components changes by different amounts when reflected on the sample, to create reflected linear polarization we need to use a phase compensator. A KD*P Pockels cell (Cleveland Crystals XQ1020) mounted on a sample holder is used for this purpose. It is easy to adjust the phase between them by tilting the angles of the Pockels cell. The polarization of light after reflection is analyzed through a second polarizer (Thorlab model LPNIR050; extinction ratio, 1000:1 for 650-2000 nm or Thorlabs LPVISE2X2) and a photodetector (LaserMate-Q Power Meter or Thorlab DET36A). Both devices are connected to the computer which can control the orientation angle ψ of the polarizer and collects the corresponding light intensity.

Table 7.1: Laser sources used in this study.

Wavelength (nm)	Laser source
514	Argon laser, Coherent 90C-A6
532	Nd:YAG laser, EKSPLA PL2143A
543.5	HeNe laser, Coherent 31-2298-000
632.8	HeNe laser, Coherent 25-LHP-073-249
832	Diode laser, Melles Griot 56ICS115
1068	Nd:YAG laser, EKSPLA PL2143A
1310	Diode laser, Thorlab LPS-1310-FC
1550	Diode laser, Qphotonics QDFBLD-1550-50N

Samples of VO_2 for this study were made by the method described in Chapter 4. The vanadium layers were deposited onto substrates of Corning glass, quartz and Zerodur, a glass ceramic with low thermal expansion. Their thicknesses are shown in Table 7.2.

Table 7.2: Thickness of samples used in this study.

Substrate	Thickness
Zerodur	50 nm
Corning Glass	110 nm
Quartz	150 nm

Figure 7.3 shows results obtained at 633 nm with the VO_2 on Zerodur sample. Transmitted intensity versus polarizer 2 orientation angle at temperatures below and above the transition temperature are given in polar coordinates. The whole experiment was done at incidence angle

$\theta_i = 75^o$. At low temperature (25°C), the reflected light is linearly polarized at $\alpha = 50^0$ but at the high temperature of 85°C, the linear polarization transforms to elliptical polarization with the new orientation angle of $\alpha = 140^o$. The relative phase difference between s- and p- components of electric field $\arg(z_r)$ in Eq. 3.46 can be expanded as

$$arg(z_r) = arg\left(\frac{r_{H,s}}{r_{H,p}}.\frac{r_{L,p}}{r_{L,s}}\right) = arg\left(\frac{r_{L,p}}{r_{L,s}}\right) - arg\left(\frac{r_{H,p}}{r_{H,s}}\right) \quad (7.1)$$

$$= (\varphi_{L,p} - \varphi_{L,s}) - (\varphi_{H,p} - \varphi_{H,s}) = \delta_{L,sp} - \delta_{H,sp} \quad (7.2)$$

where $\delta_{L,sp}$ and $\delta_{H,sp}$ are phase difference between s- and p- component of reflected electric field at low and high temperatures, respectively. In the case for low temperature, the light beam is linearly polarized so $\delta_{L,sp} = 0$, this leads to $arg(z_r) = -\delta_{H,sp}$. The calculation steps based on Eq. 3.59 give $\Delta = |arg(z_r)| = 0.78\pi$, this result is near the predicted value 0.89π by the model in Figure 3.8 and the data of Figure 6.2. This difference may be due to deviations in the values of refractive indices and thickness of the VO_2 film in the ellipsometry measurements.

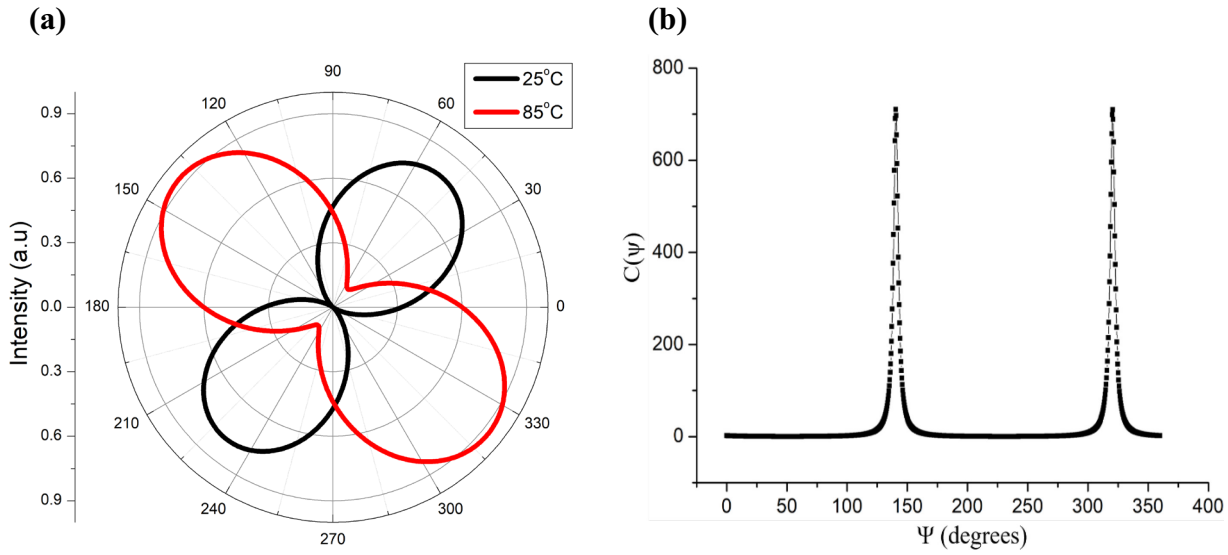

Figure 7.3: (a) Reflected light intensity at 633 nm and 75° incidence angle transmitted through polarizer 2 with VO_2 on Zerodur sample in its insulating state (black) and metallic state (red), (b) Intensity ratio between the two results versus polarizer angle.

The experimental results of Figure 7.3 also show that the reflected orientation polarizations at the high- and low-temperature states are perpendicular to each other as desired for optical switching applications discussed in Section 6.2. The relative light intensity passing through the polarizer at a given angle ψ between two states can be rewritten from Eq. 6.1 as

$$R(\psi) = \frac{S(T_H, \psi)}{S(T_L, \psi)} \tag{7.3}$$

where S is the photodetector signal, and $T_H > T_{MIT} > T_L$. $R(\psi)$ is plotted in Figure 7.3(b) showing a large modulation peak at $\psi = 140^o$, where the polarizer is orthogonal to the linearly polarized light at low temperature. The maximum contrast ratio is achieved for the case of this experiment is 700. This ratio would be sufficient for many optical switching applications. Also, note that the intensity of reflected light in both VO_2 states is almost unchanged while the polarization seems to rotate by 90°.

Similar experiments for different incidence angles from 72° to 77° also were performed on the same VO_2 on Zerodur sample, Figures 7.4-7.8. In all cases, more than two orders of magnitude for maximum contrast ratio are achieved. Especially in the case of a 73° incidence angle in Figure 7.5, the maximum contrast ratio reaches values of 4000, although the total reflected intensity at high temperature is many times smaller than that at low temperature. However, the maximum contrast ratio can depend on the quality of the polarizer and the sensitivity of the detector. Besides, when collecting the data from the experiments, an appropriate intensity of the incoming light must be selected so that minimum and maximum reflected intensities are in a same detector range. This causes some difficulties in collecting accurate data.

The experimental results below also show that the angle of incidence not only affects the relative phase shift but also affects the total reflected intensities very much. For example, the ratio

between reflections at high- and low-temperatures is 0.1 for the case of a 72° incidence angle while this value is 9 for the case of a 77° incidence angle.

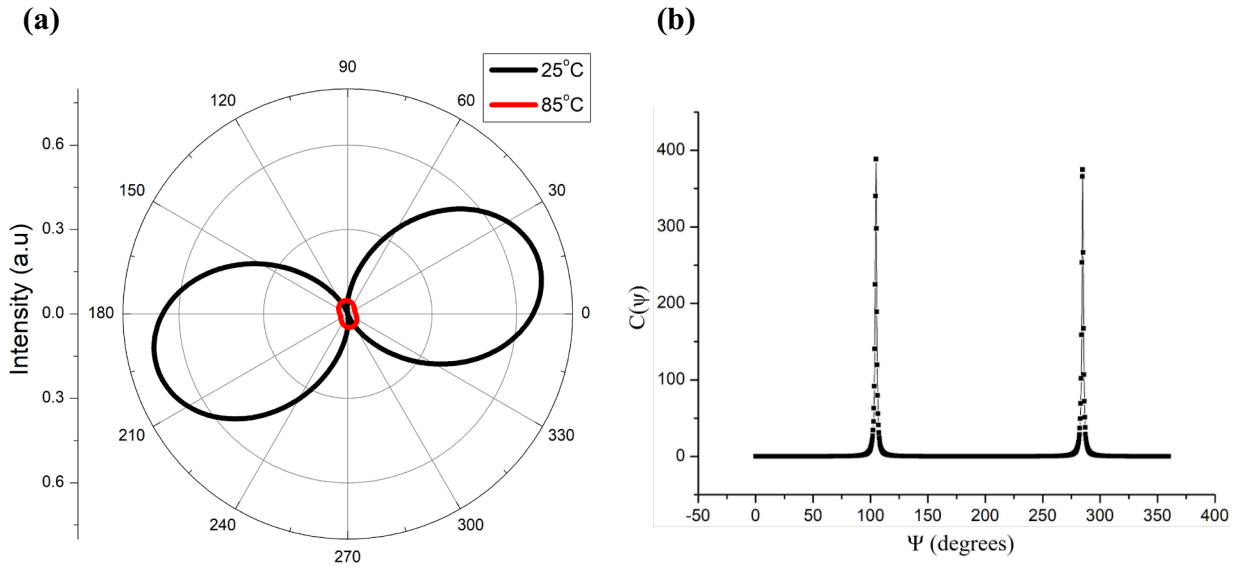

Figure 7.4: (a) Polarization states of reflected light at 633 nm and 72° incidence angle using VO_2 on Zerodur sample and (b) the corresponding contrast ratio.

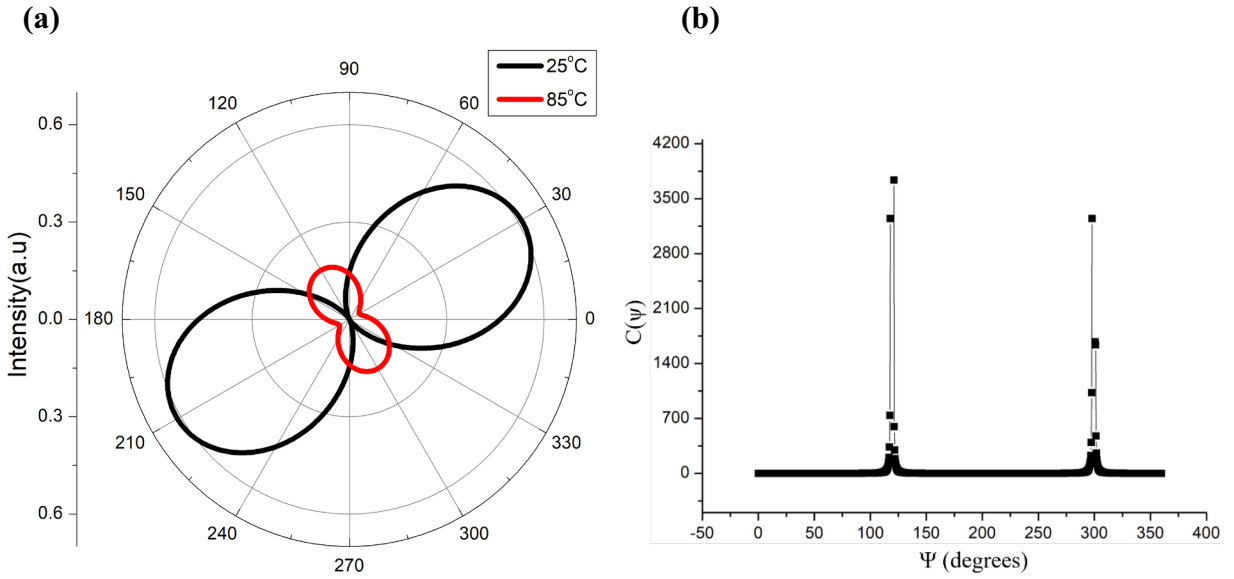

Figure 7.5: (a) Polarization states of reflected light at 633 nm and 73° incidence angle using VO_2 on Zerodur sample and (b) the corresponding contrast ratio.

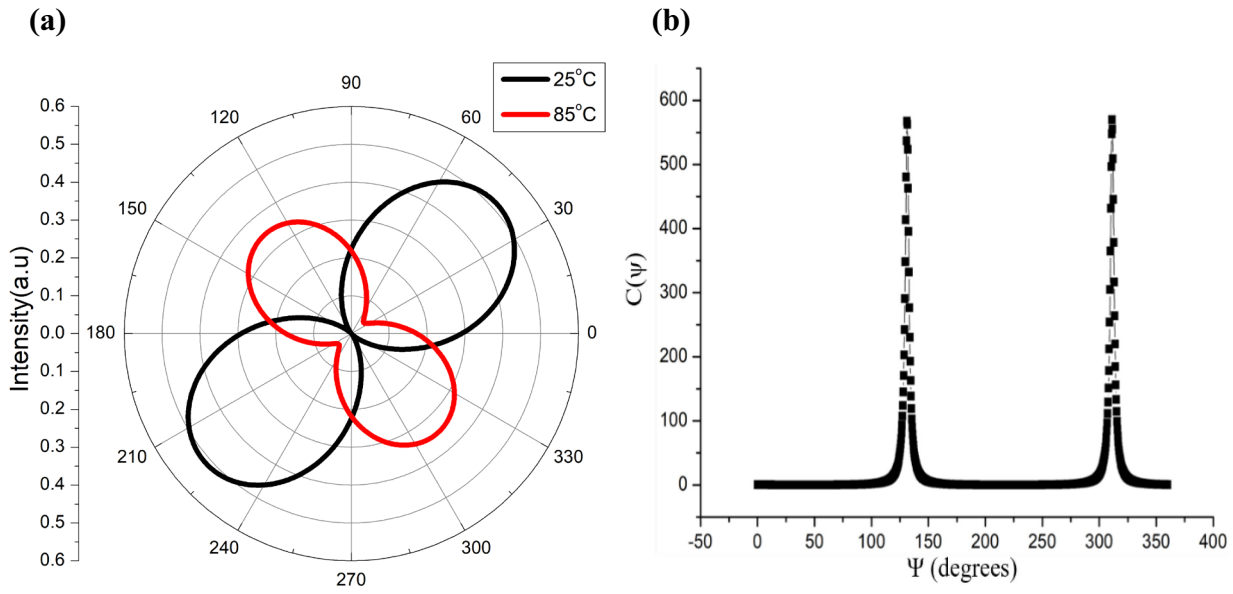

Figure 7.6: (a) Polarization states of reflected light at 633 nm and 74° incidence angle using VO_2 on Zerodur sample and (b) the corresponding contrast ratio.

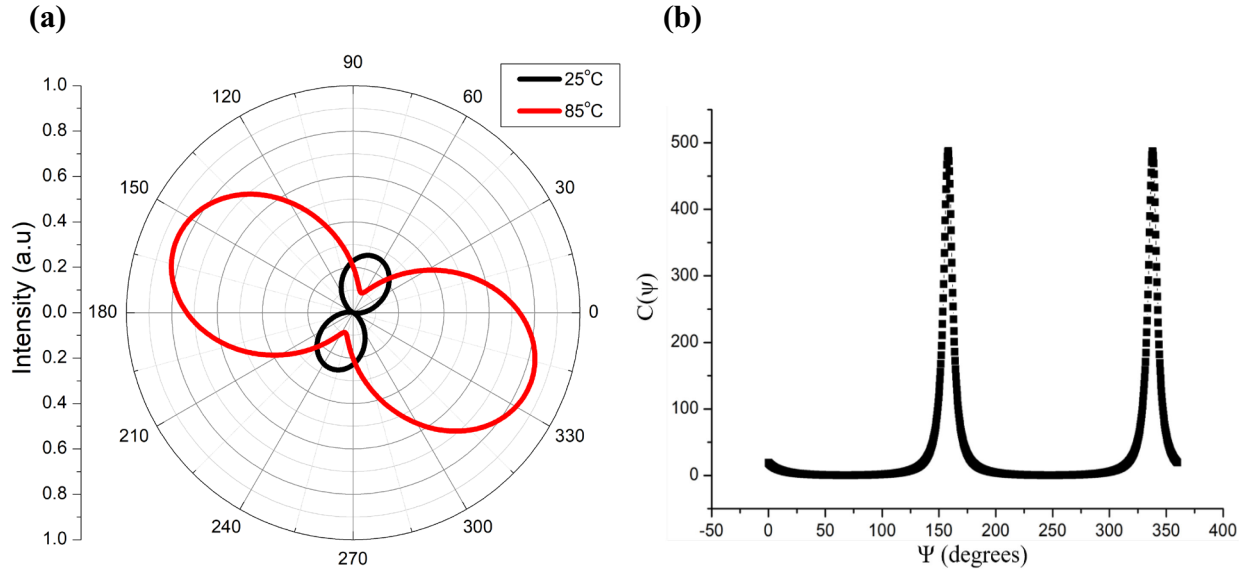

Figure 7.7: (a) Polarization states of reflected light at 633 nm and 76° incidence angle using VO_2 on Zerodur sample and (b) the corresponding contrast ratio.

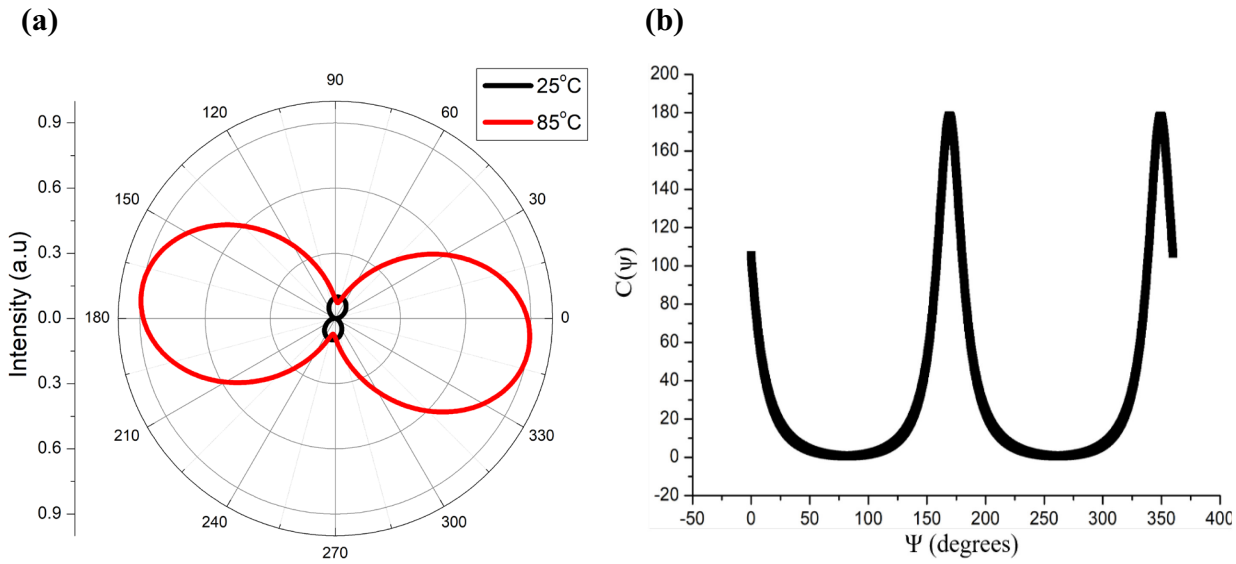

Figure 7.8: (a) Polarization states of reflected light at 633 nm and 77° incidence angle using VO_2 on Zerodur sample and (b) the corresponding contrast ratio.

Using the same VO_2 on Zerodur sample, we performed experiments with 1550 nm infrared light. To match the new wavelength, appropriate polarizers (Thorlabs model LPNIR050) and infrared detectors are used in the setup of Figure 7.2. The incidence angles from 68° to 76° are selected for the experiments based on the calculation in Figure 6.3(a). All experimental results at the 1550 nm wavelength are presented in Figures 7.9, 7.10, 7.11, 7.12 and 7.13. In all cases, the orientations of polarizations at the low- and high-temperature are perpendicular to each other. For experiments at 68° and 76° incidence angles, the linear polarization at low temperature transforms to elliptical polarization with the relative phase shifts 0.6π and 0.64π, respectively. Meanwhile, the relative phase shifts for 70°, 72° and 74° incident angles are quite high at 0.85π, 0.87π and 0.77π, respectively. Thus, both polarizations at the low- and high-temperatures are almost linear.

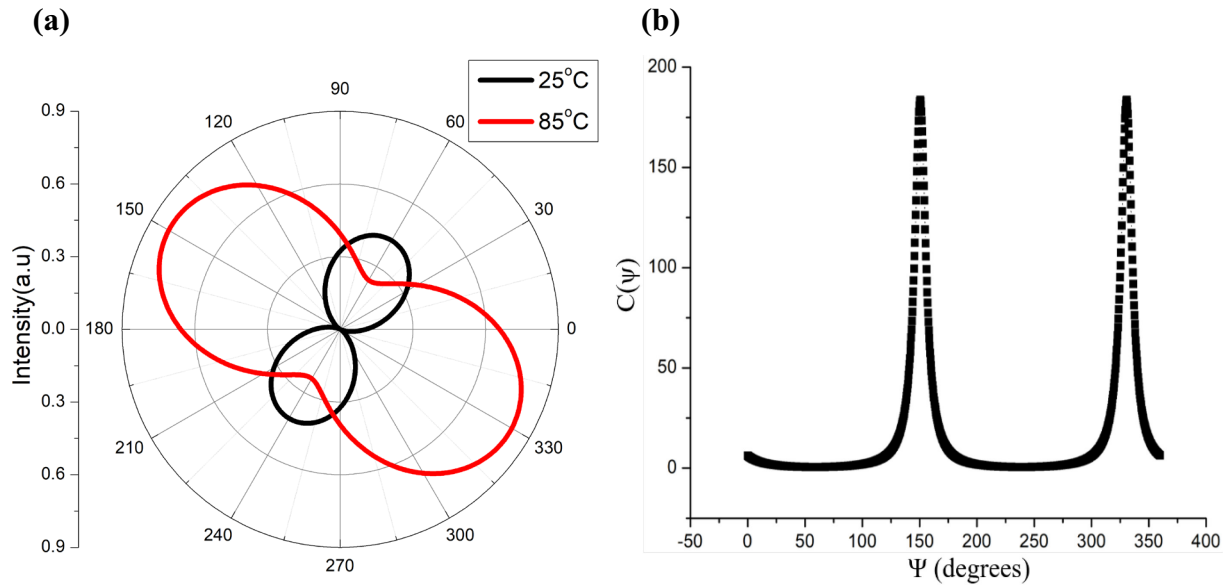

Figure 7.9: (a) Polarization states of reflected light at 1550 nm and 68° incidence angle using VO_2 on Zerodur sample and (b) the corresponding contrast ratio.

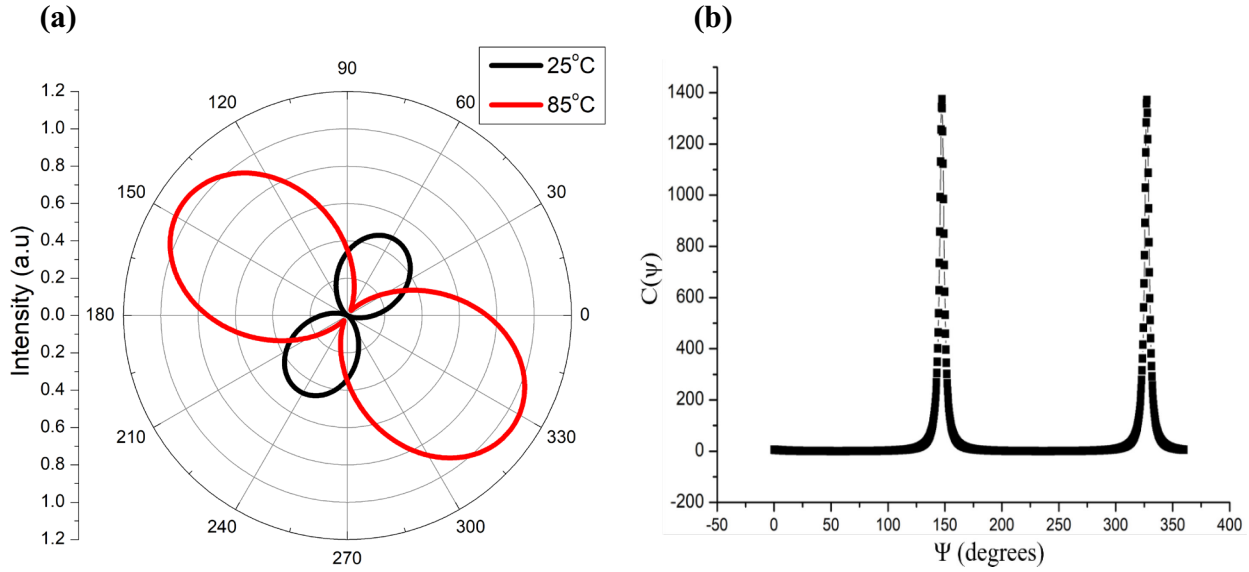

Figure 7.10: (a) Polarization states of reflected light at 1550 nm and 70° incidence angle using VO_2 on Zerodur sample and (b) the corresponding contrast ratio.

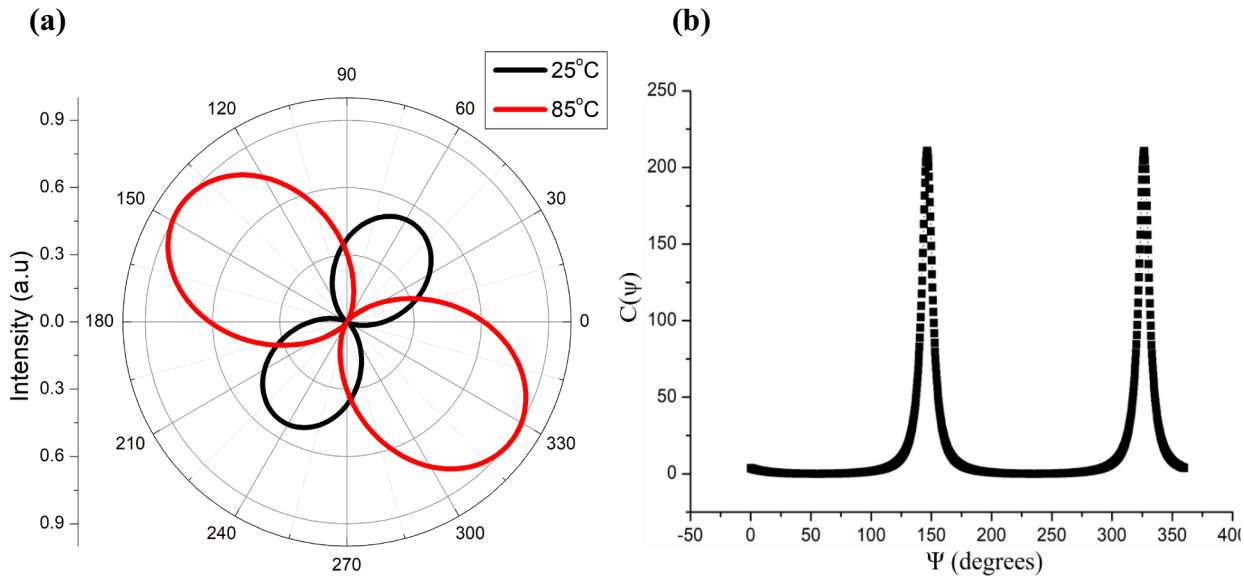

Figure 7.11: (a) Polarization states of reflected light at 1550 nm and 72° incidence angle using VO_2 on Zerodur sample and (b) the corresponding contrast ratio.

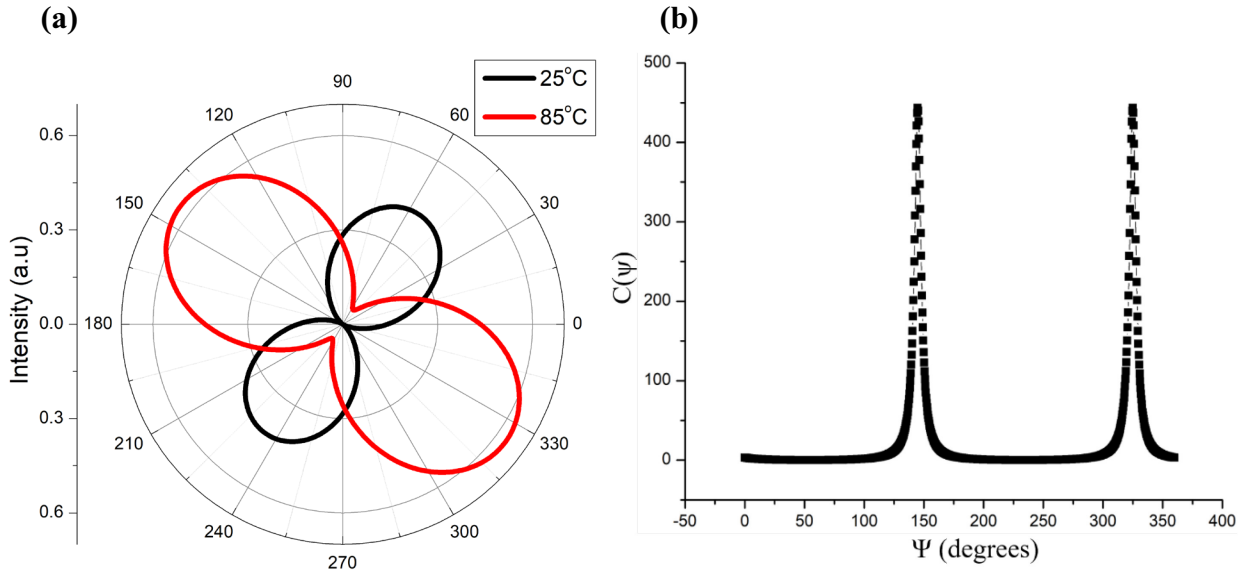

Figure 7.12: (a) Polarization states of reflected light at 1550 nm and 74° incidence angle using VO_2 on Zerodur sample and (b) the corresponding contrast ratio.

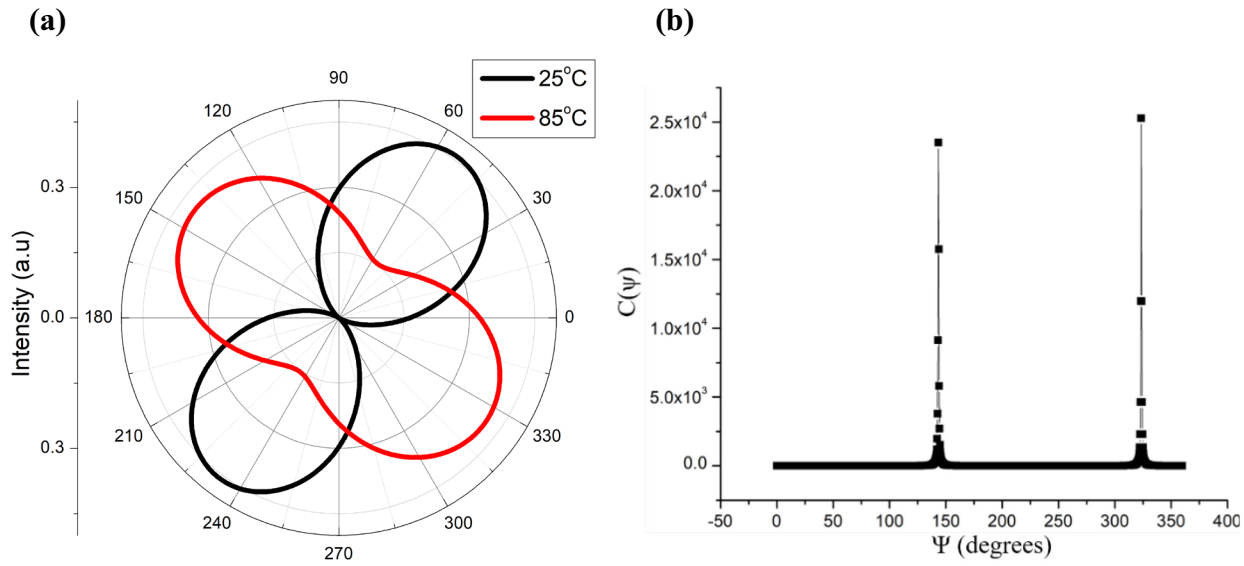

Figure 7.13: (a) Polarization states of reflected light at 1550 nm and 76° incidence angle using VO_2 on Zerodur sample and (b) the corresponding contrast ratio.

Similar experimental results were also obtained with the VO_2 on glass substrate. At 1550 nm wavelength and 74° incidence angle, the thickness of VO_2 film is not optimal for rotation of linear polarization. However, with the relative phase shift of 0.56π, the linear polarization at low temperature can transform to elliptical polarization with a 90° rotation, and the maximum contrast ratio is still very high. It reaches up to early 800, as shown in Figure 7.14.

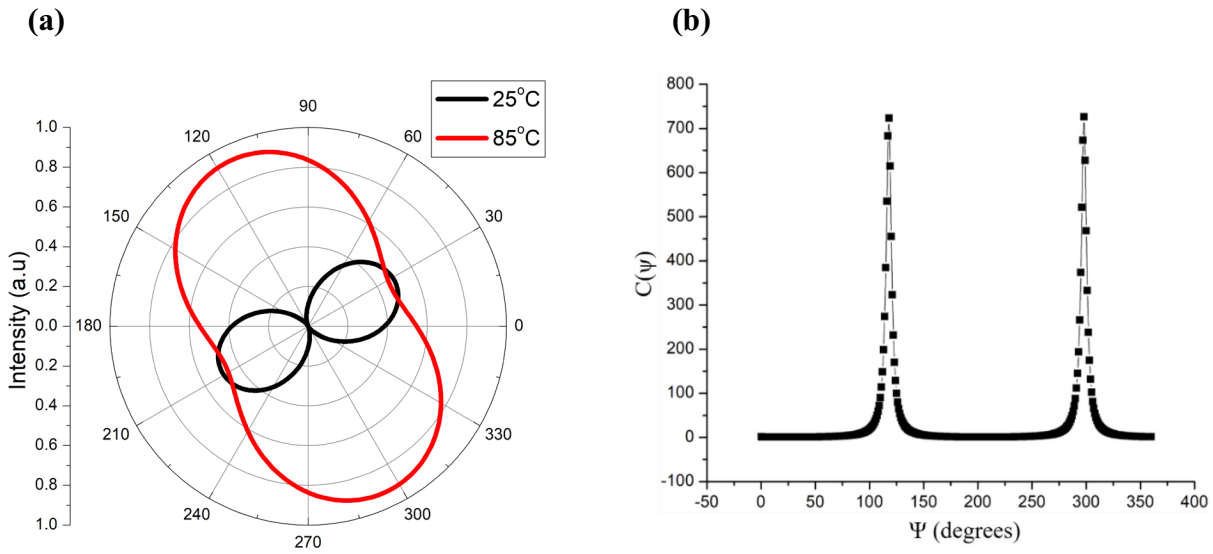

Figure 7.14: (a) Polarization states of reflected light at 1550 nm and 74° incidence angle using VO_2 on Corning glass sample and (b) the corresponding contrast ratio.

In Figure 7.15, results obtained with the VO_2 on quartz with light at 633 nm and $\theta_i = 68^o$ shows transformation between linear to circular polarization. The relative phase shift in this case is 0.49π, which is suitable for some applications as discussed in Section 3.3. The contrast ratio reaches a maximum value of 500 at the angle 160° where the polarization of electric field at low temperature is orthogonal to the transmission axis of the polarizer.

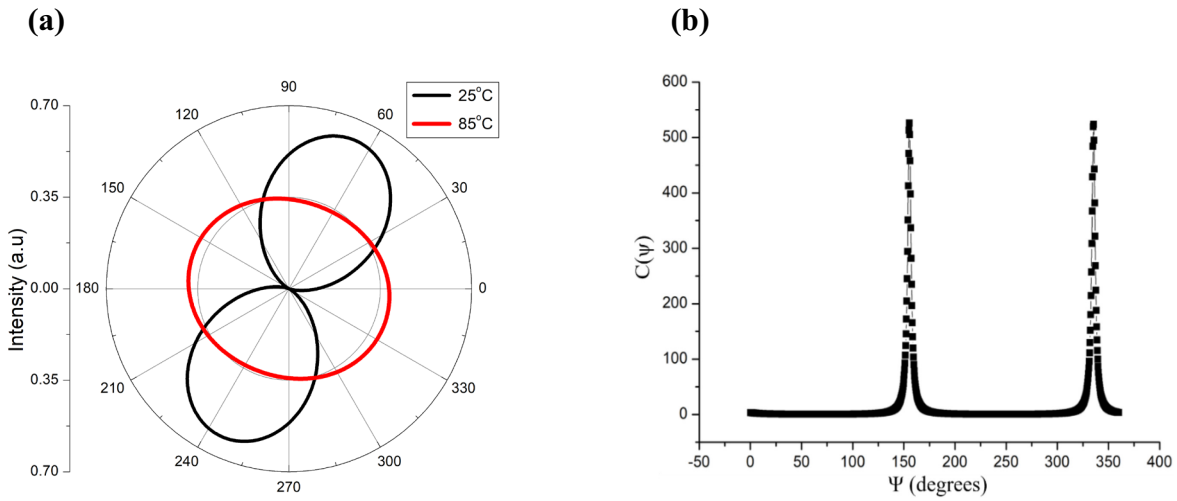

Figure 7.15: (a) Polarization states of reflected light at 633 nm and 68° incidence angle using VO_2 on quartz sample and (b) the corresponding contrast ratio.

Several other VO_2 samples were tested near the center of the visible spectrum, at a wavelength of 514 nm, where theory predicts it is difficult to alter polarization because of small changes in refractive indices [80], [83]. The phases of s- and p- components of electric field are nearly unchanged during the VO_2 phase transition. For example, the experimental results as shown in Figure 7.16 for the VO_2 on Zerodur sample at $\theta_i = 74^o$, the relative phase shift only achieves 0.05π. As a result, the polarization at the high temperature is still linear and the orientation angle only changes slightly by 5^o. Yet a maximum contrast ratio of 8 still can be achieved.

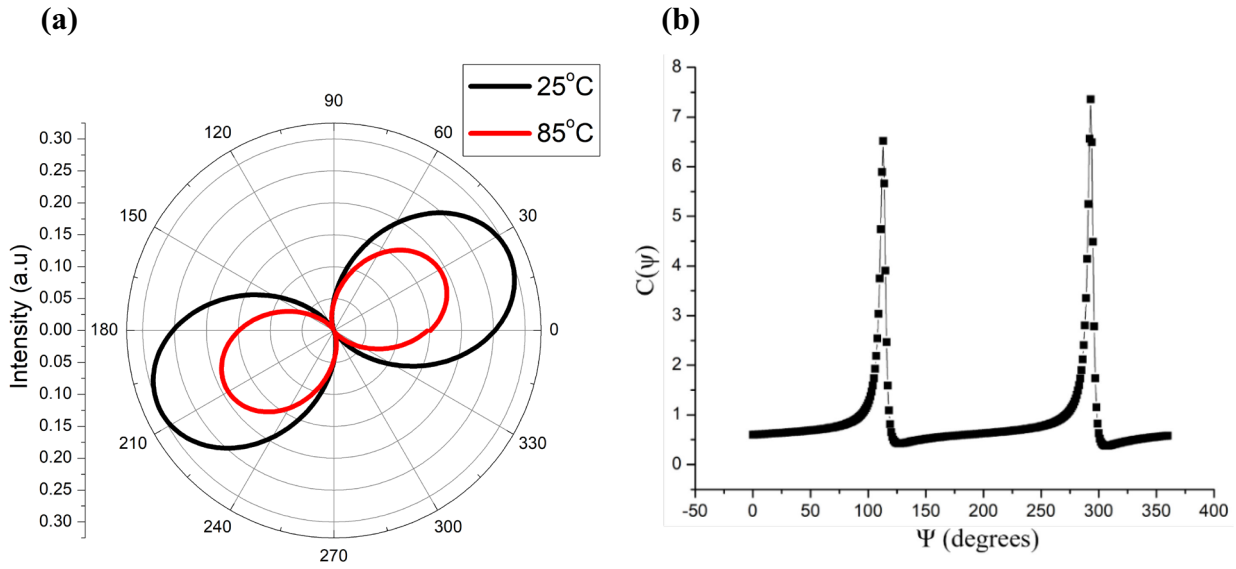

Figure 7.16: (a) Polarization states of reflected light at 514 nm and 74° incidence angle using VO_2 on Zerodur sample and (b) the corresponding contrast ratio.

To summarize this chapter, we have demonstrated theoretical and experimental results in controlling light polarization by using thin films of VO_2 activated thermally. Large changes in the refractive index of VO_2 films during phase transition cause the amplitude and phase of s- and p-components of the reflected light to change significantly. This makes the polarization states of light reflected on the sample sensitive to the state of the material. Under certain conditions, a linear

polarization at room temperature can be transformed into a new polarization state. This effect has the following advantages:

1. The polarization state of light is controlled by a simple (i.e. unpatterned) and single layer VO_2 with thicknesses around 100 nm. This is much thinner than liquid crystals (micrometers thick) and materials using the electro-optic effect (milimeters to centimeters thick).
2. The effect works in reflection.
3. The concept is suitable for a wide spectral range from the mid-visible to the infrared.
4. High light contrast ratios are obtained when VO_2 samples are combined with a polarizer. This opens new possibilities for creating high-performance modulator.

CHAPTER 8

Polarization modulation by optical activation

In the previous chapter, the changes in refractive indices of VO_2 during the phase transition have been shown to have great potential for phase retarders, polarization rotators or efficient modulation switching applications such as optical switches. But those electronic devices are required to operate at speeds as high as possible to process more information, whereas thermal activation is very low. Therefore, in this chapter we will concentrate on studying the response speed of VO_2 thin films. To carry out this study, we need to activate the phase transition rapidly by using optical pumping. The processes occurring in VO_2 film right after interacting with pump laser were discussed in Section 2.4. In general, there are two main processes at play. The first process occurs within about 1 picosecond and transforms completely the structure of VO_2 from insulator to metal. The second process takes place between nanoseconds to a few hundreds of microseconds and restores the structure to its original state. This recovery time depends very much on the pump laser intensity and the properties of the substrates. The study in this chapter was done in two stages.

- First, we used a picosecond pulsed laser to activate the phase transition in VO_2 samples and tried to repeat the same experiment as described in Chapter 7.
- Second, we measured the response time of VO_2 films deposited on Corning glass, quartz, sapphire, and Zerodur substrates.

The results and analysis of this study will be presented in the following sections.

8.1 Polarization changes by optically activated VO_2

To investigate the ability of using optically activated thin films of VO_2 in changing the polarization state of light, we modified the setup in Figure 7.2. The main laser source, a Q-switched

Nd:YAG laser, was used in the setup to provide both the pump and probe beams for the experiments. This source produces pulses at a repetition rate of 5 Hz. The probe beam at 1064 nm has a pulse duration of 215 ps (FWHM) and a weak tail that extends to 1 ns, as shown in Figure 8.1. The second-harmonic emission at 532 nm produced by a K*DP nonlinear crystal inside the laser was used as a pump beam to induce a phase transition in VO_2. Another change in the setup was to link the photodiode (Thorlab_DET36A) to an oscilloscope (Tektronix_DPO 2014B) which helps measure the light intensity at high speeds.

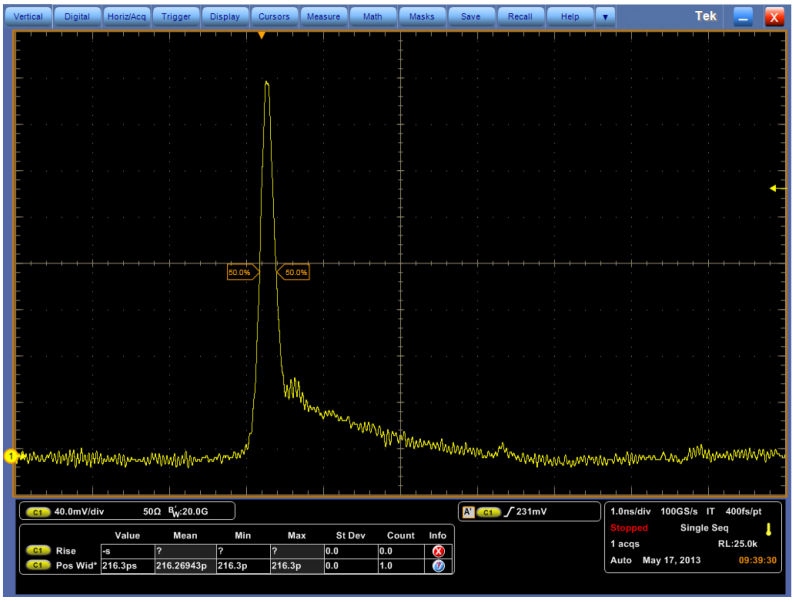

Figure 8.1: Profile of the 1064 nm probe pulse from the Nd:YAG laser.

The polarizer 1 in Figure 7.2 was replaced by a half-wave plate in order to rotate the linearly polarized probe beam to the desired angle. A filter (Melles Griot AG-780) was placed in front of the detector to cut all intensity of the strong pump beam. The optical path length of the pump beam can be adjusted by a delay line which consists of two right-angle prisms, as shown in Figure 8.2. The distance between mirrors will determine the time difference of the arrival of the probe and pump pulses onto the sample.

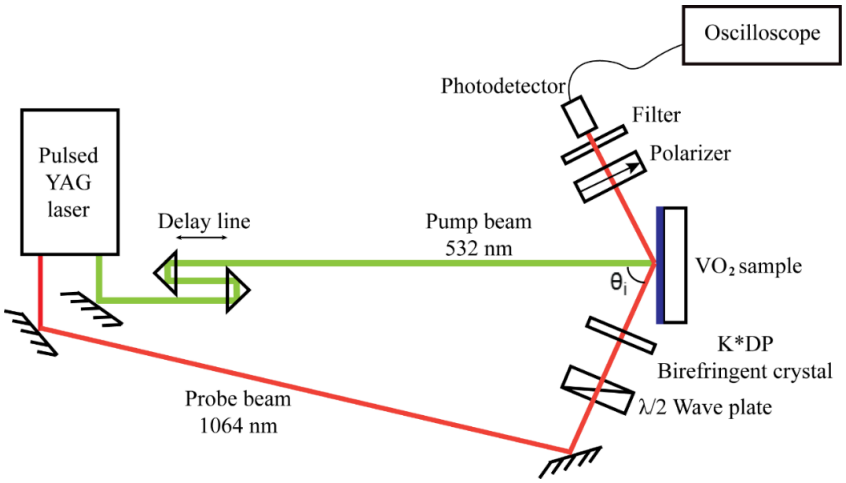

Figure 8.2: Pump and probe setup for optical activation of VO_2 and polarization change measurements.

In the experiments to control polarization, we adjusted the delay line so that the probe and the pump pulses arrived at the sample at the same time (zero delay). The size of the pump beam on the sample was chosen to be larger than that of the probe beam in order to make sure that the whole probe beam interacts with an activated VO_2 film. Light intensity was measured through the peak photodetector voltage displayed on the oscilloscope, as the angle of the polarizer is rotated.

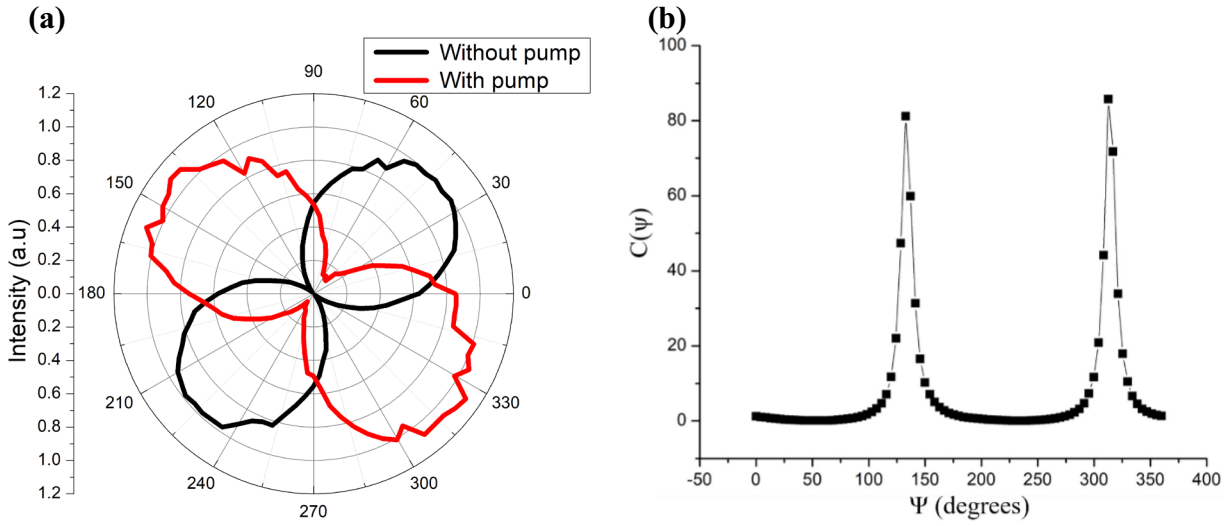

Figure 8.3: (a) Reflected probe intensity at 1064 nm measured through a polarizer as a function of polarizer angle for VO_2 on Zerodur sample, with and without pump at 532 nm (b) Intensity ratio between the intensities versus polarizer angle.

Figure 8.3(a) shows polarization states of light reflected off the VO_2 on Zerodur sample at an incidence angle of 72°. When the pump laser is off, the reflected probe beam (black curve) exhibits a linear polarization with an orientation angle at 40°. This polarization remains almost unchanged and only its axis is rotated by 90° (red curve) when the pump laser interacts with the sample. This leads to a large contrast ratio in the measured signal, as Figure 8.3(b) shows. Here, the contrast ratio as a function of polarizer angle is determined by the ratio of the signals at the photodetector between the pump laser on and off cases. At polarizer angle 130°, the contrast ratio reaches a maximum value of 80. This value can be higher if a better filter for cutting the pump beam scattering was used.

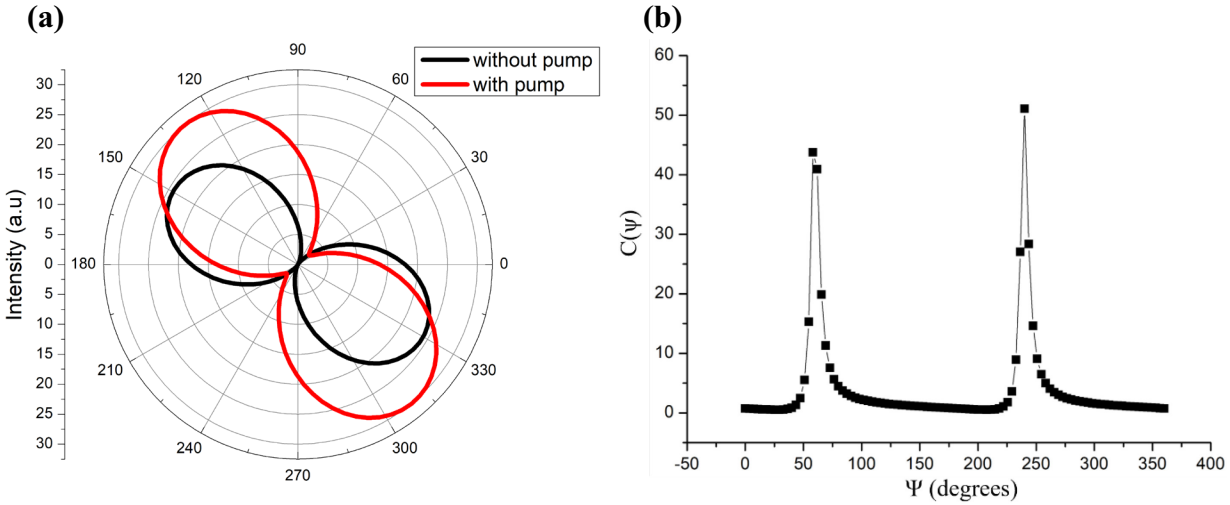

Figure 8.4: (a) Reflected probe intensity at 1064 nm measured through a polarizer as a function of the polarizer angle for VO_2 on sapphire sample, with and without pump at 532 nm (b) Intensity ratio between the two results versus polarizer angle.

The same experiments were carried out on VO_2 on sapphire substrates at 70° incidence angle. Linear polarization at 1064 nm was transformed to elliptical polarization with 20° axis rotation, as shown in Figure 8.4(a). The thickness of this sample is not optimized for the wavelength so a relative phase shift of only 0.14π was achieved after optimization of incidence

angle. However, a maximum contrast ratio of up to 50 can still be reached in reflection with polarizers.

The experimental results with the optical pumping activation are similar to the results with thermal activation described in Chapter 7. This confirms that we can use pulsed laser in experiments to change the polarization state of light. All the advantages of using VO_2 thin films in controlling polarization presented at the end of Chapter 7 remain unchanged when the sample is induced by a laser, but the dynamics is potentially much faster.

8.2 Response time of VO_2 on different substrates

To explore the applicability of VO_2 thin films in optical devices, we need to know how fast a sample can change its properties when interacting with pump laser and the time it takes to restore its initial state. This can be found by studying reflections off the sample after the sample interacts with the pump beam at a given time interval [84]. This time difference between the pump and the probe beams to the sample was made possible by adding a longer delay line in the setup, as shown in Figure 8.5.

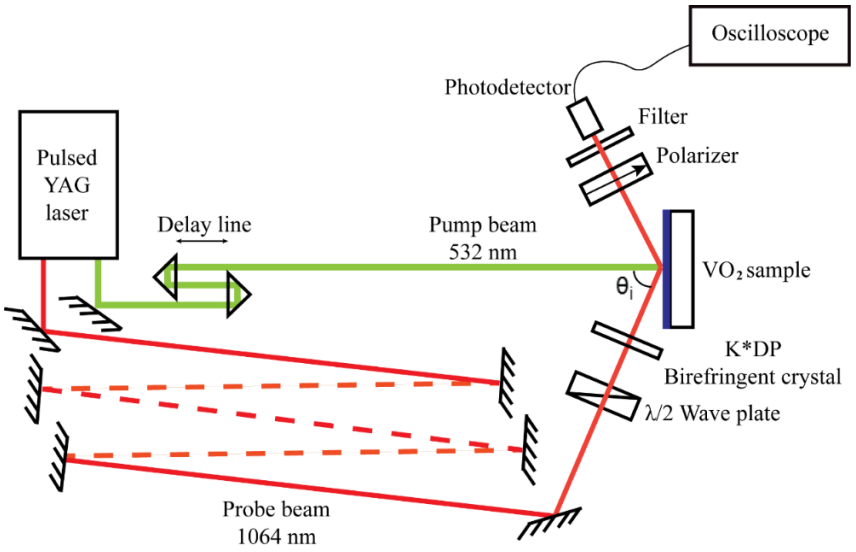

Figure 8.5: Setup for measuring rise time and recovery time of VO_2 samples under optical activation.

Let's call t_{pump} and t_{probe} are time the pump beam and the probe beam need to travel from the laser source to the sample, respectively. The probe beam arrives at the sample after the pump beam does in a delay time given by

$$t_{delay} = t_{probe} - t_{pump} = \frac{L_{probe} - L_{pump}}{c} \tag{8.1}$$

where L_{probe} and L_{pump} are optical path lengths of the probe and the pump beams, respectively, and c is the light velocity. L_{pump} can be changed slightly by the short delay line while L_{probe} is increased by allowing the probe beam to reflect on many mirrors before reaching the sample, as in Figure 8.5. The number of mirrors added to the setup determines the maximum delay time that can be measured. In practice, it is very difficult to determine $t_{delay} = 0$ through L_{probe} and L_{pump}. We only assume that $t_{delay} = 0$ when the largest change in the reflection occurs.

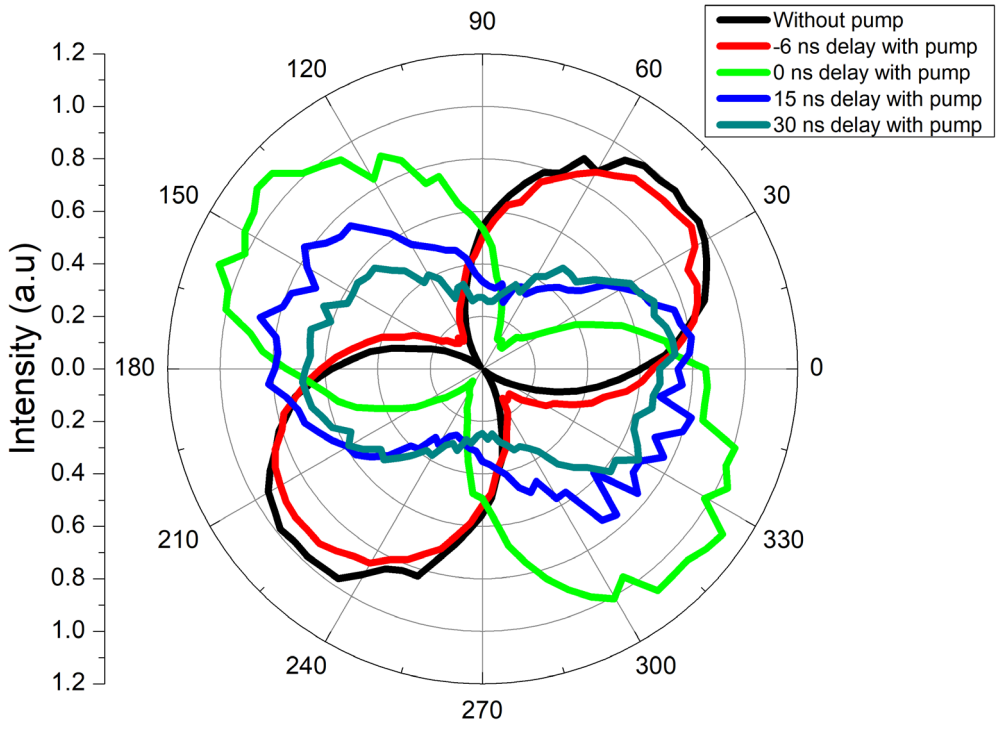

Figure 8.6: Reflected probe intensity at 1064 nm measured through a polarizer as a function of the polarizer angle for VO_2 on Zerodur at different delay times between the pump and probe beams.

To gain a better understanding of the changes inside VO_2 during the phase transition activated by pump laser as well as the reflected polarization change, we repeated the previous experiments at different delay times. The polarization dynamic is shown in Figure 8.6. From Eq. 8.1, negative (positive) delay times correspond to the probe beam arriving at the sample before (after) the pump beam. The polarization state is almost unchanged for negative delays because there is no change in VO_2 properties before interacting with the pump beam, while the properties of VO_2 change completely from insulator to metal at $t_{delay} = 0$ and the recovery happens quickly after that. At 15 ns and 30 ns delay times, the polarization state returns to initial orientation described by the black curve.

The analysis in Sections 2.3 and 2.4 shows that the transition process depends greatly on the pump intensity while the recovery process depends on the properties of substrates. In this section, we will discuss the influence of those factors to experimental results. The samples used in these experiments were made on different substrates such as Corning glass, quartz, Zerodur, sapphire. Unlike the previous experiments used to study light polarization, in our experiments we were interested in the intensity change of the probe beam under optical activation. Therefore, the setup in Figure 8.5 was simplified by removing the polarizer and the birefringent crystal K^*DP. Here, the incident probe was set to the p-polarized state for all the experiments.

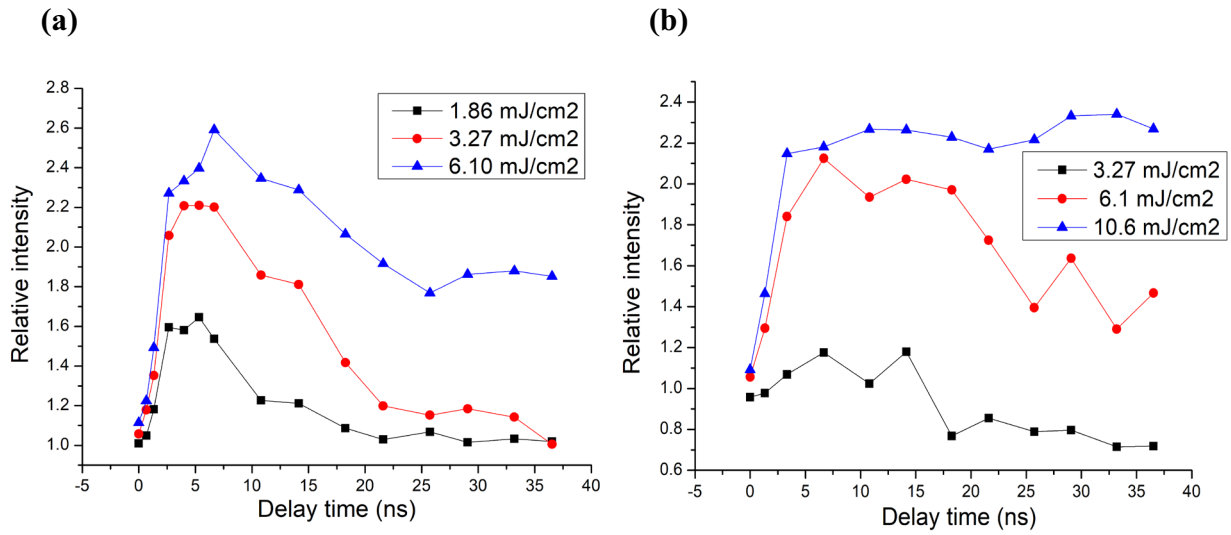

Figure 8.7: Pump-on to pump-off ratio of reflected intensity at different delay times between the pump and the probe beams, as a function of pump pulse fluence (a) for the VO_2 on sapphire sample and (b) for the VO_2 on Zerodur sample.

The effect of pump intensity on the phase transition of VO_2 is clearly demonstrated by the experimental results in Figure 8.7(a) for the VO_2 on sapphire sample and Figure 8.7(b) for the VO_2 on Zerodur sample. Here, the relative intensity is the reflected probe intensity with the pump beam on divided to reflected probe intensity without the pump beam, so that a value of 1 means no change. At low intensity, the samples do not receive enough energy to make the full transition which was checked carefully through the test with thermal activation. However, if the pump intensity is too large, VO_2 will switch rapidly from insulator to metal and keeps this state for a long period of time, as shown in Figure 8.7(b) for the case of pump fluence 10.6 mJ/cm^2. With these experimental results, we found that a pump intensity 3.2 mJ/cm^2 is suitable for the VO_2 on sapphire, glass and quartz substrates to make the full transition to metal while the VO_2 on Zerodur sample needs a little bit higher energy at 6.1 mJ/cm^2.

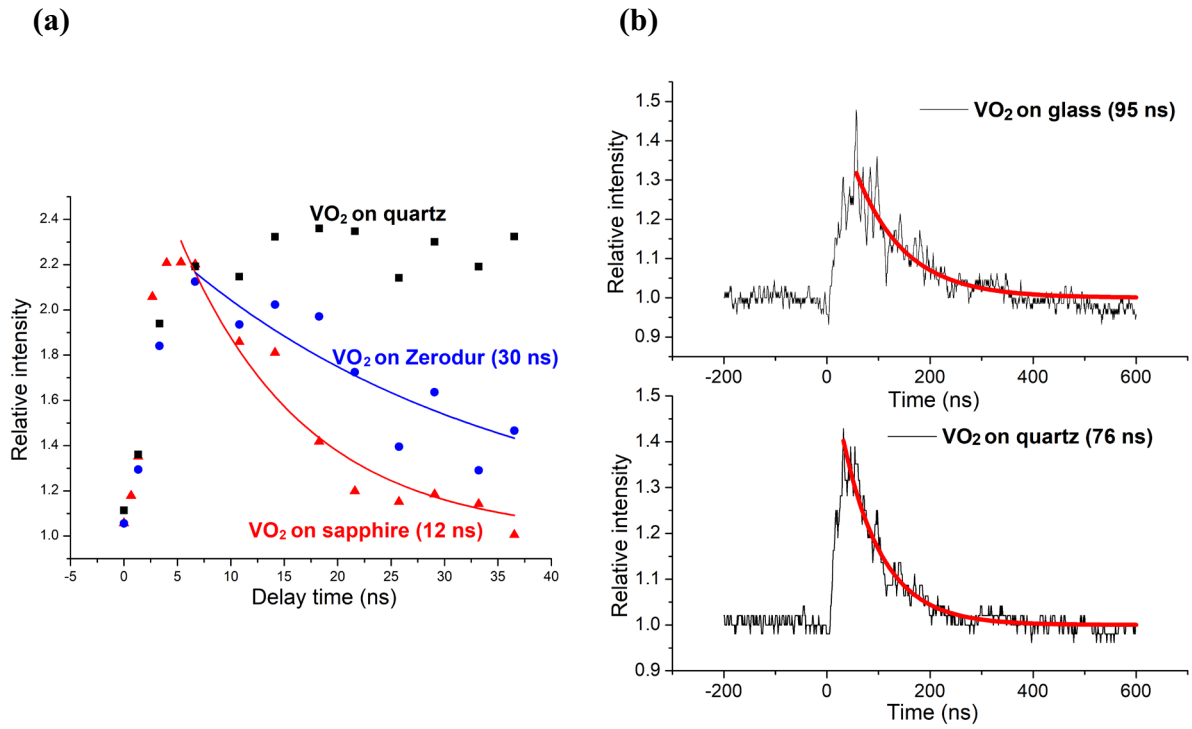

Figure 8.8: Relative reflected intensity as a function of delay time (a) with a pulsed 1064 nm probe and (b) with a continuous 832 nm probe.

For all the samples, the relative intensities take about 2 ns to reach the maximum when the pump and probes pulses overlap. This time is longer than a full-width at half maximum 215 ps of the probe pulse, this problem could be explained by the probe pulse shape, as shown in Figure 8.1. This pulse has a tail of 1 ns which contains about half the pulse energy. So, some of the energy of the probe arrives at samples before the pump does.

After reaching the peaks, the relative intensities decrease as the VO_2 samples recover to the initial state. The reflection during this recovery is modelled as an exponential decay of the form $R(t)=R_o \exp(-t/\tau)$ with τ the characteristic recovery time. This recovery time is highly dependent on the substrate, as shown in Figures 8.8(a) and 8.8(b). We obtain a relaxation time τ of 12 ns, 30 ns, 76 ns and 95 ns for the VO_2 made on sapphire, Zerodur, quartz, and Corning glass samples, respectively. These differences in relaxation time depend mainly on the heat diffusion between the

VO_2 film and the substrate. Comprehensive analysis of the effect of substrate on the relaxation time of VO_2 can be found in [85], [86].

Since the recovery times of VO_2 on quartz and on glass substrates are greater than the delay time limit of 35 ns in our pump-probe setup, a continuous laser 832 nm was used as probe beam for all experiments with these samples, as shown in Figure 8.9. In this setup, the relative reflected intensities as a function of time were measured by the 100 Mhz oscilloscope.

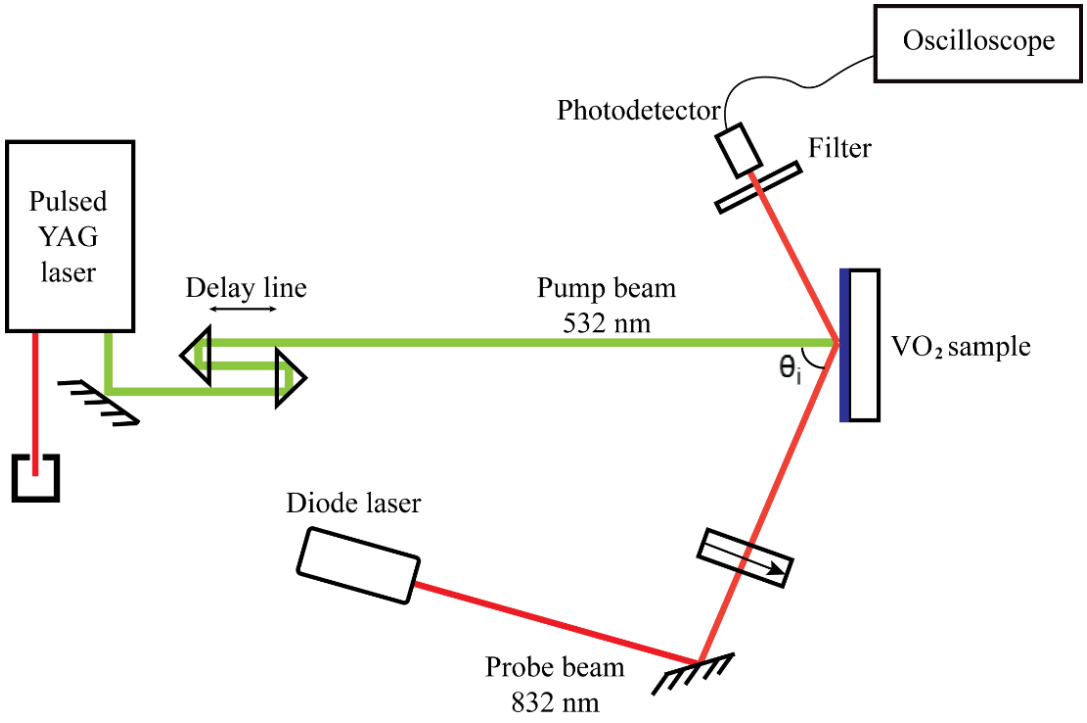

Figure 8.9: Setup with the continuous laser 832 nm for measuring recovery time of VO_2 on quartz and on glass samples.

To summarize this chapter, we changed the polarization state of reflected light by inducing a phase transition of VO_2 by mean of a pulsed laser. The experimental results have confirmed that similar polarization effects are obtained by thermal activation (Chapter 7) can be achieved by optical activation. With the ability to change the state at nanosecond time scales, VO_2 thin films demonstrate great potential for fast optical devices applications.

CHAPTER 9

Polarization modulation enhancement metallic substrates

In Chapters 7 and 8, we have demonstrated the ability of using VO_2 thin films to change the polarization state of light. And when this is combined with a polarizer, high modulation switching is achieved. In addition, with the ability to change the phase quickly along with the recovery time around nanoseconds, VO_2 thin films promise many applications in thermal sensors and optoelectronics devices. In this chapter, we enhance the properties of VO_2 samples in changing light polarization by using metallic substrates [87]. Theory and experimental results show that VO_2/metal samples can get large relative phase shifts at lower incidence angles and over a wider spectral range compared with VO_2 on dielectric samples [87]. Besides, metallic layers also tend to increase reflectance significantly. Those enhancements will be presented in the following parts.

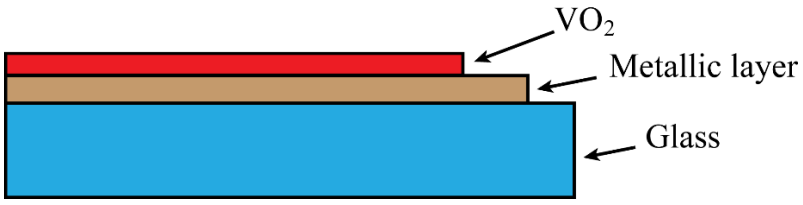

Figure 9.1: VO_2 on a metallic layer structure.

The model in Figure 9.1 was used in this part of the study to calculate relative phase shifts of reflected light for s- and p-polarizations. It includes a VO_2 layer on the top, a metallic layer and a glass substrate. The metallic layer can be made from gold, aluminum, silver, titanium, etc., and is assumed to be optically thick, so that no light interacts with the underlying glass. Figures 9.2, 9.3, and 9.4 below show calculated relative phase shifts for VO_2 on gold, aluminum, and titanium samples, respectively. Refractive indices of VO_2, gold and aluminum were experimentally measured from ellipsometry, while titanium data were taken from [88]. Compared with the result

calculated for VO_2 on glass, shown in Figure 6.3(a), the results for VO_2 on metallic layer share the following characteristics.

- The spectrum over which a π radians relative phase shift can be achieved is extended. Now, the possibility to change polarization state of wavelengths near 400 nm becomes a reality.
- Experiments can be performed at smaller incidence angles; at some wavelengths we can even achieve π radians for relative phase shift at near normal incidence angles.

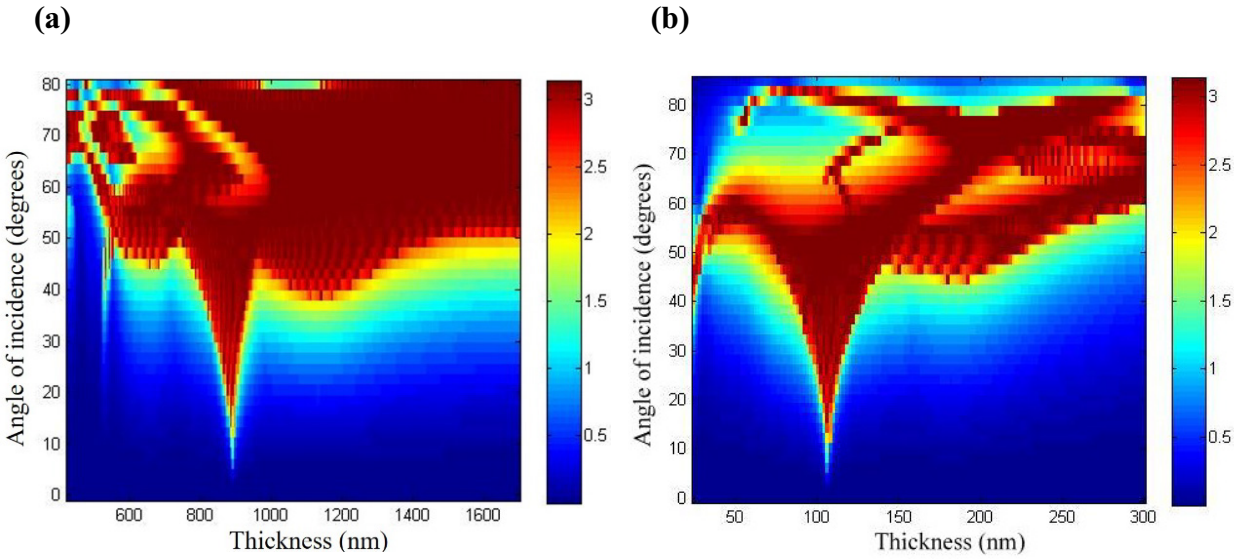

Figure 9.2: The maximum relative phase shifts calculated for VO_2 on gold film sample at (a) different wavelengths and angles of incidence (b) different VO_2 layer thicknesses and angles of incidence.

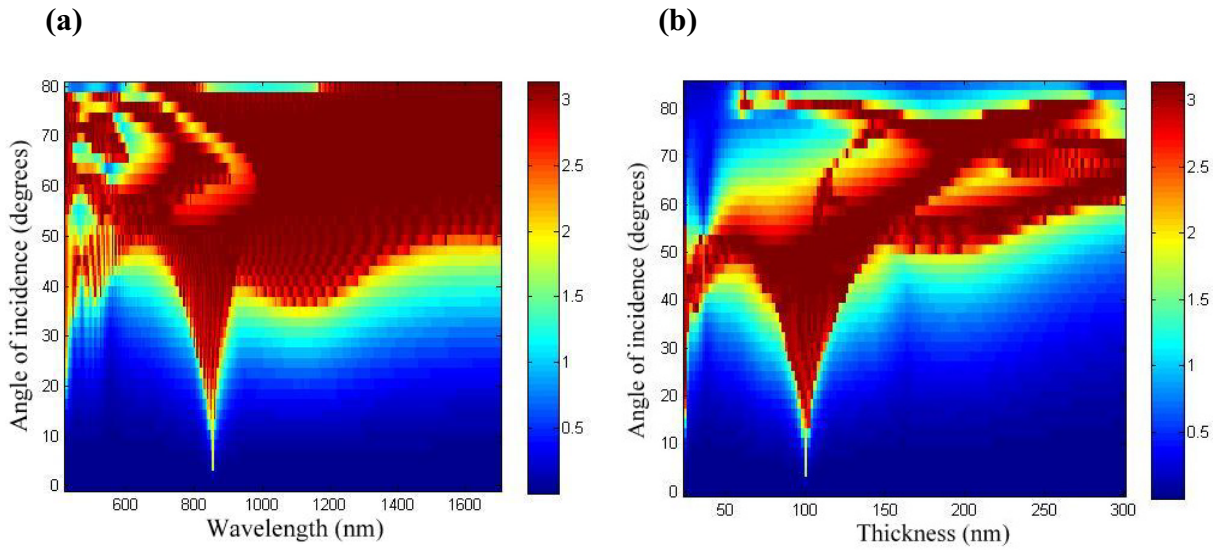

Figure 9.3: The maximum relative phase shifts calculated for VO_2 on aluminum at (a) different wavelengths and angles of incidence (b) different VO_2 layer thicknesses and angles of incidence.

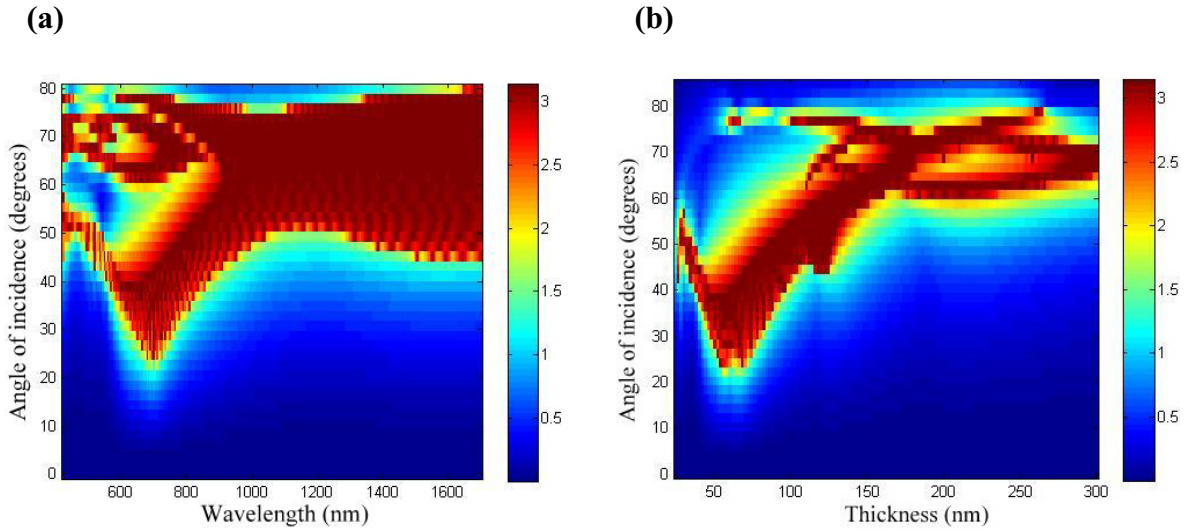

Figure 9.4: The maximum relative phase shifts calculated for VO_2 on titanium at (a) different wavelengths and angles of incidence (b) different VO_2 layer thicknesses and angles of incidence.

The calculated results for VO_2 on gold and on aluminum samples are nearly similar, with a large relative phase shift for all incidence angles in range 40^o to 80^o. Especially with wavelengths near 900 nm, the incidence angle can be reduced significantly, down to 10^o, as in Figures 9.2(a) and 9.3(a). Besides, in order to provide information about the thickness of the VO_2 layer, we also

calculated the relative phase shift at different thicknesses and angles of incidence as shown in Figures 9.2(b) and 9.3(b). For doing experiments at small angles (< 40°), the VO_2 layer thickness must be between 80 nm to 120 nm. However, this thickness is only suitable for experiments with wavelengths near 900 nm. For other wavelengths, the thickness of the VO_2 layer should be adjusted accordingly. This is clearly shown in Figures 9.5 and 9.6, which are calculated for a single wavelength. For the sample with gold substrate, the VO_2 layer thickness needs to be between 50 nm to 80 nm for doing experiment with 500 nm, while for the 1000 nm wavelength we need a thicker film in range 100 nm to 150 nm. Here, we only choose the thicknesses for small angles of incidence. Similarly, thicknesses of 150 nm to 200 nm are suitable for the 1500 nm wavelength. Compared to calculated results for the VO_2 on glass sample (see Figure 7.1), the thicknesses for those cases are increased and the ranges are extended.

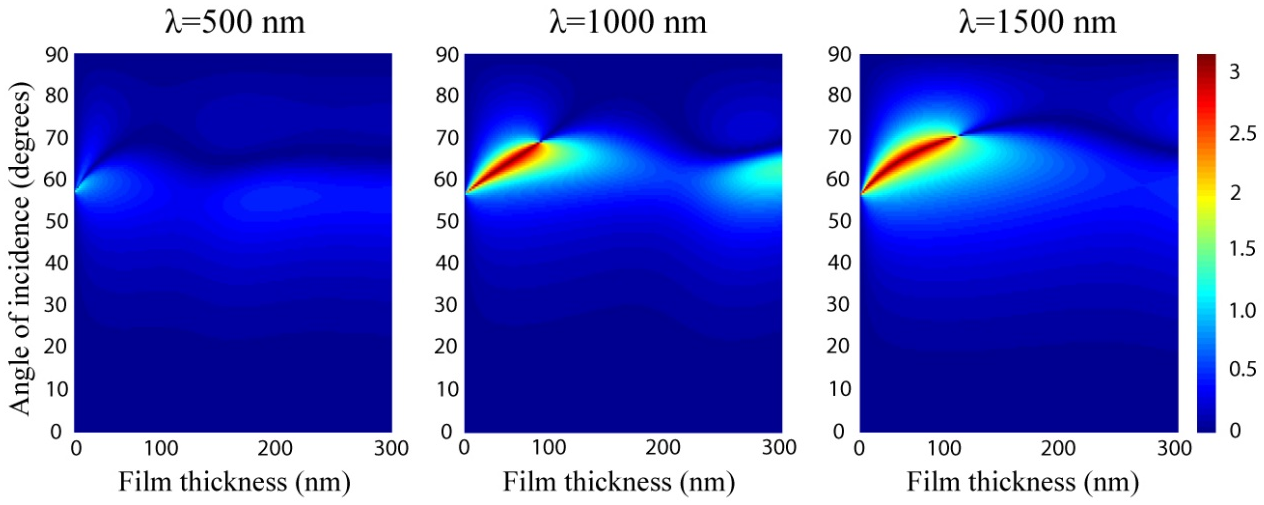

Figure 9.5: Calculated relative phase shifts for different VO_2 layer thicknesses and angles of incidence at wavelengths 500 nm, 1000 nm and 1500 nm for VO_2 on glass.

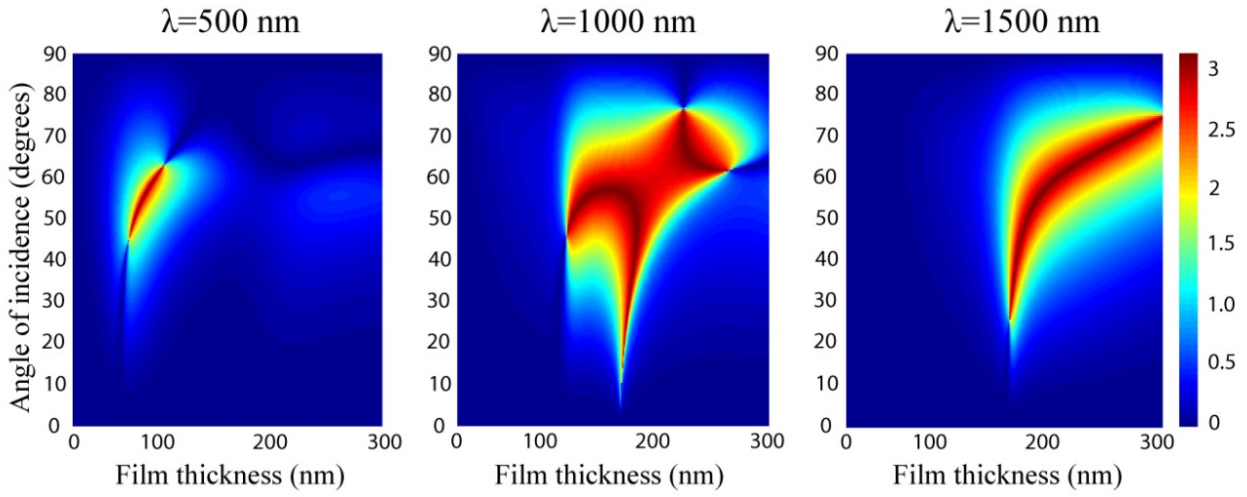

Figure 9.6: Calculated relative phase shifts for different VO_2 layer thicknesses and angles of incidence at wavelengths 500 nm, 1000 nm and 1500 nm for VO_2 on gold.

In addition to the advantages described above, the VO_2 on metal also exhibits significant enhancement of reflectivity. Calculated results in Table 9.1 shows that about 0.2 normal light intensity reflected off the VO_2 on glass sample for all film thicknesses. Meanwhile, this coefficient for the VO_2 on gold sample is 0.6 for 50 nm VO_2 thick, 0.44 for 75 nm and 0.29 for 100 nm. With thick samples (more than 200 nm), the role of metallic substrate is negligible.

Table 9.1: Calculated reflectance for 50 nm, 75 nm and 100 nm thick VO_2 layers on a gold substrate at temperatures below and above T_{MIT}.

	50 nm	**75 nm**	**100 nm**
VO_2/glass	$R_{cold} = 0.21$ $R_{hot} = 0.17$	$R_{cold} = 0.25$ $R_{hot} = 0.20$	$R_{cold} = 0.25$ $R_{hot} = 0.21$
VO_2/gold	$R_{cold} = 0.62$ $R_{hot} = 0.61$	$R_{cold} = R_{hot} = 0.44$	$R_{cold} = R_{hot} = 0.29$

For VO_2 on titanium, the minimum angle of incidence for π radians relative phase shift can be reduced to 20°, as Figure 9.4 shows. This requires a VO_2 layer with a thickness of about 50 nm

and the experiments performed at 700 nm wavelength. For most cases, an angle of incidence of 40^{o} is possible for attaining a high relative phase shift with light from visible to near infrared. Like gold and aluminum, titanium also helps to increase reflectivity significantly. In addition, it is also known for the ability to enhance the properties of VO_2 thin films as described in Section 2.3.

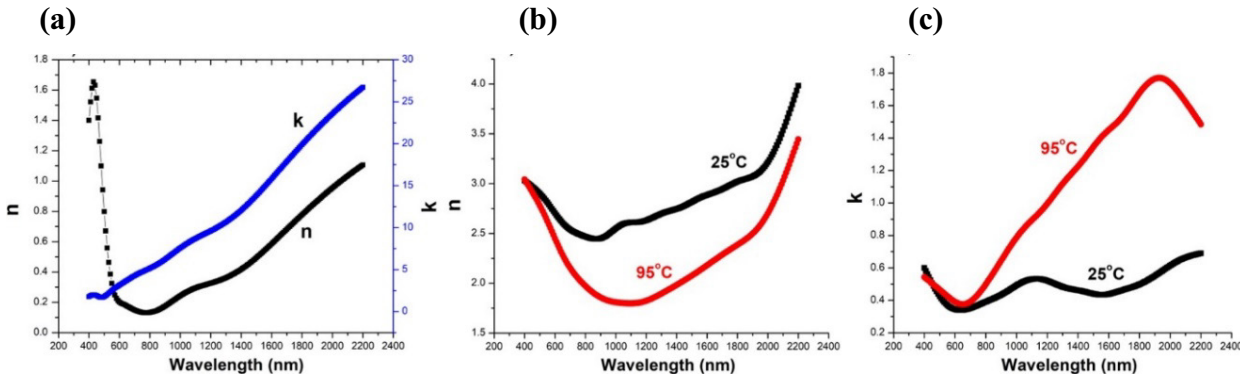

Figure 9.7: (a) Real (n) and imaginary (k) parts of the refractive indices of gold, (b) real and (c) imaginary parts of the refractive indices of VO_2 films at insulating state (25^{o}C) and metallic state (95^{o}C).

The enhancements in light polarization for VO_2 samples on metallic substrates are mainly due to absorption of the substrates, namely through the imaginary part of the refractive index. This is confirmed in calculations as shown in Figures 9.8(a) and 9.8(b). Here, we created different refractive index n and k sets for the substrate and produced maximum phase shift maps corresponding to each set for comparison. The set 1 includes all the n values of gold in Figure 9.7(a) and the k values of glass while the set 2 was created with the n values of glass and the k values of gold. Figures 9.2(a) and 9.8(b) are almost identical, indicating that the change in the value of n hardly changes the results. And the k value of metallic substrates determines angle of incidence as well as spectral range of modulation. At higher k values, the phase change of s- and p-components shift bigger amounts, details of this issue can be found in recent paper [89].

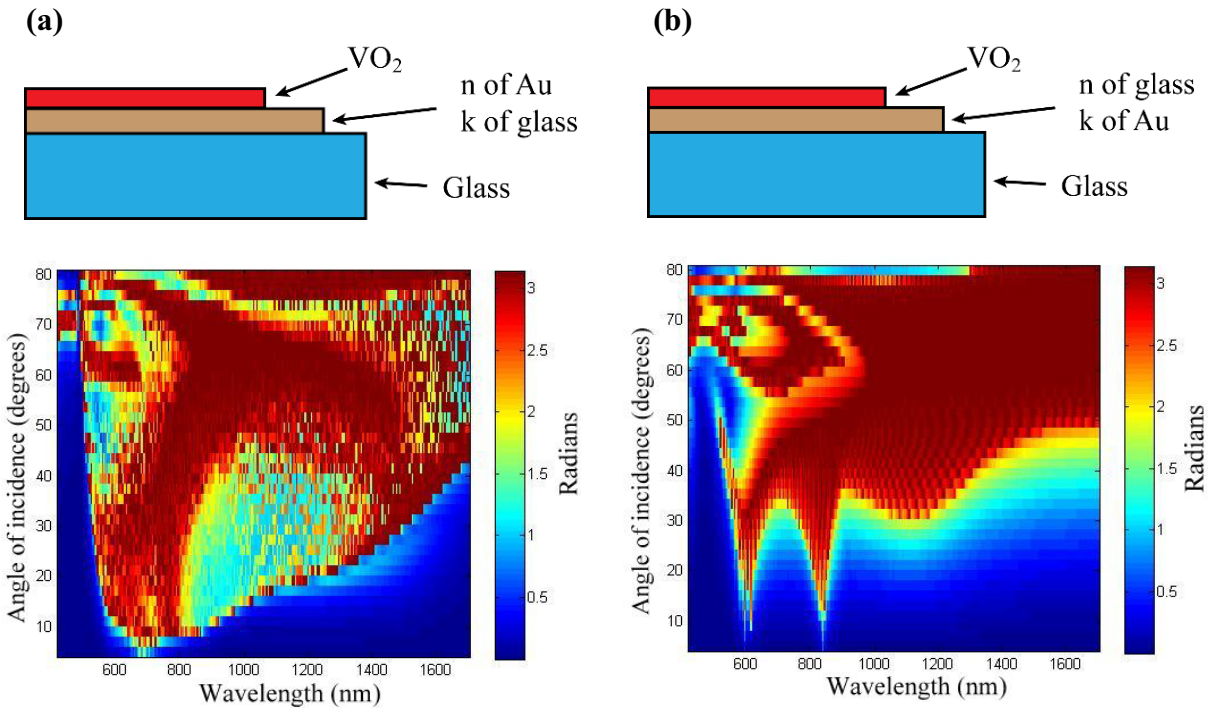

Figure 9.8: Maximum phase shift calculated for different refractive index sets of substrates: (a) set 1 has n values of gold and k values of glass and (b) set 2 has n values of glass and k values of gold.

In doing experiments to verify some of the properties described above, gold and aluminum films of 100 nm or more in thickness were deposited on glass substrates by thermal evaporation under vacuum. VO_2 films were then prepared on top of the metallic films by sputtering using the same recipe in Chapter 4. The thickness of VO_2 layers were chosen in the 85-100 nm range, values for which the calculation above shows large relative phase shifts for wavelengths from 800 to 1000 nm at small incidence angles, as Figures 9.2(b) and 9.3(b) showed. The complex refractive indices of VO_2, gold and aluminum as well as the relative phase shifts of all samples were measured by ellipsometry. Obtained data show that VO_2 formed on the metallic layer has similar refractive indices as in VO_2 on dielectric. All the VO_2 samples exhibit large refractive index changes during the phase transition around 68^{o}C.

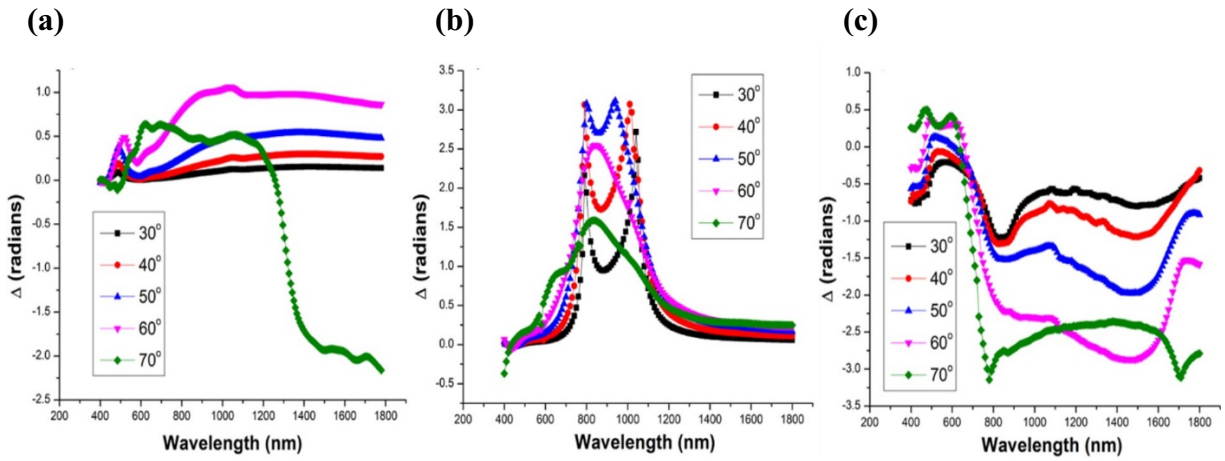

Figure 9.9: Experimental measured relative phase shifts for 86 nm thick VO_2 on (a) glass sample (b) gold sample and c) Al sample.

Figure 9.9 shows the experimentally measured relative phase shifts $\Delta = \arg(z_r)$ at different incidence angles for an 86 nm thick film of VO_2 on glass, gold and aluminum. For VO_2 on glass samples, the incidence angle should be near the Brewster's angle (from 65° to 80°) to attain $\Delta > \frac{\pi}{2}$. At angles less than 65°, the relative phase shifts do not exceed 1 radian. Meanwhile, the VO_2 on gold and on aluminum samples can produce π radians at small incidence angles down to 30°. The VO_2/gold/Corning glass model fits very well for the ellipsometry data of the VO_2 on gold sample. The real (n) and imaginary (k) parts of the refractive indices for the VO_2 layer and gold are demonstrated in Figure 9.7. The process of determining refractive indices and thickness of the VO_2 layer on aluminum is more complex. The measurement results indicate the existence of a 55 nm thick layer with properties of Al_2O_3 between Al and VO_2. This layer can be formed when aluminum is exposed to oxygen in the environment or during oxidation of V to VO_2.

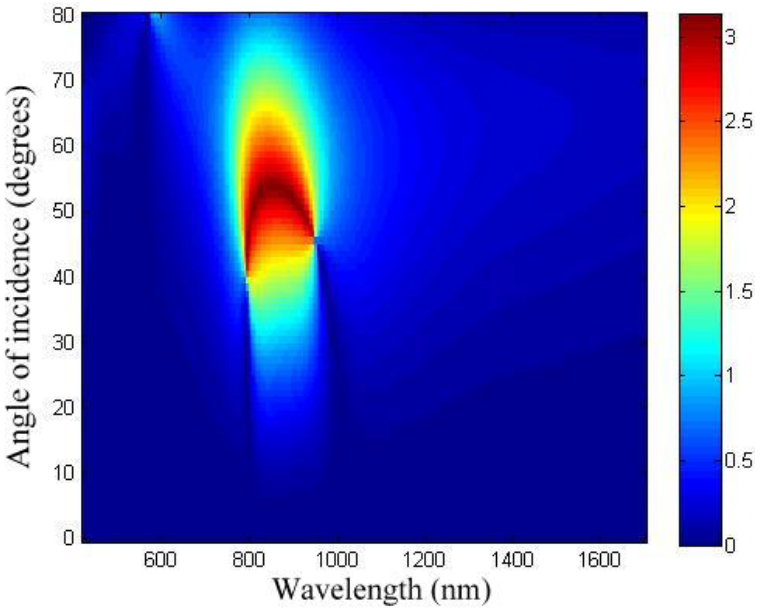

Figure 9.10: Calculated relative phase shift for the 86 nm VO_2 on gold sample at different angles of incidence and wavelengths.

Here, the VO_2 thickness of 86 nm was chosen to achieve maximum Δ at 832 nm, the laser wavelength used in polarization rotation experiments. This is confirmed by the calculated result in Figure 9.10 and the experimental results in Figure 9.9. Thinner or thicker VO_2 layers would cause the peak of Δ to move to either shorter or longer wavelengths, as described in Figures 9.5 and 9.6. The setup in Figure 7.2 was used for all experiments in this chapter. Similar to previous experiments, we used VO_2 on metal samples to change the polarization state of light. In all cases, we tried to transform a reflected linear polarization at low temperature to a new polarization with its orientation rotated by 90^o at high temperature.

Figures 9.11, 9.12 and 9.13 show results obtained at 832 nm with VO_2/gold sample at incidence angles of 60^o, 50^o and 40^o, respectively. For 60^o and 50^o incidence angles, linear polarizations are in both material states and orthogonal to each other. The maximum contrast ratio achieved can be as large as 100. This value could be improved if a better polarizer was used.

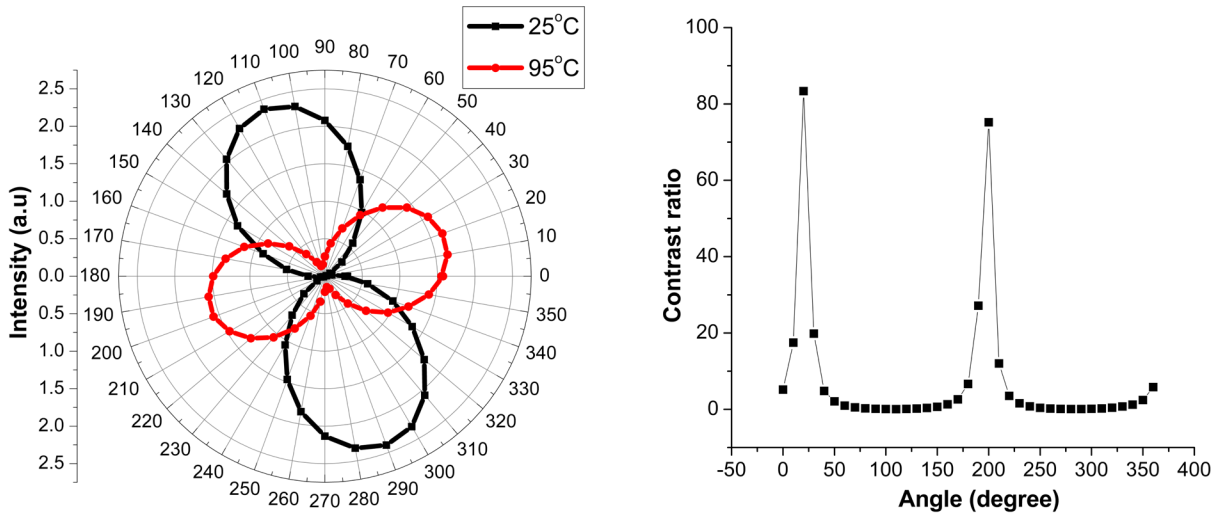

Figure 9.11: Polarization state of reflected light at 60° incidence angle and the corresponding contrast ratio for the VO_2 on gold sample.

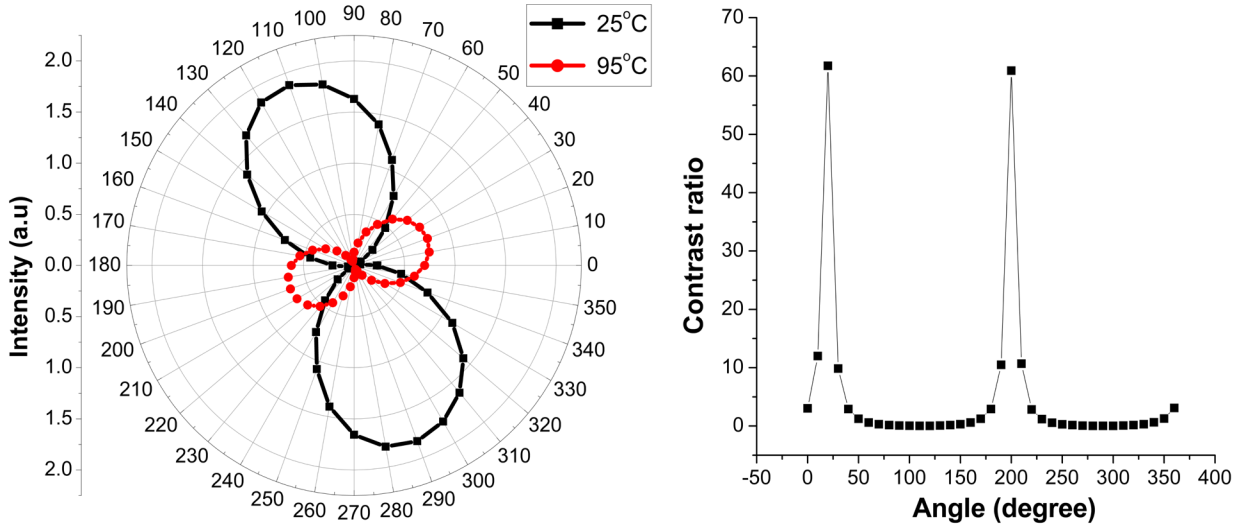

Figure 9.12: Polarization state of reflected light at 50° incidence angle and the corresponding contrast ratio for the VO_2 on gold sample.

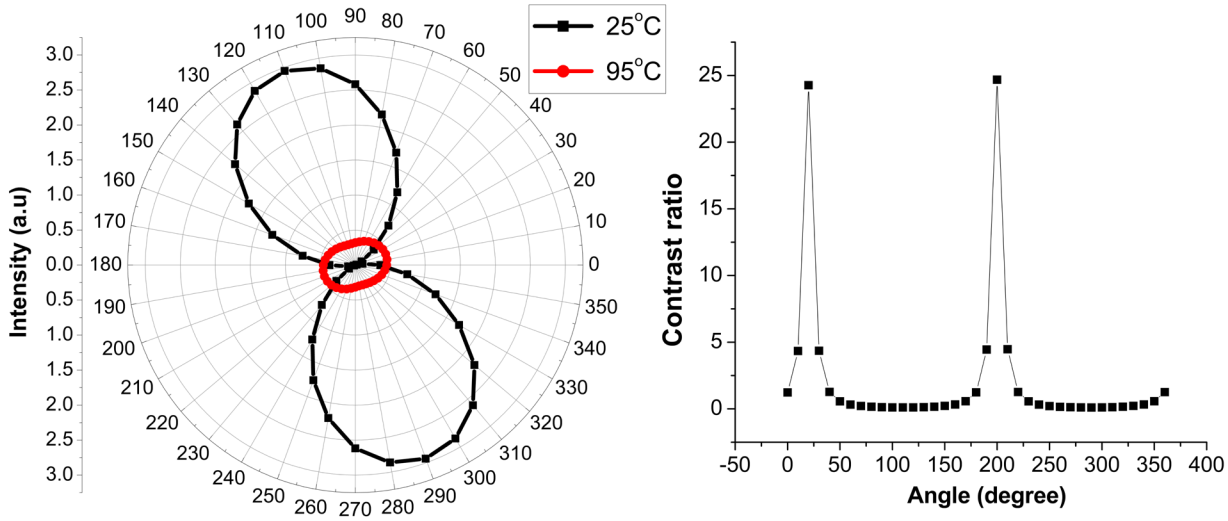

Figure 9.13: Polarization state of reflected light at 40° incidence angle and the corresponding contrast ratio for the VO_2 on gold sample.

At 40° incidence angles, the Δ value is smaller but large enough to transform a linear polarization at 25°C to elliptical polarization at 95°C. Although the polarizations of the reflected light at two temperatures are perpendicular to each other, the reflection on the metallic VO_2 is however reduced significantly so that the contrast ratios are decreased and only reach the maximum at 25.

Experiments also were performed on the VO_2 on aluminum sample at 543 nm probe beam, Figures 9.14-9.19. Thickness of the sample is not optimized for small incidence angles (<60°). Nevertheless, even these non-optimal conditions yield large contrast ratios.

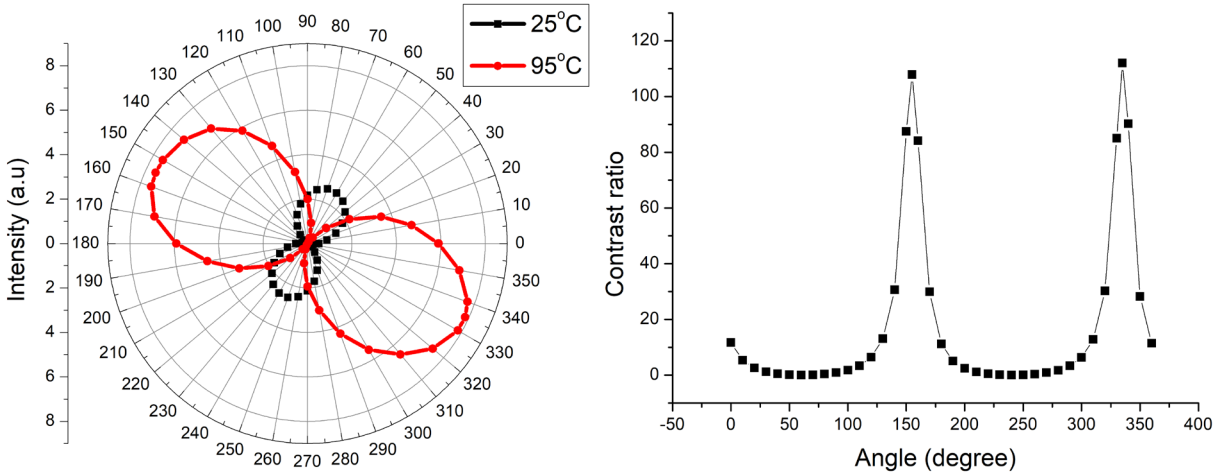

Figure 9.14: Polarization state of reflected light at 72^{o} incidence angle and the corresponding contrast ratio for the VO_2 on Al sample.

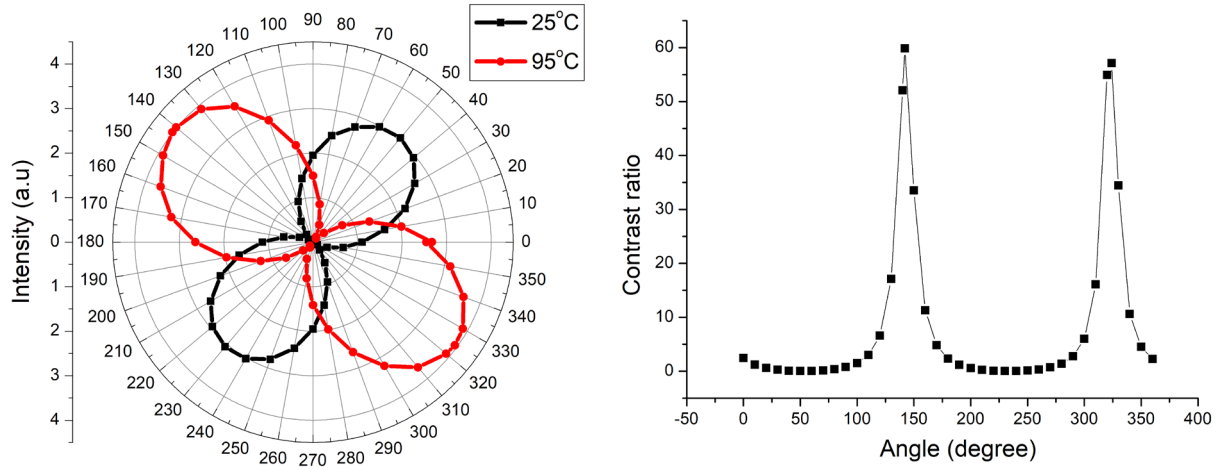

Figure 9.15: Polarization state of reflected light at 70^{o} incidence angle and the corresponding contrast ratio for the VO_2 on Al sample.

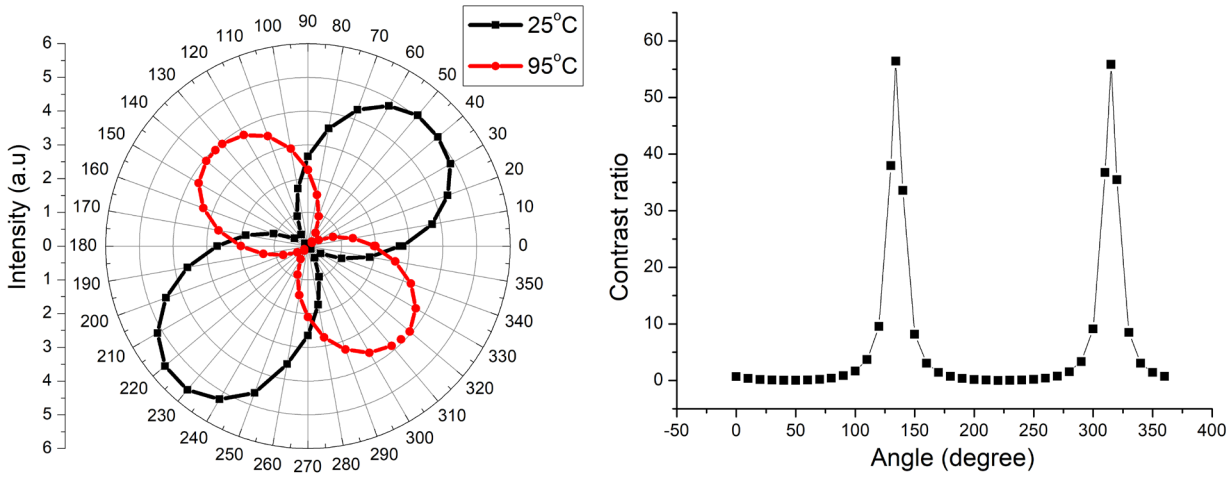

Figure 9.16: Polarization state of reflected light at 68° incidence angle and the corresponding contrast ratio for the VO_2 on Al sample.

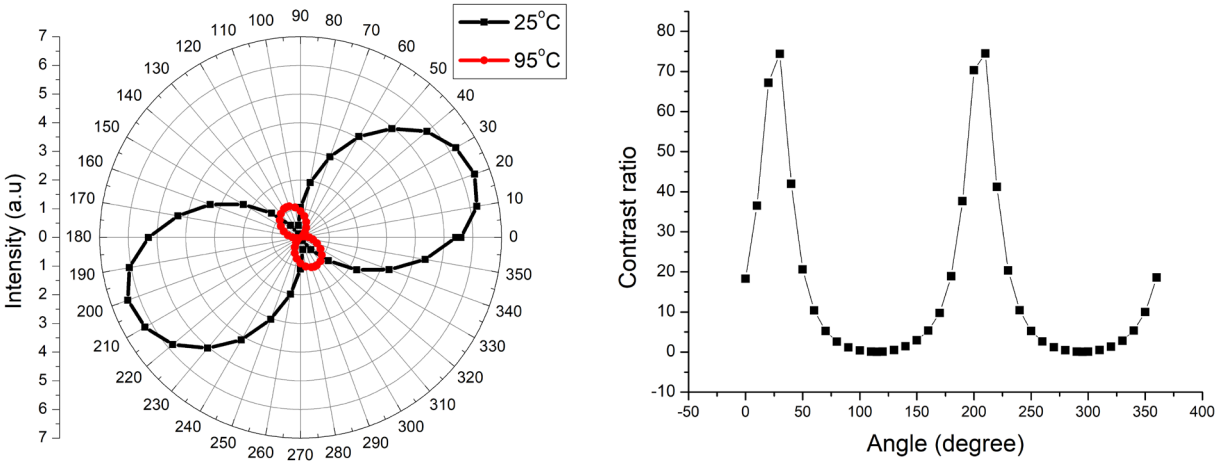

Figure 9.17 Polarization state of reflected light at 64° incidence angle and the corresponding contrast ratio for the VO_2 on Al sample.

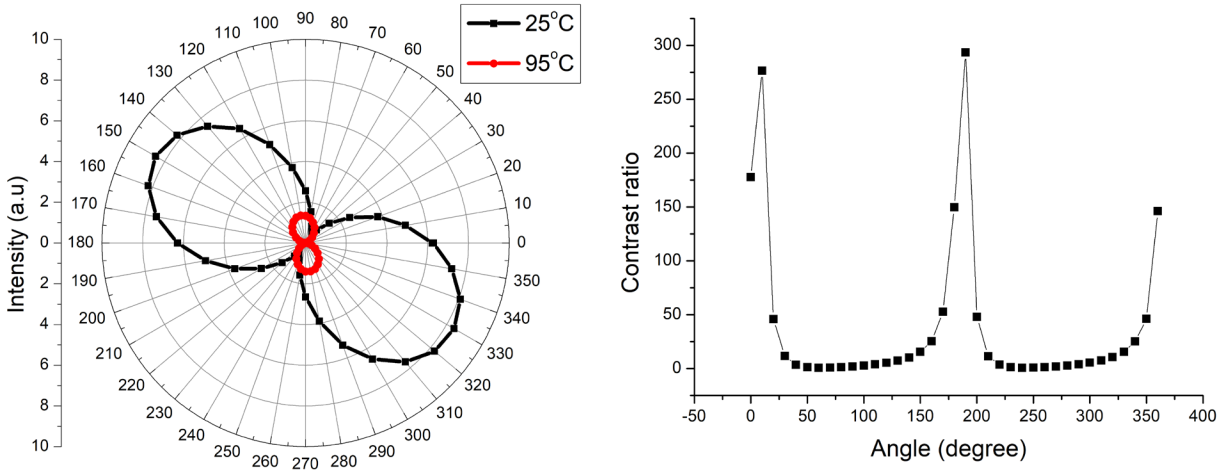

Figure 9.18: Polarization state of reflected light at 60° incidence angle and the corresponding contrast ratio for the VO_2 on Al sample.

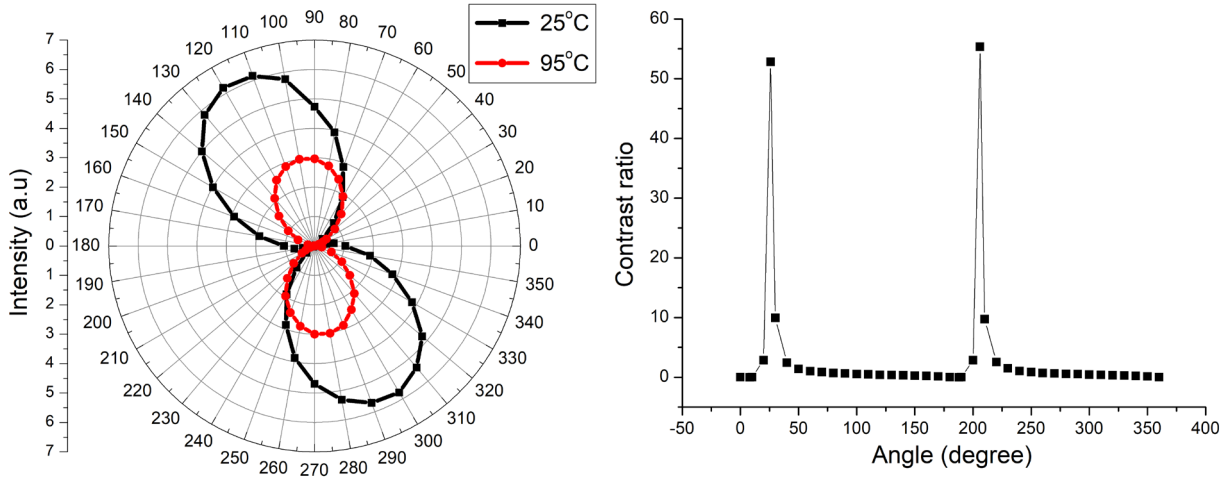

Figure 9.19: Polarization state of reflected light at 56° incidence angle and the corresponding contrast ratio for the VO_2 on Al sample.

Here, some oxide layer formed in the VO_2 on aluminum sample changes its properties and causes difficulties in doing experiments. Thus, we are looking for ways to make better samples. The structure glass/VO_2/Al with light arriving on VO_2 through the glass substrate may solve this

problem. However, the effect of the glass substrate on the polarization results must be considered carefully.

In conclusion of this chapter, we have demonstrated that metallic substrates such as gold, aluminum, titanium can enhance the ability of VO_2 samples in controlling polarization of light and help lowering incidence angles in experiment to 30^o-40^o. This has been clearly confirmed through experiments on the VO_2/gold samples. The VO_2 on aluminum samples promise better results, especially the ability to change polarization of light in the visible region. However, the oxidation of aluminum at the interface between VO_2 and Al modifies considerably the properties of the samples. The problem of oxide layer formed in VO_2 on metal samples will be studied carefully in the near future.

CHAPTER 10

Conclusions and future works

The use of amplitude variation in most optical applications of vanadium dioxide has revealed disadvantages such as limited wavelengths range of application (> 1000 nm), operation in transmission only and low optical modulation. These limit the applicability of VO_2 in many fields. In this thesis, we presented the new method of using the optical phase to change polarized light and overcome these weaknesses. The refractive index of VO_2 changes during its phase transition, thereby altering the phases of s- and p-polarized light when they reflect on or transmit through the film. As a result, a linear polarization can transform to a circular polarization or rotate its orientation to a new angle. This effect, when combined with a polarizer enhances the applicability of VO_2, with the following advantages.

1. Samples use uniform VO_2 films on a variety of substrates. They don't require nanoscale pattering or particular treatments.
2. Spectral range for application is extended into the visible region.
3. High optical modulations are achieved.

These improvements are due to the polarization control of VO_2 thin films. It has been researched and improved gradually during my doctoral studies. The main results were presented in this thesis as follows:

1. The electrical, optical and structural properties of vanadium dioxide were outlined in detail to provide an overview of the material. We analyzed the disadvantages of using amplitude variation on optical VO_2 applications. We proposed the new approach using optical phase change of light to control polarizations.

2. To implement our idea, we studied the interactions between s- and p-polarized light to a VO_2 thin film. The Fresnel equations and the thin film single-layer model were used in the calculations in order to understand the relationships between polarization states of light at different VO_2 states. This relationship is expressed through the coefficient z_r for reflection and z_t for transmission. They are functions of wavelength, angle of incidence, film thickness, state of VO_2, refractive indices of VO_2 and substrates. The absolute value of $arg(z_r)$ or $arg(z_t)$ determines polarization change, in particular there are some notable cases:
    - $arg(z_r) = \pi(1 + 2m)$ with $m = 0, \pm1, \pm2$ ...: permits a linear polarization to rotate by some angle, and sometimes by 90^o.
    - $arg(z_r) = \pi(1/2 + m)$ with $m = 0, \pm1, \pm2$ ...: permit a linear polarization transforms into a circular polarization.
3. We successfully fabricated VO_2 films with a thickness of 50 nm to 150 nm on glass, quartz, sapphire, and Zerodur substrates by sputtering metallic vanadium followed by post-treatment in oxygen method. These samples are of good quality and tested by ellipsometry measurements. In addition, VO_2 thin films were also fabricated on thick gold and aluminum layers (more than 200 nm) to enhance ability to control polarization.
4. In our first experiments on polarization control, we measured the phase changes of light as it reflected on and transmitted through VO_2 thin films during the phase transition. 800 nm and 1310 nm lasers were chosen respectively as probe beams for transmission and reflection to ensure there is no light amplitude change at different VO_2 states, only optical phase changes. The probe beams were positioned at the edge between the bare glass and VO_2 sides of the sample. These two half-beams interacting respectively with the glass and the VO_2 on the glass sample created interference fringes in the far field. And any change

in the optical thickness of the film causes the fringes to move. The relative phase changes of the light are inferred by the position of the fringes. For a 86 nm VO_2 thin film on glass, the phase differences were 0.8 radians for reflected light and 0.4 radians for transmitted light. These experimental results were obtained at normal incidence angle. The calculation showed that π radians relative phase changes can be achieved at angles of incidence around 65^o. This is the foundation of subsequent studies on polarization control.

The phase change of light was also confirmed by laser beam focusing experiments. We used a 532nm pump laser to create temperature profile on the VO_2 thin film which created a phase front curvature on light. As a result, a reflected 1310 nm beam of light was focused at a distance 50 cm away from the sample. And by changing the pumping intensity between 100 to 200 W/cm^2, the focal length varied in the 40-80 cm range.

5. Based on the refractive indices n and k of the VO_2 films obtained from ellipsometry measurements, we did calculations and analyzed the advantages and disadvantages of using change in reflectance and transmittance in optical VO_2 applications. There are two main disadvantages below:

    - Reflectance and transmittance change substantially only for wavelengths in the infrared region (>1000 nm) and almost no change is observed in the visible spectrum.
    - Modulations for reflected light are small. While, for transmission, the modulation ratios can go to 1000 or higher for thick samples where transmittance is very low. Also, for opaque substrates, the use of transmitted beams is not possible.

    Calculations with polarized light showed encouraging results that can overcome the above weaknesses, with π radians relative phase shift for reflection achieved with

wavelengths in the visible and infrared. For transmission, only a 1 radian phase difference is achieved at 1.7μm and at very large angle of incidence 80°. Because of these results, we proposed using polarized light in reflection from VO_2 sample to change the polarization state of light.

Theoretical analysis showed that the ratio of light intensity passing through the polarizer with VO_2 activated to the light passing when VO_2 is not activated can be very high. This happens if a prepared linear polarization transforms to a new polarization with its orientation rotated by 90°. Reflected linear polarization can be created easily by combining a polarizer and a birefringent crystal. However, the most important thing is to find the conditions of VO_2 film thickness, angle of incidence and wavelength so that the relative phase difference $arg(z_r)$ reaches a value of π.

6. Using experimentally measured refractive indices of VO_2 and a single thin-film model, we calculated the relative phase differences in all the cases of thickness from 25 nm to 300 nm, wavelength from 400 nm to 1700 nm and angle of incidence from 0° to 90°. For the VO_2 on glass samples, the results showed the optimal parameters for fabrication and doing experiments as follows:

   - Thickness of VO_2 thin film must be between 50 nm and 150 nm for experiments with visible and infrared light.
   - Angle of incidence is between 65° to 80° to achieve π relative phase difference.

   The above parameters were used in polarization control experiments with VO_2 on glass, quartz and Zerodur samples. For all cases, light contrast ratios reach very high values when VO_2 samples are combined with a polarizer. This has many potential applications in ultrathin, wide bandwidth, high-performance optical modulator.

7. We changed the state of VO_2 fast by using a picosecond pumping laser to photoinduce the phase transition. The results obtained by this optical activation are similar to the results with thermal activation in their magnitude, but much faster in speed. It confirms that we can control polarization state of light in a pico- to nanosecond time scale. And this switching time depends mainly on free carrier lifetime and heat diffusion between the VO_2 film and the substrate. Specifically, by measuring reflectance of light on VO_2 samples over time during the phase transition, we obtain a switch-off time of 12 ns, 30 ns, 76 ns and 95 ns for the VO_2 made on sapphire, Zerodur, quartz, and glass samples, respectively, while switch-on times for the VO_2 samples are very fast, on picoseconds scales. These results suggest that VO_2 thin films can be applied to high-speed optical devices.
8. We enhanced the polarization control of VO_2 thin films by fabricating them on metallic substrates such as gold and aluminum. Calculations showed that the angle of incidence can be reduced down to 10^o and the spectral range of modulation is extended to near 400 nm. This was confirmed by the experimental results on the VO_2 films fabricated on the gold substrates. At 40^o angle of incidence, the linear polarization can transform to the elliptical polarization with contrast ratio of 25 through a polarizer. The VO_2 on aluminum samples promise better results, especially the ability to change polarization of light in the visible region. However, the oxide layers formed during the fabrication changes their properties. So, we need to find better methods to prepare VO_2 thin films on metallic substrates.

Potential applications and future works

The positive results obtained in this thesis show that VO_2 thin films can be applied to many different fields. Their ability to modulate the optical phase of light can be compared with that of some electro-optic and ferroelectric material such as quartz, $BaTiO_3$ or KH_2PO_4 (KDP). A substantial relative phase difference between the reflected s- and p-polarization can be achieved easily between the non-activated and activated VO_2 states. However, in case using VO_2 we only need to use thin film thickness in nanometers rather than millimeters as in other devices. This could be especially useful in miniaturized optical components. Our work has also shown great potential in the application of VO_2 to high-speed, high-modulation optical devices. Research on this issue could be continued with following improvements.

- Creating perfect absorbers for some specific wavelengths.
- Using metallic thin films underneath and above VO_2 to create effective polarization rotator.
- Researching on dynamic modulation of visible spectrum and colour.
- Creating multi-layer VO_2 devices for laser beam focusing.
- Measuring refractive indices n and k of VO_2 thin films at different delay times.
- Metamaterials based on hybrid combination of metallic nanostructures and vanadium dioxide.

REFERENCES

[1] F. J. Morin, "Oxides Which Show a Metal-to-Insulator Transition at the Neel Temperature," *Phys. Rev. Lett.*, vol. 3, no. 1, pp. 34–36, Jul. 1959.

[2] T.-C. Chang, X. Cao, S.-H. Bao, S.-D. Ji, H.-J. Luo, and P. Jin, "Review on thermochromic vanadium dioxide based smart coatings: from lab to commercial application," *Adv. Manuf.*, vol. 6, no. 1, pp. 1–19, Mar. 2018.

[3] M. Soltani, M. Chaker, E. Haddad, and R. Kruzelesky, "1 × 2 optical switch devices based on semiconductor-to-metallic phase transition characteristics of VO_2 smart coatings," *Meas. Sci. Technol.*, vol. 17, no. 5, pp. 1052–1056, May 2006.

[4] R. M. Briggs, I. M. Pryce, and H. A. Atwater, "Compact silicon photonic waveguide modulator based on the vanadium dioxide metal-insulator phase transition," *Opt. Express*, vol. 18, no. 11, pp. 11192–11201, May 2010.

[5] B.-J. Kim, Y. W. Lee, B.-G. Chae, S. J. Yun, S.-Y. Oh, H.-T. Kim, and Y.-S. Lim, "Temperature dependence of the first-order metal-insulator transition in VO_2 and programmable critical temperature sensor," *Appl. Phys. Lett.*, vol. 90, no. 2, p. 023515, Jan. 2007.

[6] S. Bonora, G. Beydaghyan, A. Haché, and P. V. Ashrit, "Mid-IR laser beam quality measurement through vanadium dioxide optical switching," *Opt. Lett.*, vol. 38, no. 9, pp. 1554–1556, May 2013.

[7] S. Bonora, U. Bortolozzo, S. Residori, R. Balu, and P. V. Ashrit, "Mid-IR to near-IR image conversion by thermally induced optical switching in vanadium dioxide," *Opt. Lett.*, vol. 35, no. 2, pp. 103–105, Jan. 2010.

[8] Y. Chen, S. Zhang, F. Ke, C. Ko, S. Lee, K. Liu, B. Chen, J. W. Ager, R. Jeanloz, V. Eyert, and J. Wu, "Pressure–Temperature Phase Diagram of Vanadium Dioxide," *Nano Lett.*, vol. 17, no. 4, pp. 2512–2516, Apr. 2017.

[9] M. J. Tadjer, V. D. Wheeler, B. Downey, Z. R. Robinson, D. J. Meyer, and C. R. Eddy, "Temperature and Electric Field Induced Metal-Insulator Transition in Atomic Layer Deposited Vanadium Dioxide Thin Films," *Solid State Electron.*, vol. 136, pp. 30–35, Oct. 2017.

[10] R. M. Wentzcovitch, W. W. Schulz, and P. B. Allen, "VO_2: Peierls or Mott-Hubbard? A view from band theory," *Phys. Rev. Lett.*, vol. 72, no. 21, pp. 3389–3392, May 1994.

[11] R. M. Wentzcovitch, W. W. Schulz, and P. B. Allen, "Wentzcovitch et al. Reply," *Phys. Rev. Lett.*, vol. 73, no. 22, pp. 3043–3043, Nov. 1994.

[12] A. Cavalleri, T. Dekorsy, H. H. W. Chong, J. C. Kieffer, and R. W. Schoenlein, "Evidence for a structurally-driven insulator-to-metal transition in VO_2: A view from the ultrafast timescale," *Phys. Rev. B*, vol. 70, no. 16, Oct. 2004.

[13] Rice TM, Launois H, and Pouget JP, "Comment on 'VO_2: Peierls or Mott-Hubbard? A view from band theory,'" *Phys. Rev. Lett.*, vol. 73, no. 22, p. 3042, Nov. 1994.

[14] H.-T. Kim, Y. W. Lee, B.-J. Kim, B.-G. Chae, S. J. Yun, K.-Y. Kang, K.-J. Han, K.-J. Yee, and Y.-S. Lim, "Monoclinic and Correlated Metal Phase in VO_2 as Evidence of the Mott Transition: Coherent Phonon Analysis," *Phys. Rev. Lett.*, vol. 97, no. 26, p. 266401, Dec. 2006.

[15] F. Bloch, "Bemerkung zur Elektronentheorie des Ferromagnetismus und der elektrischen Leitfähigkeit," *Z. Für Phys.*, vol. 57, no. 7–8, pp. 545–555, Jul. 1929.

[16] M. Imada, A. Fujimori, and Y. Tokura, “Metal-insulator transitions,” *Rev. Mod. Phys.*, vol. 70, no. 4, pp. 1039–1263, Oct. 1998.
[17] A. H. Wilson, “The theory of electronic semi-conductors,” *Proc R Soc Lond A*, vol. 133, no. 822, pp. 458–491, Oct. 1931.
[18] Sommerfeld, W.V.Houston, and C.Eckart, *Z.Physik*, vol. 47, no. 1, 1928.
[19] J. H. de Boer and E. J. W. Verwey, “Semi-conductors with partially and with completely filled 3 d -lattice bands,” *Proc. Phys. Soc.*, vol. 49, no. 4S, p. 59, 1937.
[20] N. F. Mott and R. Peierls, “Discussion of the paper by de Boer and Verwey,” *Proc. Phys. Soc.*, vol. 49, no. 4S, pp. 72–73, Aug. 1937.
[21] N. F. Mott and W. D. Twose, “The theory of impurity conduction,” *Adv. Phys.*, vol. 10, no. 38, pp. 107–163, Apr. 1961.
[22] G. B. Norris and K. K. Bajaj, “Exciton-plasma Mott transition in Si,” *Phys. Rev. B*, vol. 26, no. 12, pp. 6706–6710, Dec. 1982.
[23] J. Hubbard, “Electron Correlations in Narrow Energy Bands,” *Proc. R. Soc. Math. Phys. Eng. Sci.*, vol. 276, no. 1365, pp. 238–257, Nov. 1963.
[24] M. Fowler, “Electrons in One Dimension: the Peierls Transition,” p. 11.
[25] R. E. Thorne, “Charge-Density-Wave Conductors,” *Phys. Today*, vol. 49, no. 5, pp. 42–47, May 1996.
[26] P. W. Anderson, “Absence of Diffusion in Certain Random Lattices,” p. 14.
[27] A. Lagendijk, B. van Tiggelen, and D. S. Wiersma, “Fifty years of Anderson localization,” *Phys. Today*, vol. 62, no. 8, pp. 24–29, Aug. 2009.
[28] J.-J. Wang, Y.-Z. Xu, R. Mazzarello, M. Wuttig, and W. Zhang, “A Review on Disorder-Driven Metal-Insulator Transition in Crystalline Vacancy-Rich GeSbTe Phase-Change Materials,” *Mater. Basel Switz.*, vol. 10, no. 8, Jul. 2017.
[29] T. Ying, Y. Gu, X. Chen, X. Wang, S. Jin, L. Zhao, W. Zhang, and X. Chen, “Anderson localization of electrons in single crystals: $LixFe_7Se_8$,” *Sci. Adv.*, vol. 2, no. 2, Feb. 2016.
[30] Y. Yanase and N. Yorozu, “Localization and Superconductivity in Doped Semiconductors,” *J. Phys. Soc. Jpn.*, vol. 78, no. 3, p. 034715, Mar. 2009.
[31] H. v. Löhneysen, “Metal-insulator transition in heavily doped semiconductors,” *Curr. Opin. Solid State Mater. Sci.*, vol. 3, no. 1, pp. 5–15, Feb. 1998.
[32] Q. Meng, “Metal Insulator Transition,” p. 10.
[33] A. S. McLeod, E. van Heumen, J. G. Ramirez, S. Wang, T. Saerbeck, S. Guenon, M. Goldflam, L. Anderegg, P. Kelly, A. Mueller, M. K. Liu, I. K. Schuller, and D. N. Basov, “Nanotextured phase coexistence in the correlated insulator V_2O_3,” *Nat. Phys.*, vol. 13, no. 1, pp. 80–86, Jan. 2017.
[34] J. Laverock, A. R. H. Preston, D. Newby, K. E. Smith, S. Sallis, L. F. J. Piper, S. Kittiwatanakul, J. W. Lu, S. A. Wolf, M. Leandersson, and T. Balasubramanian, “Photoemission evidence for crossover from Peierls-like to Mott-like transition in highly strained VO_2,” *Phys. Rev. B*, vol. 86, no. 19, p. 195124, Nov. 2012.
[35] C. Sun, L. Yan, B. Yue, H. Liu, and Y. Gao, “The modulation of metal–insulator transition temperature of vanadium dioxide: a density functional theory study,” *J. Mater. Chem. C*, vol. 2, no. 43, pp. 9283–9293, Oct. 2014.
[36] M. Cyrot, “Theory of Mott transition: Applications to transition metal oxides,” *J. Phys.*, vol. 33, no. 1, pp. 125–134, 1972.

[37] D. Meyers, J. Liu, J. W. Freeland, S. Middey, M. Kareev, J. Kwon, J. M. Zuo, Y.-D. Chuang, J. W. Kim, P. J. Ryan, and J. Chakhalian, "Pure electronic metal-insulator transition at the interface of complex oxides," *Sci. Rep.*, vol. 6, no. 1, Sep. 2016.
[38] V. Heine and L. F. Mattheiss, "Metal-insulator transition in transition metal oxides," *J. Phys. C Solid State Phys.*, vol. 4, no. 10, p. L191, 1971.
[39] Z. Yang, C. Ko, and S. Ramanathan, "Oxide Electronics Utilizing Ultrafast Metal-Insulator Transitions," *Annu. Rev. Mater. Res.*, vol. 41, no. 1, pp. 337–367, Jul. 2011.
[40] A. V. Il'inskiy, M. E. Pashkevich, and E. B. Shadrin, "Stage-by-stage modeling of the mechanism of semiconductor–metal phase transition in vanadium dioxide," *St Petersburg Polytech. Univ. J. Phys. Math.*, vol. 3, no. 3, pp. 181–186, Oct. 2017.
[41] K. D. Rogers, "An X-ray diffraction study of semiconductor and metallic vanadium dioxide," *Powder Diffr.*, vol. 8, no. 04, pp. 240–244, Dec. 1993.
[42] J. B. Goodenough, "The two components of the crystallographic transition in VO_2," *J. Solid State Chem.*, vol. 3, no. 4, pp. 490–500, Nov. 1971.
[43] C. Sun, L. Yan, B. Yue, H. Liu, and Y. Gao, "The modulation of metal–insulator transition temperature of vanadium dioxide: a density functional theory study," *J. Mater. Chem. C*, vol. 2, no. 43, pp. 9283–9293, Oct. 2014.
[44] T. J. Huffman, C. Hendriks, E. J. Walter, J. Yoon, H. Ju, R. Smith, G. L. Carr, H. Krakauer, and M. M. Qazilbash, "Insulating phases of vanadium dioxide are Mott-Hubbard insulators," *Phys. Rev. B*, vol. 95, no. 7, Feb. 2017.
[45] A. Pergament, "Metal–insulator transition: the Mott criterion and coherence length," *J. Phys. Condens. Matter*, vol. 15, no. 19, p. 3217, 2003.
[46] D. Khomskii, *Transition metal compounds*. Cambridge, United Kingdom: Cambridge University Press, 2014.
[47] Y. Muraoka, Y. Ueda, and Z. Hiroi, "Large modification of the metal–insulator transition temperature in strained VO_2 films grown on TiO_2 substrates," *J. Phys. Chem. Solids*, vol. 63, no. 6, pp. 965–967, Jun. 2002.
[48] D. H. Kim and H. S. Kwok, "Pulsed laser deposition of VO_2 thin films," *Appl. Phys. Lett.*, vol. 65, no. 25, pp. 3188–3190, Dec. 1994.
[49] T. Maruyama and Y. Ikuta, "Vanadium dioxide thin films prepared by chemical vapour deposition from vanadium (III) acetylacetonate," *J. Mater. Sci.*, vol. 28, no. 18, pp. 5073–5078, Jan. 1993.
[50] J. Livage, "Optical and electrical properties of vanadium oxides synthesized from alkoxides," *Coord. Chem. Rev.*, vol. 190–192, pp. 391–403, Sep. 1999.
[51] T. V. Son, K. Zongo, C. Ba, G. Beydaghyan, and A. Haché, "Pure optical phase control with vanadium dioxide thin films," *Opt. Commun.*, vol. 320, pp. 151–155, Jun. 2014.
[52] R. T. Kivaisi and M. Samiji, "Optical and electrical properties of vanadium dioxide films prepared under optimized RF sputtering conditions," *Sol. Energy Mater. Sol. Cells*, vol. 57, no. 2, pp. 141–152, Feb. 1999.
[53] M. Nazari, Y. Zhao, Y. Zhu, V. V. Kuryatkov, A. A. Bernussi, Z. Fan, and M. Holtz, "Optical, Structural, and Electrical Properties of Vanadium Dioxide Grown on Sapphire Substrates with Different Crystallographic Orientations," *MRS Proc.*, vol. 1494, Jan. 2012.
[54] B.-G. Chae, H.-T. Kim, S.-J. Yun, B.-J. Kim, Y.-W. Lee, D.-H. Youn, and K.-Y. Kang, "Highly Oriented VO_2 Thin Films Prepared by Sol-Gel Deposition," *Electrochem. Solid-State Lett.*, vol. 9, no. 1, p. C12, 2006.

[55] R. G. Mani and S. Ramanathan, "Observation of a uniform temperature dependence in the electrical resistance across the structural phase transition in thin film vanadium oxide (VO_2)," *Appl. Phys. Lett.*, vol. 91, no. 6, p. 062104, Aug. 2007.
[56] K. G. West, Jiwei Lu, Jiani Yu, D. Kirkwood, Wei Chen, Yonghang Pei, J. Claassen, and S. A. Wolf, "Growth and characterization of vanadium dioxide thin films prepared by reactive-biased target ion beam deposition," *J. Vac. Sci. Technol. Part -Vac. Surf. Films*, vol. 26, no. 1, pp. 133–139, Jan. 2008.
[57] A. Crunteanu, M. Fabert, J. Cornette, M. Colas, J.-C. Orlianges, A. Bessaudou, and F. Cosset, "Electric field-assisted metal insulator transition in vanadium dioxide (VO_2) thin films: optical switching behavior and anomalous far-infrared emissivity variation," in *Proc. SPIE 9364, Oxide-based Materials and Devices VI*, 2015, p. 93640J.
[58] Y. Cui and S. Ramanathan, "Substrate effects on metal-insulator transition characteristics of rf-sputtered epitaxial VO_2 thin films," *J. Vac. Sci. Technol. Part -Vac. Surf. Films*, vol. 29, no. 4, p. 041502, Jul. 2011.
[59] Z. Ling, T. Jianhui, F. Hao, and C. Jingzhong, "Study on mixed vanadium oxide thin film deposited by RF magnetron sputtering and its application," *Phys. Procedia*, vol. 18, pp. 73–76, 2011.
[60] H. Kakiuchida, P. Jin, S. Nakao, and M. Tazawa, "Optical Properties of Vanadium Dioxide Film during Semiconductive–Metallic Phase Transition," *Jpn. J. Appl. Phys.*, vol. 46, no. 2L, p. L113, Jan. 2007.
[61] D. Ruzmetov, D. Heiman, B. B. Claflin, V. Narayanamurti, and S. Ramanathan, "Hall carrier density and magnetoresistance measurements in thin film vanadium dioxide across the metal-insulator transition," *Phys. Rev. B*, vol. 79, no. 15, Apr. 2009.
[62] A. L. Pergament, G. B. Stefanovich, N. A. Kuldin, and A. A. Velichko, "On the Problem of Metal-Insulator Transitions in Vanadium Oxides," *ISRN Condensed Matter Physics*, May-2013. .
[63] D. Fu, K. Liu, T. Tao, K. Lo, C. Cheng, B. Liu, R. Zhang, H. A. Bechtel, and J. Wu, "Comprehensive study of the metal-insulator transition in pulsed laser deposited epitaxial VO_2 thin films," *J. Appl. Phys.*, vol. 113, no. 4, p. 043707, Jan. 2013.
[64] R. A. Aliev, V. N. Andreev, V. M. Kapralova, V. A. Klimov, A. I. Sobolev, and E. B. Shadrin, "Effect of grain sizes on the metal-semiconductor phase transition in vanadium dioxide polycrystalline thin films," *Phys. Solid State*, vol. 48, no. 5, pp. 929–934, May 2006.
[65] P. Jin, K. Yoshimura, and S. Tanemura, "Dependence of microstructure and thermochromism on substrate temperature for sputter-deposited VO_2 epitaxial films," *J. Vac. Sci. Technol. Vac. Surf. Films*, vol. 15, no. 3, pp. 1113–1117, May 1997.
[66] L. Kang, Y. Gao, Z. Zhang, J. Du, C. Cao, Z. Chen, and H. Luo, "Effects of Annealing Parameters on Optical Properties of Thermochromic VO2 Films Prepared in Aqueous Solution," *J. Phys. Chem. C*, vol. 114, no. 4, pp. 1901–1911, Feb. 2010.
[67] B. Rajeswaran and A. M. Umarji, "Effect of W addition on the electrical switching of VO_2 thin films," *AIP Adv.*, vol. 6, no. 3, p. 035215, Mar. 2016.
[68] W. R. Roach and I. Balberg, "Optical induction and detection of fast phase transition in VO_2," *Solid State Commun.*, vol. 9, no. 9, pp. 551–555, May 1971.
[69] D. Wegkamp and J. Stähler, "Ultrafast dynamics during the photoinduced phase transition in VO_2," *Prog. Surf. Sci.*, vol. 90, no. 4, pp. 464–502, Dec. 2015.

[70] E. Radue, L. Wang, S. Kittiwatanakul, J. Lu, S. A. Wolf, E. Rossi, R. A. Lukaszew, and I. Novikova, "Substrate-induced microstructure effects on the dynamics of the photo-induced metal–insulator transition in VO_2 thin films," *J. Opt.*, vol. 17, no. 2, p. 025503, 2015.
[71] A. Pashkin, C. Kübler, H. Ehrke, R. Lopez, A. Halabica, R. F. Haglund, R. Huber, and A. Leitenstorfer, "Ultrafast insulator-metal phase transition in VO_2 studied by multiterahertz spectroscopy," *Phys. Rev. B*, vol. 83, no. 19, May 2011.
[72] D. J. Hilton, R. P. Prasankumar, S. Fourmaux, A. Cavalleri, D. Brassard, M. A. El Khakani, J. C. Kieffer, A. J. Taylor, and R. D. Averitt, "Enhanced Photosusceptibility near Tc for the Light-Induced Insulator-to-Metal Phase Transition in Vanadium Dioxide," *Phys. Rev. Lett.*, vol. 99, no. 22, Nov. 2007.
[73] C. Kübler, H. Ehrke, R. Huber, R. Lopez, A. Halabica, R. F. Haglund, and A. Leitenstorfer, "Coherent Structural Dynamics and Electronic Correlations during an Ultrafast Insulator-to-Metal Phase Transition in VO_2," *Phys. Rev. Lett.*, vol. 99, no. 11, Sep. 2007.
[74] W.-P. Hsieh, M. Trigo, D. A. Reis, G. Andrea Artioli, L. Malavasi, and W. L. Mao, "Evidence for photo-induced monoclinic metallic VO_2 under high pressure," *Appl. Phys. Lett.*, vol. 104, no. 2, p. 021917, Jan. 2014.
[75] J. Leroy, A. Crunteanu, A. Bessaudou, F. Cosset, C. Champeaux, and J.-C. Orlianges, "High-speed metal-insulator transition in vanadium dioxide films induced by an electrical pulsed voltage over nano-gap electrodes," *Appl. Phys. Lett.*, vol. 100, no. 21, p. 213507, May 2012.
[76] Y.-X. Ji, S.-Y. Li, G. A. Niklasson, and C. G. Granqvist, "Durability of thermochromic VO_2 thin films under heating and humidity: Effect of Al oxide top coatings," *Thin Solid Films*, vol. 562, pp. 568–573, Jul. 2014.
[77] A. Haché, P. A. Do, and S. Bonora, "Surface heating by optical beams and application to mid-infrared imaging," *Appl. Opt.*, vol. 51, no. 27, p. 6578, Sep. 2012.
[78] T. V. Son, C. O. F. Ba, R. Vallée, and A. Haché, "Nanometer-thick flat lens with adjustable focus," *Appl. Phys. Lett.*, vol. 105, no. 23, p. 231120, Dec. 2014.
[79] I. Gerdova, X. Zhang, and A. Haché, "Optically tunable hollow Gaussian beams with thin metal films," *JOSA B*, vol. 23, no. 9, pp. 1934–1937, Sep. 2006.
[80] P. Cormier, T. V. Son, J. Thibodeau, A. Doucet, V.-V. Truong, and A. Haché, "Vanadium dioxide as a material to control light polarization in the visible and near infrared," *Opt. Commun.*, vol. 382, pp. 80–85, Jan. 2017.
[81] H. Kakiuchida, P. Jin, S. Nakao, and M. Tazawa, "Optical Properties of Vanadium Dioxide Film during Semiconductive–Metallic Phase Transition," *Jpn. J. Appl. Phys.*, vol. 46, no. 2L, p. L113, Jan. 2007.
[82] J. B. Kana Kana, J. M. Ndjaka, G. Vignaud, A. Gibaud, and M. Maaza, "Thermally tunable optical constants of vanadium dioxide thin films measured by spectroscopic ellipsometry," *Opt. Commun.*, vol. 284, no. 3, pp. 807–812, Feb. 2011.
[83] T. V. Son, V. V. Truong, P. A. Do, and A. Haché, "Ultra-thin, single-layer polarization rotator," *AIP Adv.*, vol. 6, no. 8, p. 085102, Aug. 2016.
[84] T. V. Son, V. V. Truong, J.-F. Bisson, and A. Haché, "Nanosecond polarization modulation in vanadium dioxide thin films," *Appl. Phys. Lett.*, vol. 111, no. 4, p. 041103, Jul. 2017.
[85] S. Lysenko, A. Rúa, V. Vikhnin, F. Fernández, and H. Liu, "Insulator-to-metal phase transition and recovery processes in VO_2 thin films after femtosecond laser excitation," *Phys. Rev. B*, vol. 76, no. 3, Jul. 2007.
[86] M. Rodriguez-Vega, M. T. Simons, E. Radue, S. Kittiwatanakul, J. Lu, S. A. Wolf, R. A. Lukaszew, I. Novikova, and E. Rossi, "Effect of inhomogeneities and substrate on the

dynamics of the metal-insulator transition in VO_2 thin films," *Phys. Rev. B*, vol. 92, no. 11, Sep. 2015.
[87] T. V. Son, P. A. Do, V.-V. Truong, G. Bader, and A. Haché, "Polarization modulation by vanadium dioxide on metallic substrates," *Opt. Commun.*, vol. 427, pp. 511–516, Nov. 2018.
[88] "Refractive index of Ti (Titanium) - Johnson." [Online]. Available: https://refractiveindex.info/?shelf=main&book=Ti&page=Johnson. [Accessed: 29-Jun-2018].
[89] K. Katsumata and S. Sasaki, "Reflection and Refraction of Light in Absorbing Media," *J. Phys. Soc. Jpn.*, vol. 87, no. 5, p. 054401, May 2018.